REPUBLIC OF IRAQ
MINISTRY OF HIGHER EDUCATION AND SCIENTIFIC RESEARCH
AL-FURAT AL-AWSAT TECHNICAL UNIVERSITY
ENGINEERING TECHNICAL COLLEGE - NAJAF

AN EXPERIMENTAL STUDY OF AXIAL CONDUCTION THROUGH AN EVACUATED TUBE HEAT PIPE SOLAR COLLECTOR INTEGRATED WITH PHASE CHANGE MATERIAL

A THESIS

SUBMITTED TO THE POWER TECHNICAL ENGIEENERING DEPARTMENT IN PARTIAL FULFILMENT OF THE REQUIREMENTS FOR THE DEGREE OF TECHNICAL MASTER IN MECHANICAL ENGINEERING –THERMAL

BY

NOORA SALEH MAHDI

(B.SC MECHANICAL ENGINEERING 2013)

Supervisor by

Asst. Prof. Dr. MOHAMED A. AL-FAHHAM

2021

رَبِّ أوزعني أَنْ أَشْكُرَ نعمتك الّتِي أَنْعَمْتَ عَلَيَّ وَعَلَىٰ وَالِدَيَّ وَأَنْ أعمل صَالِحًا تَرْضَاهُ وأصلح لِي فِي ذُرِّيَّتِي ۖ إِنِّي تُبْتُ إِلَيْكَ واني مِنَ الْمُسْلِمِينَ

....

صَدَقَ اللَّهُ الْعَلِيُّ الْعَظِيمُ

سورة الأحقاف: آية ١٥

DISCLAIMER

I confirm that the work submitted in this thesis is my own work and has not been submitted to another organization or for any other degree.

Noora S. Mahdi

Signature:

Date: 20/6/2021

ACKNOWLEDGMENT

Before everyone and above all estimators, all praise and gratitude to ALLAH almighty for his uncountable blessings, and his assistance during the preparation of this thesis.

Mainly, I would like to send my deepest grateful to my thesis advisors, ***Asst. Prof. Dr. Mohamed A. Al-Fahham*** *and* ***Asst. Prof. Dr. Adel A. Eidan****, for their guidance and support throughout this research. They are giving me an exciting opportunity to work on fantastic and vital thesis subject regarding the Renewable Energy. By their guidance, I have learned a lot about the solar energy especially the solar collector systems, I have got new skills such as topic researching and choosing the appropriate courses skill regarding my thesis. They have worked with me as a friend and colleague, not a student, and their offices' door open for my questions and experimental issues most of the time. Their support encouraged me to achieve my thesis goals that I maybe wouldn't do without them.*

Special thanks to the dean of college, head, and members of the Mechanical Power Techniques Engineering department for their assistance. I would like to thanks to my colleagues for their great assistant and great encouragement. My deepest thanks and gratitude are due to each member of my family, especially my dearest husband for their patience, support, and encouragement during the period of my study.

Noora Saleh Mahdi

2021

Supervisor Certification

We certify that this thesis titled**" An Experimental Study of Axial Conduction Through an Evacuated Tube Heat Pipe Solar Collector Integrated with Phase Change Material"** which is being submitted by **Noora Saleh Mahdi** was prepared under our supervision at the Power Techniques Engineering Department, Engineering Technical faculty-Najaf, AL- Furat Al-Awsat Technical University, as partial fulfillment of the requirements for the degree of Master of technical in thermal Engineering.

Signature:

Name: **Asst. Prof. Dr. Mohamed A .Al-Fahham**

(Supervisor)

Date / / 2021

In view of the available recommendation, we forward this thesis for debate by the examining committee.

Signature:

Name: **Prof. Dr. Dhafer Manea Hachim**

(Head of power Tec.Eng.Dept.)

Date: / / 2021

Committee Report

We certify that we have read this thesis titled **"An Experimental Study of Axial Conduction Through an Evacuated Tube Heat Pipe Solar Collector Integrated with Phase Change Material "** which is being submitted by **Noora Saleh Mahdi** and as Examining Committee, examined the student in it is contents. In our opinion, the thesis is adequate for an award of degree of Master of Technical in Thermal Engineering.

Signature:

Name: **Asst. Prof. Dr. Mohamed A. Al-Fahham**
(Supervisor)

Date / / 2021

Signature:

Name: **Asst. Prof. Dr. Bassim Hameed Aboud**

(Member)

Date / / 2021

Signature:

Name: **Asst. Prof. Dr. Mahdi Hatf Kadhum**

(Member)

Date / / 2021

Signature:

Name: **Asst. Prof. Dr. Hassanain Ghani Hameed**

(Chairman)

Date / / 2021

Approval of the Engineering Technical College – Najaf.

Signature:

Name: **Asst. Prof. Dr. Hassanain Ghani Hameed**

Dean of Technical Engineering College -Najaf

Date: / / 2021

Abstract

Next-generation solar collectors, more specifically evacuated tube solar collector (ETSC) system concepts. For instance, the drop in the heat energy during the absence of solar intensity. One of the unique technologies is utilizing an adiabatic section within the gravity assistance heat pipe (GAHP-ETSC) system, such as a thermal breaker within the adiabatic section of the GAHP that is significantly various from the traditional HP-ETSC system.

Four experimental GAHP-ETSC models are two GAHP-ETSC with and without PCM and both with thermal breaker, and the other two with and without PCM and both without thermal breaker have been manufactured, developed, and operated to attain the desired benefits. The four various models were studied by dividing into two cases based on the water load amount in the storage tank. The first and second cases are studying the influence of applying 1 Liter/Hour load and 2 Liter/Hour load of water on the daily efficiency and performance of the four various experimental devices, respectively.

The empirical study was completed in Al-Najaf city of Iraq at outdoor conditions for the period from September 2020 to April 2021. Where, the tilt angle (45^{o}), filling ratio 70% with acetone as a working fluid, and 3.6 kg of paraffin wax as a PCM for each device of the four-apparatus. The results show that the thermal breaker enhances the daily efficiency by extending the total operating hours of the solar collector around (3 Hours) during the night. Also, the system with both thermal breaker and PCM has the highest daily efficiency compared to the other apparatuses, where it increased from 31% to 41% at 1 L/H load, and 42% to 47 % at 2 L/H load. Moreover, the water outlet temperature (The primary output of the GAHP-ETSC) improvement percentage between the apparatus with both thermal breaker and PCM and the apparatus without both is 55% and 55.5% at 1 L/H and 2 L/H load, respectively.

A mathematical model of GAHP has been analyzed by solving Partial Differential Equation (PDE) in order to get the temperature distribution profiles of the present system by using a numerical analysis (MATLAB Software) for future works.

By identifying and understanding the principal challenges and possibilities provided by the technology, this thesis further contributes to defining a roadmap of the new technology ETSC system for future research.

CONTENTS

LIST OF TABLES

LIST OF FIGURES

NOMENCLATURE

Symbol	Definition	Unite
A	The area of solar collector	m^2
C□	Specific heat coefficient	J/kg.K
C_L	Specific heat coefficient of Liquid	J/kg.K
C_S	Specific heat coefficient of Solid	J/kg.K
H	Enthalpy	kJ/kg
P	Pressure	N/m^2
q	Conduction heat transfer rate	W
t	Time	sec
G_T	Global radiation	W/ m^2
h	Coefficient of heat transfer	$W/ m^2. K$
g	Acceleration	m/sec^2
V	Volume	m^3
I	Total solar irradiance	W/ m^2
k	Constant of thermal conductivity	W/ m. K
K_s	Constant of thermal conductivity for solid	W/ m. K
K_L	Constant of thermal conductivity for liquid	W/ m. K
K_c	Constant of thermal conductivity for copper	W/ m. K
R_{exp}	The overall thermal resistance	°C/W
$\bar{q}$	Average heat flux	W/m^2
L	Collector length	m
l	Distance between plate and covers	m
ṁ	The flow rate of mass	kg/sec
Nu	Nusselt number	Dimensionless
Q	Thermal energy	W
$\dot{Q}_u$	Total useful thermal energy	W
H_p^*	Old value of (H) at grid point J	-
T	Temperature	^{o} C
T□	Melting point temperature	^{o} C

x,y,z	Cartesian coordinate directions	-
u,v,w	Velocity component in x, y and z direction respectively	-
i,j,k	Vector in x, y, z direction respectively	-

Greek Symbols		
β	Coefficient of expansion	K^{-1}
ξ	Dummy variable	-
$\mathcal{L}$	Diffusion coefficient	$N.s/m^2$
η	Efficiency	Dimensionless
ρ	Density	kg/m^3
ν	kinematics viscosity of air	m^2/sec
τ	Kirchhoff temperature	^{o} C
$\mathcal{M}$	Source term	-
α	Thermal diffusivity	m^2/sec
ϕ	Incidence angle	degree
μ	Dynamic viscosity	kg/m.s
λ	Latent heat	kJ/kg
Δt	Time interval	sec
ΔT	Temperature difference	K
Δv	Volume of element	m^3
Δx	x- Direction width of the control volume	m
Δy	y- Direction width of the control volume	m
Δz	z- Direction width of the control volume	m
δx	x-direction distance between two adjacent grid points	m
δy	y-direction distance between two adjacent grid points	m
δz	z-direction distance between two adjacent grid points	m

Abbreviations

Symbol	Description
ETSC	Evacuated tube solar collector
FPSC	Flat plate solar collector
GAHP	Gravity Assistance Heat Pipe
FR	Filling Ratio
HP	Heat pipe
PCM	Phase change material
PDE	Partial Differential Equation
FDM	Finite Difference Method
BC	Boundary Conditions

Subscripts

Symbol	Description
amb	Ambient
air	Air
B	Bottom neighbor of grid P
b	Control-volume face between P and B
c	Copper
E	East neighbor of grid P
e	Control-volume face between P and E
i	Initial
in	Water at inlet
l	Liquid of PCM
m	Mushy zone, Melting
N	North neighbor of grid P
n	Control-volume face between P and N
out	Water at outlet
P	Grid point
S	South neighbor of grid P
s	Control-volume face between P and S, solid of PCM, start (initial)
solar	Solar energy
T	Top neighbor of grid P
t	Control-volume face between P and T

W	West neighbor of grid P
v	Vapor
w	Control-volume face between P and W, water

Chapter One

Introduction

1. Introduction

1.1. Renewable Solar Energy

Recently, Renewable energy spreads and develops so fast around the world. Stable, clean, and sustainable energy are considered the fundamentals of Renewable energy that can be provided by this type. In recent times, the global depends on fossil fuel as the main source to produce energy which represents a big concern and fears of depleting these resources in the future especially with the tremendous need for energy due to the population growth rate around the world [1]. Renewable energy has many different source types such as solar energy, wind power, hydropower, geothermal energy, etc. with very low pollution and emissions rate compared to the fossil fuels energy which is one of the major factors of Global Warming (friendly to the environment) [2].

The solar energy is deemed the main type of renewable energy that is used widely to provide heat energy and produce electrical power. The agency of the international energy (IEA) states that renewable sources especially solar energy in 2050 will produce less than 46% of the global energy demand (generate heat and supply clean electricity power) [1]. Furthermore, Renewable energy power plants contributed to produce 28% (Heat energy and electrical power) of the total power plants around the world, while the remaining energy which is 72% produced by the other power plant stations that depend on the fossil fuels [3].

Solar energy is utilized by photovoltaics (PV system), solar heating and cooling, solar chemical fuel (sunlight artificial photosynthesis), solar thermal energy system, etc. The solar photovoltaic PV system is supply energy to the world by almost around 401,000 MW at the end of 2017 [4]. In other words, this power capacity represented 2.1% of the consumed energy (electrical power consumption) by the worldwide. In 2017, solar energy was raised and developed faster in the continent of Asia especially China where solar energy produced more around 51% of the total world solar energy production [4]. Also, at the end of 2016, in India, the production of solar energy is around 86300 MW [5]. However, the European Union was contributed by 28%, the north and south of America represented 19%, and the Middle East provided 2% of the total worldwide solar

energy production in 2017. In 2018, the continent of Asia produced solar energy which is around 75% of the total worldwide production, and the remaining energy represented by the rest of the world. Solar energy is continued to increase during the time to be approximately 635 GW and 760 GW in 2019 and 2020 respectively as shown in Figure

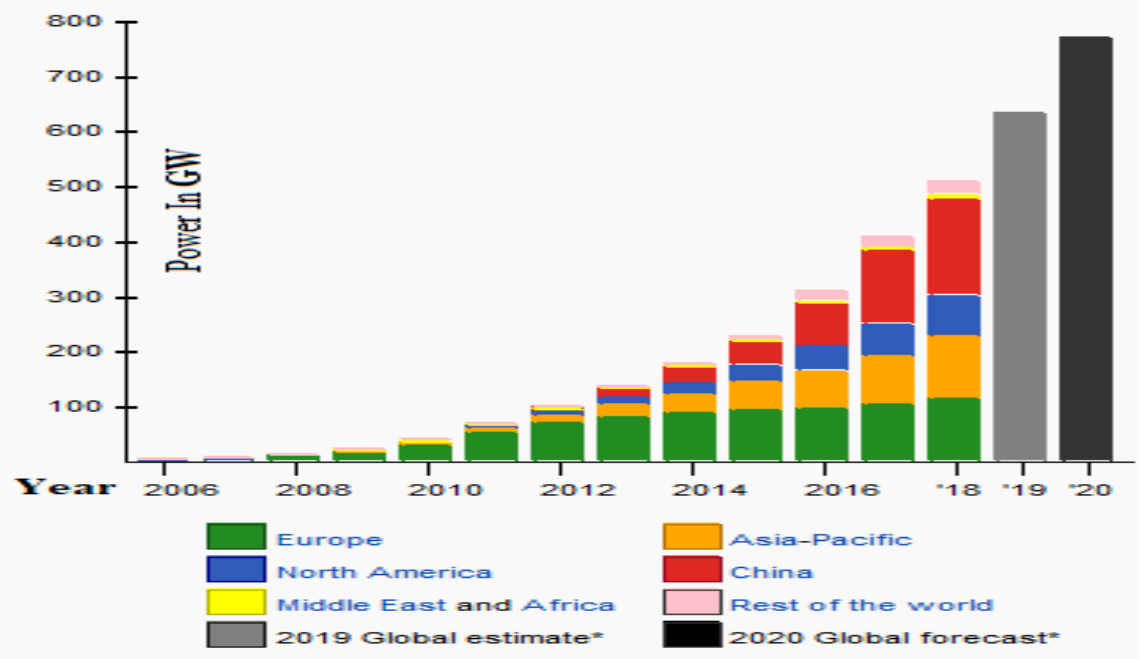

(1-1) [6][7].

Figure (1-1): Global Renewable Solar Energy Growth [7]

1.2. Project Overview and Scope

One of the Renewable solar energy kinds is solar thermal energy (solar thermal energy takes advantage of solar energy) that used to integrate latent heat energy storage. The most common applications of solar thermal energy are thermal energy storage and solar collector. The researchers are working hard to improve the performance of the solar collector to absorbing heat as much as is achievable and to increase the density of the thermal energy storage and the heat transfer rate with less expensive and smaller size components. The researchers have achieved that target by using an evacuated tube and

phase change materials (PCM) which are integrated with the solar collector and thermal storage components depending on the temperature [8].

1.2.1. Evacuated Tube Solar Collector

Solar thermal energy specifically (Domestic Solar Water Heating (DSWH)) is one of the most common techniques of harvesting solar energy [9]. Thermal energy storage and solar collector are the important components of Solar Water Heater. A solar collector can be considered a heat exchanger which is used to convert sun energy (Solar Radiation) into heat energy, and this heat energy stores in the thermal energy storage components. There are two types of solar collectors: the Evacuated Tube Solar Collector (ETSC) and Flat Plate Solar Collector (FPSC). The evacuated tube ETSC is supplying the thermal solar energy tanks fluid with higher temperature and lower heat energy loss compared to the flat plate (FPSC) due to the vacuum insulation between the glass tubes. Also, the ETSC can be used in different weather conditions such as clear, cloudy, windy, hot, and cold weather, it's working in weather with high, medium, and low temperature, so it’s more efficient than the FPSC. In addition, the ETSC's shape helps to be less sensitive to the sun angle and direction compared to FPSC, ETSC doesn’t need to solar radiation tracker. However, ETSC is a little bit expensive, the design is more complex, and the expectation of life cycle is shorter, and it has a normal performance around the year compared to the flat plat (FPSC) [10].

Evacuated Tube Solar Collector (ETSC) has various evacuated tube construction designs, the principal differences are the absorber's shapes and manufacturing materials as shown in Figure (1-2). The two ETSC major types are cylindrical absorber shape and tubes with an all-glass material, and an absorber with a copper material and fin shape, and tubes with glass-metal materials as shown in Figure (1-2) a and b, respectively. Different types of heat exchangers may be used in evacuated tubes. For instance, evacuated tube heat pipes exchanger, evacuated tube double pipes heat exchanger (evacuated tube direct flow heat exchanger), and evacuated tube U-tubes heat exchanger as shown in Figure (1-2)c, d, and e, respectively. In Figure (1-2) a, the cylindrical absorber evacuated tube has a selective coating surface such as (Al-N/Al or AlN/AlN-

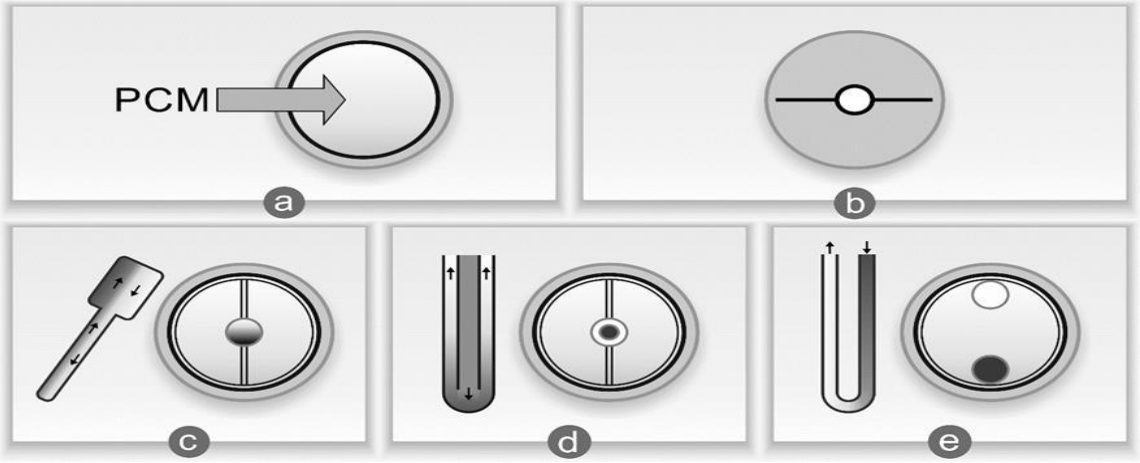

SS/Cu) that is absorbing highly solar radiation over it and less thermal radiation reflection with vacuum insulation space around it [11]. The purpose of fabricating a vacuum area around the absorber to reduce the convection and conduction heat transfer energy losses.

Figure (1-2): Evacuated Tubes Categorization [11]: (a) cylindrical absorber, (b) copper fin absorber, (c) heat pipe exchanger, (d) direct flow heat exchanger, (e) u-tube heat exchanger

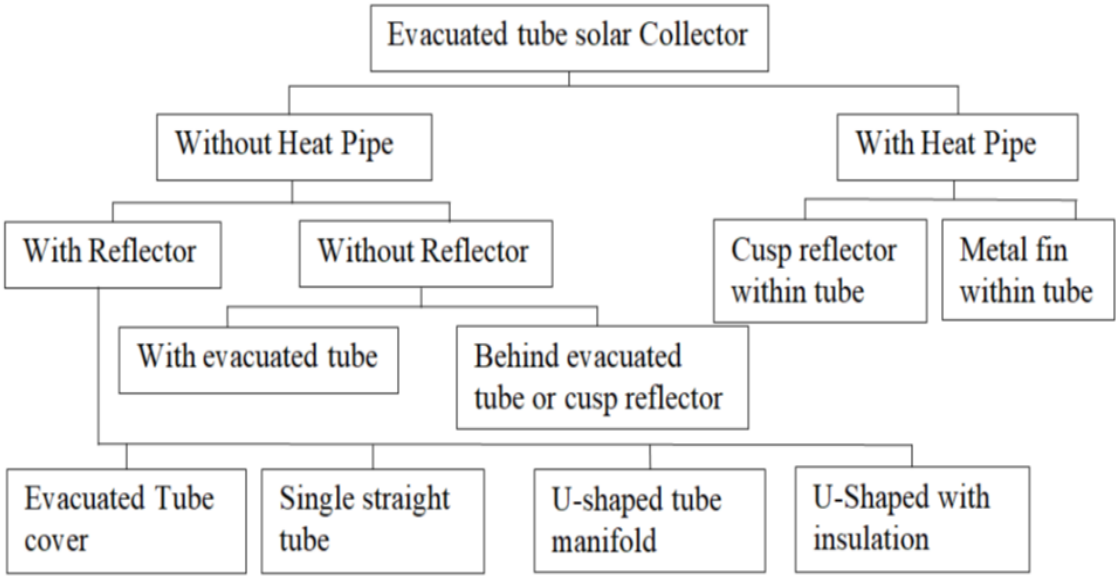

There are many different types of Evacuated Tube solar collectors (ETSC) designs. ETSC can be classified into two main types (Evacuated Tube solar collectors with Heat Pipes and without Heat Pipes). Also, these two main types may further classify into various types as illustrated in Chart (1-1) [11].

Chart (1-1): ETSC Classification [12]

1.2.2. Heat Pipe Evacuated Tube Solar Collector

The Heat pipe evacuated tube solar collector type means there is a hollow heat pipe made from a highly conductive metallic material and at its one end there is a recognizable bulb which is considered the condenser of the heat pipe. This heat pipe located inside the glass or metal-glass tube surrounded by a selective coating surface which absorbs highly solar radiation with less solar radiation reflection; between the selective coating surface and the glass or metal-glass tube, there is a vacuum insulation area which is created to reduce the convection and conduction heat transfer energy losses and helping the evacuated tube to operate at various temperature. Also, the heat pipes condensers are located inside the heat exchanger (Manifold) that contains fluid (water) flow. Moreover, there two types of heat pipe are Evacuated Heat Pipe which is filled with a slight amount of liquid (water) and heated to release all air from it [13]. The second type is Heat Pipe that is filled with phase change materials (PCM) [14]. Heat Pipes are designed to transfer the heat energy from the absorber to the tank (in one direction only). Specifically, it designs to transfer heat energy between the cold liquid in the storage tank (water) and the heat pipe condenser which contains vapor because of the absorbing solar radiation that changes the liquid (phase change material (PCM)) into vapor. Then, the vapor around the heat pipe condenser change back to a warm liquid, and it comes back to the pipe's bottom because the density of the cold liquid (water) is bigger than hot water, and the cycle repeats over and over until dark comes. However, the cold liquid in the storage tank (water) turns into a hot liquid. In some cases, fins and phase change materials (PCM) are adding to the heat pipe evacuated tube to increase efficiency [12].

1.2.2. Thermosyphon Evacuate Tube Solar Collector

Thermosyphon evacuated tube solar collector can be divided into two main types which are with heat pipe (without a wick) and without heat pipe. The wickless heat pipe Thermosyphon (gravity-assisted heat pipe) is utilized in this research. Thermosyphon is consist of two all-glass or glass-metal tubes sealed together at their one of the end side,

between the two glass tubes a vacuum insulation space which is created to reduce the convection and conduction heat transfer energy losses and making the evacuated tube to operate at different weather conditions. The outer surface of the inner glass tube is coated by a high absorbing selective coating material surface which absorbs highly solar radiation with less emissivity. In contrast to the heat pipe type, the sealed end side of the tubes connects directly to a horizontal thermal storage tank [15].

The Thermosyphon mechanism is the thermal energy transfer from the absorber to the cold liquid (water) inside the inner glass tube to be a hot liquid (water). Then, the hot water rises to the storage tank, where there is cold water inside it, and it turns part of the storage cold water into hot water because of the natural convection heat transfer. Then, it displaces the remaining cold water of the storage tank to the bottom of the glass tube because of the gravity force. Thus, the lack of water is substituted by cold water and the cycle repeats over and over as long as solar radiation exists [16]. Figure (1-3) represents the Thermosyphon and heat pipe evacuated tube solar collector.

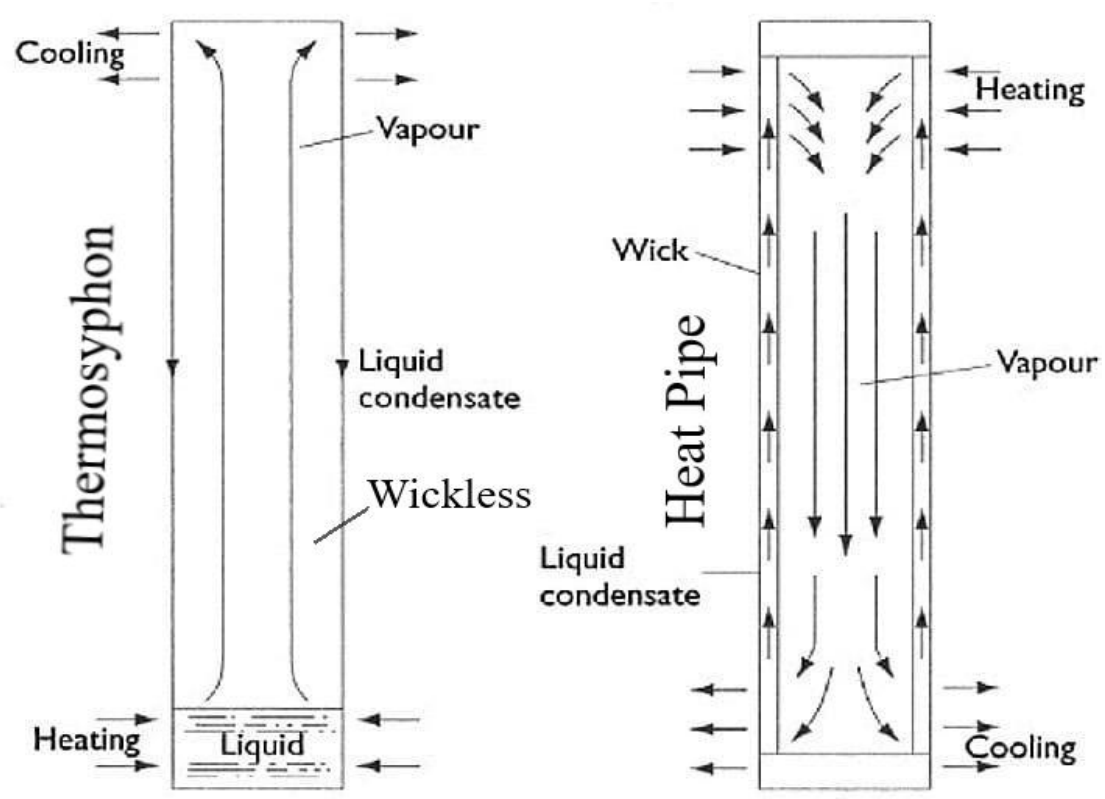

Figure (1-3): (A) Thermosyphon (Wickless Heat Pipe). **(B)** Heat Pipe (Wick) [17]

1.2.4. Phase Change Material (PCM)

A phase change material (PCM) is a substance characterized by having a high melting point temperature (heat of fusion); in contrast to the traditional sensible storage materials, PCM is capable of absorbing and emitting high heat energy at an almost steady temperature. Also, the phase change or state change material phenomenon is considered one of the PCM benefits. In other words, when PCM materials change from one phase to another phase (liquid to solid and vice versa), a transfer of heat energy occurs; for this reason, PCM is also known as latent heat storage. Moreover, PCM has been deemed highly efficient materials since the heat of fusion for various types of phase change materials are available at any temperature range (from -5 to 190 C^{o}). Originally, in solid to liquid phase change when the PCM material absorbs heat, the temperature of (A) increases similar to traditional s ge materials. However, the t y that stores in the PCM mater (B) at storage) is much higher than the traditional (sensible) heat storage material. For instance, latent heat stored in PCM materials around (5-14) times more heat per volume unit than the traditional storage materials [18]. Examples of sensible storage materials are solid and fluid storage materials such as oil and water, metal and rock, respectively. Furthermore, the cost-effectiveness of a PCM, and the availability of a particular PCM (Abundant). These two factors are important, and the selection of phase change materials is depending on these two factors also. The properties that affect the selection of the PCM for the desired heat storage system are thermal, kinetic, physical, and chemical properties factors [19].

1.2.5. Thermosyphon Adiabatic Section

There were many techniques and experiments have been utilized to increase the thermal efficiency of the Thermosyphon solar collector systems. Some of the scientists are manipulating the important parameters and factors that are directly affecting the overall

heat transfer coefficient, thermal efficiency, evaporation, and condensation heat transfer coefficient, and heat flux, etc. Other scientists are working on changing the design and manufacturing of the Thermosyphon solar collector. Recently, some researchers have been working on the principal design of wickless heat pipe Thermosyphon [20]. Where these researchers adding a new section (adiabatic section) to the two conventional sections (evaporator and condenser sections) in some solar cooling and heating applications. Thus, a full real case study experimentally and mathematically analysis for this potential technique (adding an adiabatic section with thermal break for the other two sections) is a significant opportunity to enhance the Thermosyphon solar collector performance.

1.3 Aim of the Study

The primary aim of this research is to increase the daily thermal efficiency of the gravity-assisted heat pipe evacuated tube solar collector system experimentally and numerically by adding an adiabatic section (a specific thermal break part within the GAHP-ETSC system). In other words, create an appropriate solar collector model with a high daily thermal efficiency especially throughout the sunset period.

The tasks of this research are:

1. Develop a methodology to analyze the gravity-assisted heat pipe evacuated tube solar collector (GAHP-ETSC) and studying the challenges that face this tube of the solar collector.

2. Reviewing the significance conditions for the characteristics of the wax (paraffin)

3. Manufacture four gravity-assisted heat pipe evacuated tube solar collector systems at the most favorable tilt angle and filling ratio based on a previous experimental study with similar outdoor weather conditions in order to investigate the influence of using a PCM on the thermal performance of the solar collector system specifically the GAHP-ETSC.

4. Manufacture an appropriate adiabatic section thermal break material within the GAHP-ETSC to enhance the thermal performance of the solar collector system.

5. Build a mathematical model by using MATLAB software to analysis the temperature distribution profiles of the present system.

Chapter Two

Literature Review

2. Literature Review

2.1. Introduction

Newly, the global is in a fierce rivalry to discover and develop renewable energy resources to be an alternative to traditional resources of energy that depend on fossil fuel due to the sustained depletion of the fossil fuel especially the huge growth rate of the population globally. Solar energy is the most promising renewable energy source that can be utilized in numerous various approaches such as electricity, heating, cooling, etc. Also, solar thermal collectors are utilizing solar radiation to provide thermal energy for particular purposes.

This chapter of the research is discussed the researchers attempted to develop the performance and efficiency of the evacuated tube solar collector types especially gravity-assisted heat pipe (GAHP-ETSC) throughout the last years. Also, they explained the effects of adding an adiabatic section with thermal break on the performance of a gravity-assisted heat pipe.

2.2. Gravity-Assisted Heat Pipe (GAHP-ETSC)

The researchers Daghigh and Shafieian [21] analyzed the evacuated tube solar collector heat pipe energy and exergy for water heating applications. They used different types of the working fluid are ethanol, petroleum ether, chloroform, acetone, methanol, and hexane, and three wind velocities start from (2-4) m/s. It showed that the maximum energy and exergy efficiency occurs when the working fluid is chloroform with 4 m/s wind velocity and acetone with 2 and 3 m/s wind velocity. The circumstances that the investigators used to get these results are the number of the collector pipes is 15 (which is considered the perfect number for the collector pipes as they suggest). In the morning, the outlet initial temperature is around 29.5 ^{o}C, and it continues to increase reaching 52 ^{o}C approximately at 1:00 p.m. the maximum temperature reaches 56.3 ^{o}C between 3:00 and 4:00 p.m.

The investigators Behnam and Shafii [22] studied and analyzed experimentally the methods that could help increase the daily efficiency and the freshwater production of a new solar desalination system by adding a heat pipe evacuated tube solar collector and an air bubble humidifier. The researchers did some modifications to the heat pipe ETSC such as filling the evacuated tube with oil (the heat pipe surrounded by oil). The results of this study are the daily efficiency, and freshwater production is dramatically increased to be 65% and 6.275 kg/ day·m2, respectively.

Zhu et al. [23] added micro heat pipe arrays to the evacuated tube and manipulated the kinetic properties of the evacuated tube solar collector's working fluid to develop the performance and efficiency of ETSC. The investigators discovered that the efficiency of the system increased when fluid inlet velocity decreased to a certain limit because of heat energy loss reduction (heat emissivity). The results of this study showed that thermal efficiency increased to (50-70) % daily. Eventually, the ETSC system saves around (0.77 kg of coal) of burning fuel daily, and this saving value reduces the CO_2 emissions by (2.13 Kg daily) to the environment. The researchers suggested that if one-third of the northern cities of China (coldest cities in China) replace their conventional heat systems with evacuated tube solar collector systems. As result, 4.27 million tons of coal equivalent (Burned Fuel) will be saved each year. Then, a large percentage of the emission gases will be reduced.

Essa and Mustafa [24] prophesied the temperature distribution and flow profile of the Thermosyphon evacuated tube solar collector including the boundary conditions of solar radiation by using empirical and theoretical methods. The theoretical results were compatible with the empirical results where the relative percentage error reduced to be (4.2-7.8) % throughout the tube. Also, Sobhansarbandi et al. [25] explained the benefits of adding multi-practical absorber sheets to the evacuated tube solar collector. The researchers noticed that the ETSC absorbed around 98% of the incident solar radiation (spectral absorption) on the evacuated tubes between 600 and 1100 nm. Moreover, the extra amount of solar radiation enhanced the performance of the solar heater. Also, these results prove that a special type of multi-practical absorber sheets (carbon nanotube)

would increase the solar radiation significantly and improve the performance of the system subsequently.

Kong et al. [26] expected and analyzed the thermal effectiveness for one type of the evacuated tube solar collector which is the Thermosyphon Solar Heating Water system. Their mathematical model was based on integrated energy conversation equations of the fluid and solid parts (two-node graph theory). Also, they evaluated a comparison between the thermal storage tanking working fluid temperature (measured) and the theoretical fluid temperature (expected). The results of this study showed that the measured fluid temperature varies from the expected fluid temperature by 1.4 C^o maximum for a one-day test and the energy relative error is within 5%.

Eidan et al. [27] provide a research on the heat pipe evacuated tube solar collector performance by using Aluminum and Copper Oxide nanofluids (Al_2O_3 and CuO) and acetone as the working fluid and getting advantage of the gravity-assisted heat pipe (GAHP). The researchers divided their work into more than two parts. The first task was to design a system with the maximum performance and efficiencies by changing the slope angles of the collector and the filling ratio of the working fluid which is acetone of course without any nanoparticles additive. The slope angles start (30^o-60^o), while the filling ratio starts from (40-80) %. The second task was allocated to enhance the thermal performance of the heat pipe ETSC by adding the Aluminum and Copper Oxide nanoparticles (Al_2O_3 and CuO) to the working fluid (acetone) experimentally. The results showed the optimum performance and efficiencies can be achieved when the slope angle equal to 45 and the filling ratio around 70%. Also, The system efficiency with 0.5% volumetric concentration was higher compared to 0.25% volumetric concentration for both (Al_2O_3 and CuO) nanofluid. Moreover, the enhancement of the evaporation heat transfer coefficient (EHTC) could be reached from (34 -73) % maximum for both nanofluids volumetric concentration values 0.025 % and 0.05%.

2.3. PCM Embed Within Gravity-Assisted Heat Pipe (GAP-ETSC)

Chopra et al. [8] investigated experimentally two water heater models examined at the same weather conditions. The first model is a heat pipe evacuated tube solar collector

with SA-67 phase change material PCM. The second model is a heat pipe evacuated tube solar collector without PCM. The experimental results showed that the first system throughout 1500 thermal cycle treatment has a better thermal and chemical stability at each cycle than the second system. Also, the researchers used 5 various water flow rates (8-24) liter/hour to predict the thermal performance of the two systems. The experiment results showed that the daily thermal efficiency range in between (79–87) % for the first model, while (42–55) % for the second model. Additionally, the daily energy efficiency of the first system is higher than the second system.

AL-HARIS [17] investigated numerically and experimentally adding a paraffin wax (PCM) to improve the performance of a thermosyphon evacuated tube solar collector by storing the latent heat temperature to raise the water temperature of the ETSC storage tank, specifically when the solar radiation intensity is insufficient (during the cloudy weather and night). The experiment has been analyzed with and without PCM and load, and the water flow rate (load) ranging from (0.15-0.866) liter/hour. The properties of the paraffin wax that are used in his work are the melting temperature is 38-43 °C, the charge period is 9 hours, the mass is 3.6 kg, and the filling ratio of the working fluid is 50%. The numerical and experimental results presented that the heat flux increased by 33.3%, the storage tank water average temperature raised by 23.37%, and the PCM melting temperature-time speed decreased by 25%. Also, the maximum performance of the system is achieved at 0.36 L/h with 750 W/m^2 heat flux with load and PCM.

Ali [28] investigated experimentally the effect of PCM on the (GAHP-ETSC) also, but the researcher had integrated a vibration motor into the (GAHP-ETSC) model. Where this idea is considered a new technique to improve the thermal performance and the efficiency of the gravity-assisted heat pipe evacuated tube solar collector. The researcher has been utilized four identical apparatus with and without vibration and PCM. The properties of the paraffin wax that are used in his work are the melting temperature is 38-43 °C, the charge period is 9 hours, the mass is 7.2 kg, and the filling ratio is 70% of the working fluid which is acetone. Also, five different vibration frequencies (21.1-50) Hz have been applied. As result, the efficiency of the system is increased by 78% when vibration and PCM are involved within the system.

Feliński and Sekret [11] analyzed practically the effect of using paraffin wax as a PCM on a domestic hot water heater system performance (heat pipe evacuated tube solar collector). The paraffin wax stores the extra-solar thermal energy during the sunshine to increase the temperature of the hot water in the storage tank, especially throughout the sunset period. The results showed that the evacuated tube solar collector charging efficiency is increased from 33% to 66% based on the intensity of solar radiation. Also, the solar fraction of the domestic water heater system is raised by 20.5% annually [29].

2.4. Heat Pipe Adiabatic Section with Thermal Break

Guo and Nutter [30] analyzed practically the axial conduction influence through the pipe wall on the thermosyphon performance. The researchers used two identical thermosyphons (both of them have the same design, structure, and both filled by R134a partly) except one of them has a polycarbonate thermal break (insulation) within the adiabatic section located between the evaporator and condenser sections in order to prevent the axial conduction heat transfer. The investigators have utilized a constant hot water temperature as a heat energy source, and cooled water by using a heat exchanger. The results of the experiment showed that the overall, evaporation, and condensation heat transfer coefficients increased because of the effect of axial conduction heat transfer in the thermosyphon without thermal break. While, when the heat flux decreased, the fraction of heat transfer increased. For instance, when the temperature is high (60 C) the evaporation and condensation heat transfer coefficients are negligible. Whilst, when the heat flux is low (30 C) the condensation and evaporation heat transfer coefficients are 25% and 100%, respectively. The authors have recommended this research to apply in the cooling of turbine blades, deicing of roads, and other heat exchangers applications.

2.5. Summary

According to the described researches, the researchers have two essential approaches (principles) to enhance the performance of the evacuated tube solar collector system. In the first approach, the investigators try to manipulate the design of the apparatus (such as material, dimensions, incidence angle, and reflector.... etc.) and the working fluid type and filling ratio. In the second approach, the researchers try to add new techniques to the traditional ETSC system such as adding phase change materials, working fluid additive (nanoparticles and nanofluids) [31], and vibration.

In this experimental research, four apparatus of gravity-assisted heat pipe evacuated tube solar collectors (GAHP-ETSC) have been utilized, the design of these apparatus, selecting the working fluid type and filling ratio, and choosing the phase change material (PCM) based on a previous experimental study that belongs to (Eidan et al. [27] 2018 which is described in the background). The new technique involves a thermal break (insulation) within the adiabatic section located between the evaporator and condenser sections of the GAHP, and this is considered a promising technique in the ETSC system.

Chapter Three

Data Reduction

3. Data Reduction

This chapter represents the mathematical analysis for the whole system of the Gravity Assistance Heat Pipe evacuated tube solar collector (GAHP-ETSC). This mathematical model is used to solving partial differential equations to obtain the temperature distribution profiles of the present system by utilizing a numerical analysis (MATLAB Software) for recommended future work.

3.1. Gravity Assistance Heat Pipe (GAHP)

The heat pipe is a hollow pipe made from a copper material mostly sealed from one end, and there is a bulb (or valve) at the other end to charge and vacuum the liquid inside the tube (working fluid such as an acetone). The pipe is splitting into three sections which are the evaporator, adiabatic, and condenser section. The heat pipe is designed to transfer the thermal energy between the cold liquid section (evaporator) and the condenser section. Normally, the solar radiation (external source) provides the thermal energy to the evaporator part throughout the wall of the heat pipe then to the working fluid inside the GAHP [32]. Later, the working fluid (acetone) starts to obtain the heat energy, then the liquid phase status of the acetone begins to convert into a vapor phase gradually. Thus, the acetone's vapor phase transfers to the condenser section where the condensation process in the condenser section (transferring the thermal energy to the cold water of the storage tank) begins especially when the low-temperature water of the storage tank wraps around the condenser part. Thereafter, the GAHP working fluid (acetone) move down to the evaporator section because of the density and gravity.

The governing equations that were used to analysis the GAHP were performed for a cylindrical shape, transient state, and three-dimension cylindrical coordinates (r, ∅, z) of a selected small element with six faces [33].

3.1.1. Thermal Equilibrium

Energy balance or equilibrium is an important equation to analyze the heat energy in the GAHP. Equilibrium of heat energy means the sum of all the heat energy input and

output must equal zero. The heat equilibrium equation applies for the six faces of the small element. The energy balance governing equations are shown [17, 34, 35]:

$$\sum q_{in\ all\ faces} - q_{storage} = 0 \qquad \text{.... (3.1)}$$

OR

$$[KA\frac{dT}{dX}]_{in\ all\ face} - \left[\rho V C_p \frac{dT}{dt}\right]_{storge} = 0 \qquad \text{.... (3.2)}$$

$$q_{in\ all\ face} = q_r + q_\emptyset + q_z + q_{solar} \quad \text{.... (3.3)}$$

$$q_r = q_{n-r} + q_{s-r} \qquad \text{.... (3.4)}$$

$$q_r = KA_n\frac{dT}{\Delta r} + KA_s\frac{dT}{\Delta r} \qquad \text{.... (3.5)}$$

$$q_r = \frac{K}{\Delta r}\left[A_n\left({T_{i,j,k}}^n - {T_{i+1,j,k}}^n\right) + A_s\left({T_{i,j,k}}^n - {T_{i-1,j,k}}^n\right)\right] \quad \text{...(3.6)}$$

$$q_r = -\frac{K}{\Delta r}\left[A_n{T_{i+1,j,k}}^n - (A_n + A_s)\,{T_{i,j,k}}^n + A_s\,{T_{i-1,j,k}}^n\right] \text{.... (3.7)}$$

$$q_\emptyset = q_{e-\emptyset} + q_{w-\emptyset} \quad \text{.... (3.8)}$$

$$q_\emptyset = \frac{K}{r_i\Delta\emptyset}\left[A_e\left({T_{i,j,k}}^n - {T_{i,j+1,k}}^n\right) + A_w\left({T_{i,j,k}}^n - {T_{i,j-1,k}}^n\right)\right] \text{.... (3.9)}$$

$$A_e = A_w = A_\emptyset \quad \text{.... (3.10)}$$

$$q_\emptyset = -\frac{KA_\emptyset}{r_i\Delta\emptyset}\left[{T_{i,j+1,k}}^n - 2{T_{i,j,k}}^n + {T_{i,j-1,k}}^n\right] \text{.... (3.11)}$$

$$q_z = q_{t-z} + q_{b-z} \quad \text{... (3.12)}$$

$$q_z = \frac{K}{\Delta z}\left[A_t\left({T_{i,j,k}}^n - {T_{i,j,k+1}}^n\right) + A_b\left({T_{i,j,k}}^n - {T_{i,j,k-1}}^n\right)\right] \text{.... (3.13)}$$

$$A_t = A_b = A_z \text{ .... (3.14)}$$

$$q_z = -\frac{KA_z}{\Delta z}\left[{T_{i,j,k+1}}^n - 2{T_{i,j,k}}^n + {T_{i,j,k-1}}^n\right] \text{.... (3.15)}$$

$$q_{storge} = \rho\, C_p V\left[\frac{{T_{i,j,k}}^{n+1} - {T_{i,j,k}}^n}{\Delta t}\right] \text{.... (3.16)}$$

Where: the sub letters s, n, e, w, t, and b represent south, north, east, west, top, and bottom, respectively [36].

Now, substituting Eq. (3.7,11,15,16) in Eq. (3.1) yield to be:

$$\rho\, C_p V \left[\frac{{T_{i,j,k}}^{n+1} - {T_{i,j,k}}^{n}}{\Delta t} \right] = -\frac{K}{\Delta r}\left[A_n {T_{i+1,j,k}}^{n} - (A_n + A_s)\, {T_{i,j,k}}^{n} + A_s\, {T_{i-1,j,k}}^{n} \right]$$
$$-\frac{KA_\emptyset}{r_i \Delta \emptyset}\left[{T_{i,j+1,k}}^{n} - 2{T_{i,j,k}}^{n} + {T_{i,j-1,k}}^{n} \right] - \frac{KA_z}{\Delta z}\left[{T_{i,j,k+1}}^{n} - 2{T_{i,j,k}}^{n} + {T_{i,j,k-1}}^{n} \right] + q_{solar}$$
$$\ldots. \textit{(3.17)}$$

Now, equation (3.17) is multiplying by ($\Delta t / \boldsymbol{\rho\, C_p V}$) and simplified to obtained:

$${T_{i,j,k}}^{n+1} = {T_{i,j,k}}^{n} - \frac{\alpha \Delta t}{V \Delta r}\left[A_n {T_{i+1,j,k}}^{n} - (A_n + A_s)\, {T_{i,j,k}}^{n} + A_s\, {T_{i-1,j,k}}^{n} \right] -$$
$$\frac{\alpha \Delta t A_\emptyset}{V r_i \Delta \emptyset}\left[{T_{i,j+1,k}}^{n} - 2{T_{i,j,k}}^{n} + {T_{i,j-1,k}}^{n} \right] - \frac{\alpha \Delta t A_z}{V \Delta z}\left[{T_{i,j,k+1}}^{n} - 2{T_{i,j,k}}^{n} + {T_{i,j,k-1}}^{n} \right] +$$
$$\frac{\Delta t}{V \rho \boldsymbol{C_p}}\, q_{solar} \quad \ldots. \textit{(3.18)}$$

Where: ($\alpha = \frac{K}{\rho \boldsymbol{C_p}}$)

3.1.2. Evaporator Section

The Evaporator of the GAHP that is containing the working fluid is divided into two regions liquid and vapor [37].

The evaporator liquid section of GAHP can be analyzed by divided the pipe into various nodes in three-dimension cylindrical coordinates (r, ∅, z) as shown in Figure (3-1). Where 9 nodes in ∅ direction, 7 nodes in r direction, and 49 nodes in the z direction.

The nodes in the r direction will be analyzed as follow:

- Node number 1 in the center of GAHP are [38]:

$$V = \frac{\pi}{4}(\frac{\Delta r}{2})^2 \Delta z \ldots. (3.19)$$

$$A_s = 0$$
$$A_n = \frac{\Delta r}{2}\Delta\emptyset\Delta z \ldots. (3.20)$$

$$A_e = A_w = \frac{\Delta r}{2}\Delta r\Delta z = A_\emptyset \ldots. (3.21)$$

$$A_t = A_b = \frac{\Delta r}{2}\Delta r\Delta\emptyset = A_z \ldots. (3.22)$$

$$K = K_L$$

[$a = \frac{\alpha\Delta t\, A_n}{V\Delta r}$, $b = \frac{\alpha\Delta t}{V\Delta r}(A_n + A_s)$, $c = \frac{\alpha\Delta t\, A_s}{V\Delta r}$, $d = \frac{\alpha\Delta t A_\emptyset}{V r_i \Delta\emptyset}$, $e = \frac{\alpha\Delta t A_z}{V\Delta z}$, $f = \frac{\Delta t}{V\rho \boldsymbol{C_p}}$] *sub in eq (3.18) become*

$$T_{i,j,k}{}^{n+1} = T_{i,j,k}{}^{n} - \left[aT_{i+1,j,k}{}^{n} - b\,T_{i,j,k}{}^{n} + cT_{i-1,j,k}{}^{n}\right] - d\left[T_{i,j+1,k}{}^{n} - 2T_{i,j,k}{}^{n} + T_{i,j-1,k}{}^{n}\right] - e\left[T_{i,j,k+1}{}^{n} - 2T_{i,j,k}{}^{n} + T_{i,j,k-1}{}^{n}\right] + f\, q_{solar} \ldots. (3.23)$$

- It may be obtained the temperature distribution by deriving nodes number 2&3 as node number 1 above for the working fluid portion (Acetone), as shown in Figure (3-2) below:

$$V = r_i\Delta r\, \Delta\emptyset\, \Delta z \ldots. (3.24)$$

$$A_n = (r_i + \frac{\Delta r}{2})\Delta\emptyset\Delta z \ldots. (3.25)$$

$$A_s = (r_i - \frac{\Delta r}{2})\Delta\emptyset\Delta z \ldots. (3.26)$$

$$A_e = A_w = \Delta r\Delta z = A_\emptyset \ldots. (3.27)$$

$$A_t = A_b = r_i\Delta\emptyset\Delta r = A_z \ldots. (3.28)$$

$$K = K_L$$

$$T_{i,j,k}{}^{n+1} = T_{i,j,k}{}^{n} - \left[aT_{i+1,j,k}{}^{n} - b\,T_{i,j,k}{}^{n} + cT_{i-1,j,k}{}^{n}\right] - d\left[T_{i,j+1,k}{}^{n} - 2T_{i,j,k}{}^{n} + T_{i,j-1,k}{}^{n}\right] - e\left[T_{i,j,k+1}{}^{n} - 2T_{i,j,k}{}^{n} + T_{i,j,k-1}{}^{n}\right] + f\, q_{solar} \ldots. (3.29)$$

$$where:\ [\ a=\frac{\alpha\Delta t\ A_n}{V\Delta r}\ ,\ b=\frac{\alpha\Delta t}{V\Delta r}(A_n+A_s)\ ,\ c=\frac{\alpha\Delta t\ A_s}{V\Delta r}\ ,\ d=\frac{\alpha\Delta tA_{\emptyset}}{Vr_i\Delta\emptyset}\ ,\ e=\frac{\alpha\Delta tA_z}{V\Delta z}\ ,\ f=\frac{\Delta t}{V\rho\boldsymbol{C_p}}\ ]$$

- The interface nodes which are 4 for the acetone and 5 for the GAHP solid pipe part are estimated by:

$$V=r_i\frac{\Delta r}{2}\ \Delta\emptyset\ \Delta z\ \ldots.\ (3.30)$$

$$A_n=(r_i+\frac{\Delta r}{2})\Delta\emptyset\Delta\ \ldots.\ (3.31)$$

$$A_s=r_i\Delta\emptyset\Delta z\ \ldots.\ (3.32)$$

$$A_e=A_w=\Delta r\Delta z=A_{\emptyset}\ \ldots.\ (3.33)$$

$$A_t=A_b=r_i\Delta\emptyset\Delta r=A_z\ \ldots.\ (3.34)$$

$$K=K_C$$

$$q_r=\ K_cA_n\frac{dT}{\Delta r}+h_{\text{acetone}}A_s\Delta T\ \ldots.\ (3.35)$$

$$q_r=\frac{K_cA_n}{\Delta r}\left[\ \left({T_{i,j,k}}^n-{T_{i+1,j,k}}^n\right)\ \right]+\left[\ h_{\text{acetone}}A_s\left({T_{i,j,k}}^n-{T_{i-1,j,k}}^n\right)\ \right]\ \ldots.\ (3.36)$$

$$q_r=-\left[\frac{K_cA_n}{\Delta r}{T_{i+1,j,k}}^n-\left(\frac{K_cA_n}{\Delta r}+h_{\text{acetone}}A_s\right){T_{i,j,k}}^n+h_{\text{acetone}}A_s{T_{i-1,j,k}}^n\right]\ldots.\ (3.37)$$

Sub eq (3.37) in eq (3.3) yield

$${T_{i,j,k}}^{n+1}={T_{i,j,k}}^n-\left[a{T_{i+1,j,k}}^n-b\ {T_{i,j,k}}^n+c{T_{i-1,j,k}}^n\right]-d\left[\ {T_{i,j+1,k}}^n-2{T_{i,j,k}}^n+{T_{i,j-1,k}}^n\right]-e\left[\ {T_{i,j,k+1}}^n-2{T_{i,j,k}}^n+{T_{i,j,k-1}}^n\right]+f\ q_{solar}\ \ldots.\ (3.38)$$

$$where:\ [\ a=\frac{\alpha\Delta t\ A_n}{V\Delta r}\ ,\ b=\frac{\alpha\Delta t}{V}\left(\frac{A_n}{\Delta r}+\frac{h_{\text{acetone}}}{K_c}A_s\right)\ ,\ c=\frac{\alpha\Delta th_{\text{acetone}}\ A_s}{K_c}\ ,\ d=\frac{\alpha\Delta tA_{\emptyset}}{Vr_i\Delta\emptyset}\ ,\ e=\frac{\alpha\Delta tA_z}{V\Delta z}\ ,\ f=\frac{\Delta t}{V\rho\boldsymbol{C_p}}\ ]$$

- the temperature distribution of node number 6 can derive like nodes number 2&3 which is considered a pure conduction. Also, the GAHP material (copper) properties are considered too as shown:

$$V = r_i \Delta r \, \Delta \emptyset \, \Delta z \; \ldots. \; (3.39)$$

$$A_n = (r_i + \frac{\Delta r}{2}) \Delta \emptyset \Delta z \; \ldots. \; (3.40)$$

$$A_s = (r_i - \frac{\Delta r}{2}) \Delta \emptyset \Delta z \; \ldots. \; (3.41)$$

$$A_e = A_w = \Delta r \Delta z = A_\emptyset \; \ldots. \; (3.42)$$

$$A_t = A_b = r_i \Delta \emptyset \Delta r = A_z \; \ldots. \; (3.43)$$

$$K = K_c$$

$$T_{i,j,k}{}^{n+1} = T_{i,j,k}{}^{n} - \left[a T_{i+1,j,k}{}^{n} - b\, T_{i,j,k}{}^{n} + c T_{i-1,j,k}{}^{n} \right] - d\left[T_{i,j+1,k}{}^{n} - 2T_{i,j,k}{}^{n} + T_{i,j-1,k}{}^{n} \right] - e\left[T_{i,j,k+1}{}^{n} - 2T_{i,j,k}{}^{n} + T_{i,j,k-1}{}^{n} \right] + f\, q_{solar} \; \ldots. \; (3.44)$$

$$where: \; [\, a = \frac{\alpha \Delta t \, A_n}{V \Delta r} \;, b = \frac{\alpha \Delta t}{V \Delta r}(A_n + A_s) \;, c = \frac{\alpha \Delta t \, A_s}{V \Delta r} \;, d = \frac{\alpha \Delta t A_\emptyset}{V r_i \Delta \emptyset} \;, e = \frac{\alpha \Delta t A_z}{V \Delta z} \;,$$

$$f = \frac{\Delta t}{V \rho \boldsymbol{C_p}} \,]$$

- The convection temperature distribution of node 7 which represents copper metal is calculated by using the equations:

$$q_r = h_{air} A_n \Delta T + K_c A_s \frac{dT}{\Delta r} \; \ldots. \; (3.45)$$

$$V = r_i \frac{\Delta r}{2} \, \Delta \emptyset \, \Delta z \; \ldots. \; (3.46)$$

$$A_n = r_i \Delta \emptyset \Delta z \; \ldots. \; (3.47)$$

$$A_s = (r_i - \frac{\Delta r}{2}) \Delta \emptyset \Delta z \; \ldots. \; (3.48)$$

$$A_e = A_w = \Delta r \Delta z = A_\emptyset \; \ldots. \; (3.49)$$

$$A_t = A_b = r_i \Delta \emptyset \Delta r = A_z \; \ldots. \; (3.50)$$

$$K = K_c$$

Sub eq (3.45) in eq (3.3) yield

$$T_{i,j,k}{}^{n+1} = T_{i,j,k}{}^{n} - \left[aT_{i+1,j,k}{}^{n} - b\,T_{i,j,k}{}^{n} + cT_{i-1,j,k}{}^{n}\right] - d\left[T_{i,j+1,k}{}^{n} - 2T_{i,j,k}{}^{n} + T_{i,j-1,k}{}^{n}\right] - e\left[T_{i,j,k+1}{}^{n} - 2T_{i,j,k}{}^{n} + T_{i,j,k-1}{}^{n}\right] + f\,q_{solar} \quad \text{.... (3.51)}$$

$$where: \left[a = \frac{\alpha\Delta t\, h_{air}}{VK_c}\ , b = \frac{\alpha\Delta t}{V}\left(\frac{A_n h_{air}}{K_c} + \frac{A_s}{\Delta r}\right),\ c = \frac{\alpha\Delta t\, A_s}{V\Delta r}\ ,\ d = \frac{\alpha\Delta t A_\emptyset}{Vr_i\Delta\emptyset}\ ,\ e = \frac{\alpha\Delta t A_z}{V\Delta z},\ f = \frac{\Delta t}{V\rho \boldsymbol{C_p}}\right]$$

- The evaporator vapor section of GAHP can be analyzed similar to the liquid section by using vapor properties only.

3.1.3. Condenser Section

The condenser section has the same procedure as the evaporator section except for node number 7 a convection heat transfer that happens between the water of the storage tank and the pipe walls in the condenser. As results, the temperature distribution is estimated as below:

$$q_r = h_w A_n \Delta T + K_c A_s \frac{dT}{\Delta r} \quad \text{.... (3.52)}$$

$$V = r_i \frac{\Delta r}{2}\ \Delta\emptyset\ \Delta z \quad \text{.... (3.53)}$$

$$A_n = r_i \Delta\emptyset\Delta z \quad \text{.... (3.54)}$$

$$A_s = (r_i - \frac{\Delta r}{2})\Delta\emptyset\Delta z \quad \text{.... (3.55)}$$

$$A_e = A_w = \Delta r\Delta z = A_\emptyset \quad \text{.... (3.56)}$$

$$A_t = A_b = r_i\Delta\emptyset\Delta r = A_z \quad \text{.... (3.57)}$$

$$K = K_c$$

Sub eq (3.52) in eq (3.3) yield

$$T_{i,j,k}{}^{n+1} = T_{i,j,k}{}^{n} - \left[aT_{i+1,j,k}{}^{n} - b\,T_{i,j,k}{}^{n} + cT_{i-1,j,k}{}^{n}\right] - d\left[T_{i,j+1,k}{}^{n} - 2T_{i,j,k}{}^{n} + T_{i,j-1,k}{}^{n}\right] - e\left[T_{i,j,k+1}{}^{n} - 2T_{i,j,k}{}^{n} + T_{i,j,k-1}{}^{n}\right] + f\,q_{solar} \quad \text{.... (3.58)}$$

$$where: \left[a = \frac{\alpha\Delta t\, h_w}{VK_c},\ b = \frac{\alpha\Delta t}{V}\left(\frac{A_n h_w}{K_c} + \frac{A_s}{\Delta r}\right),\ c = \frac{\alpha\Delta t\, A_s}{V\Delta r},\ d = \frac{\alpha\Delta t A_\emptyset}{Vr_i\Delta\emptyset},\ e = \frac{\alpha\Delta t A_z}{V\Delta z},\ f = \frac{\Delta t}{V\rho \boldsymbol{C_p}}\right]$$

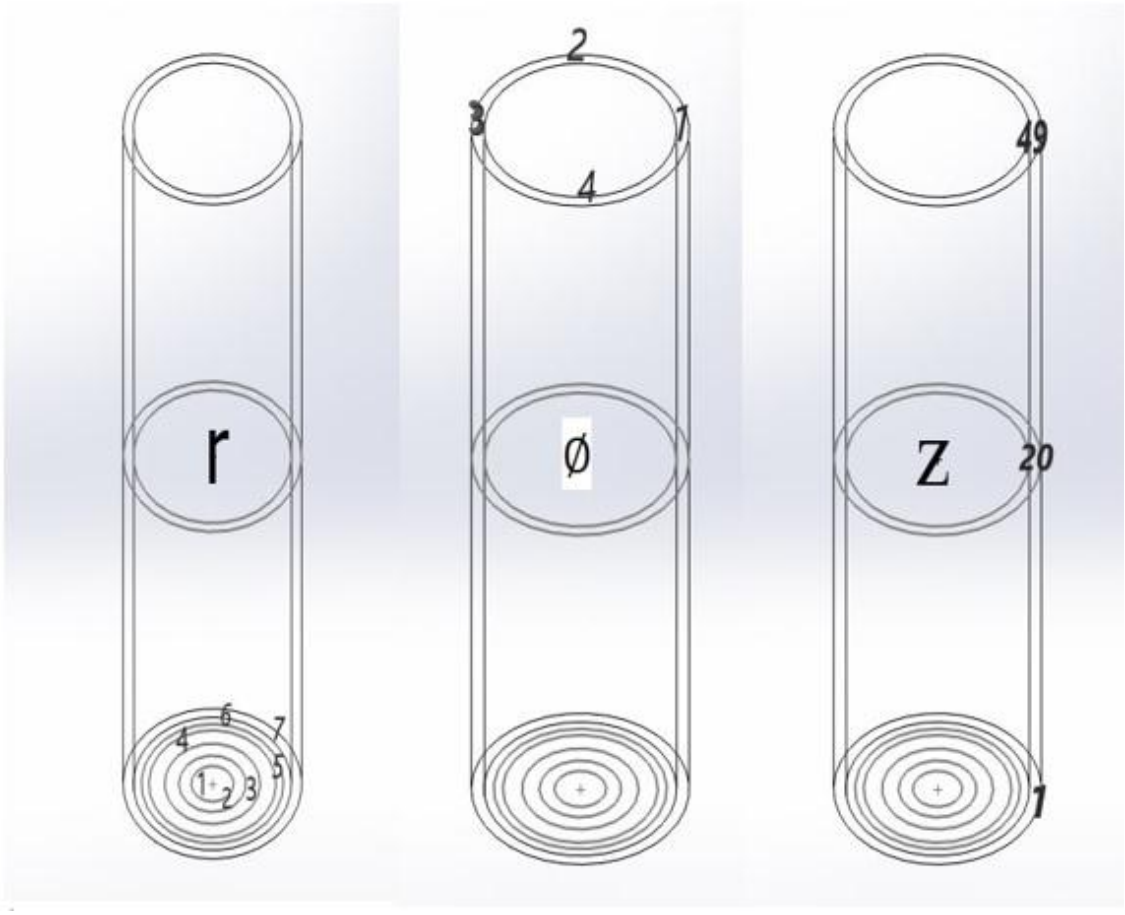

Figure (3-1): Distribution of Nodes in Gravity Assistance Heat Pipe (GAHP)

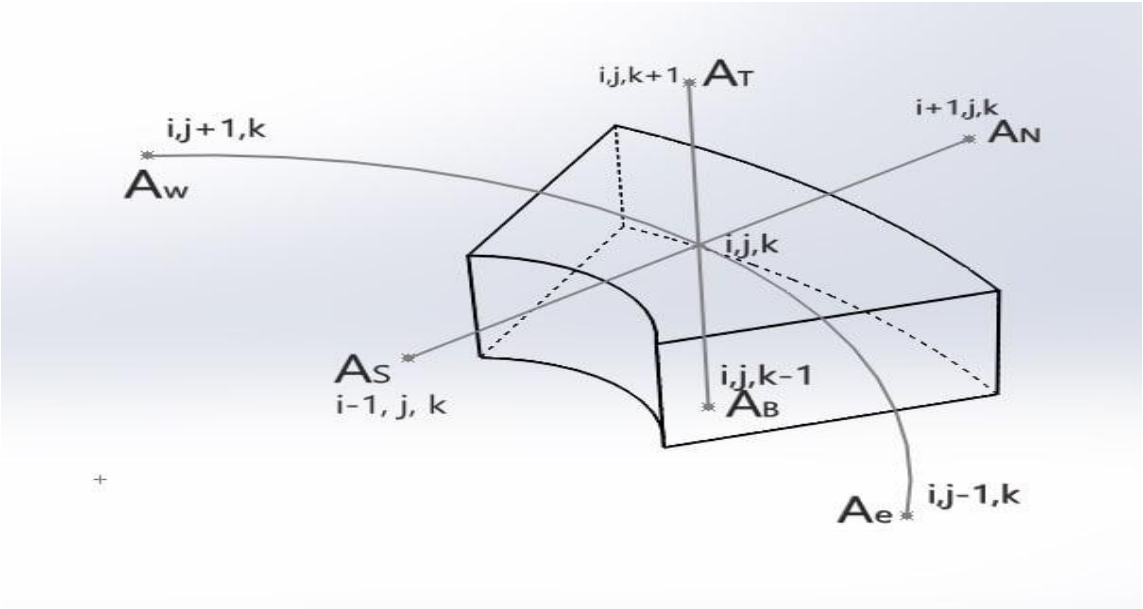

Figure (3-2): General Node for Finite Difference Node

Chapter Four

Experimental Work

4. Experimental Work

4.1. Introduction

The experimental study was utilized to determine the thermal parameter values that influence the solar collector performance in equilibrium state conditions. In addition, making a comparison between the experimental results of different cases and parameters that have been tested. These criteria are solar radiation flux, GAHP thermal energy performance with phase change materials (PCM), and without as well, all the tested cases with the load. The empirical study was completed in Al-Najaf city of Iraq for the period from September 2020 to April 2021. During that time, the experimental devices (rig) are remanufactured, manufacturing the adiabatic section thermal break of the GAHP, and the empirical measurements for the different cases.

4.2. Experimental Rigs

Four identical rigs that are utilized in this empirical study showing in Figure (4-1A&B). This part of the research study illustrates the experimental procedure and verifies the formerly described work of each part experimentally by investigating various factors that affect the thermal performance of the experimental devices such as the adiabatic section and solar intensity. The four-system apparatus are composed of a water storage tank, phase change material (PCM) container, gravity-assisted heat pipe evacuated tube solar collector (GAHP-ETSC), curved (part of an ellipse) reflector, working fluid (Acetone) inside the (GAHP), iron stand structure, and other equipment. However, the only difference between the four devices is: the first apparatus has both an adiabatic section with a thermal breaker within the GAHP and a PCM together. The second one has an adiabatic section with a thermal breaker within the GAHP and hasn't had a PCM. The third rig without a thermal breaker and with a PCM. The last rig hasn’t had both an adiabatic section with a thermal breaker within the GAHP and PCM. Also, the utilizing assistance tools, such as the pressure gage (that is used to measure the charging and vacuuming pressure of heat pipe), thermocouples which is utilized to measure the

temperature in multi-different places of the apparatus, data acquisition apparatus, and others are illustrated in Figure (4-2).

Figure (4-1A): The Four Experimental Apparatus of the GAHP-ETSC

Figure (4-1B): The Four Experimental Apparatus of the GAHP-ETSC (Back View)

Figure (4-2): Schematic of the GAHP-ETSC with Equipment

4.2.1. Evacuated Tube Solar Collector

The ETSC is providing the water storge tank and the PCM container thermal energy with high temperature and low heat energy loss by comparing to FPSC [45]. Also, ETSC is the suitable type for AL-Najaf city and Iraq because it can be used in different weather circumstances especially in weather with high and low temperature. The cylindrical shape of the ETSC helps to be less sensitive to the sun angle and direction. The cylindrical absorber evacuated tube has a selective coating surface such as (Al-N/Al or AlN/AlN-SS/Cu) that is absorbing highly solar radiation over it and less thermal radiation reflection with vacuum insulation space around it [11]. The purpose of fabricating a vacuum space around the absorber to reduce the convection and conduction heat transfer energy losses and enhance the evacuated tube to operate at various temperature.

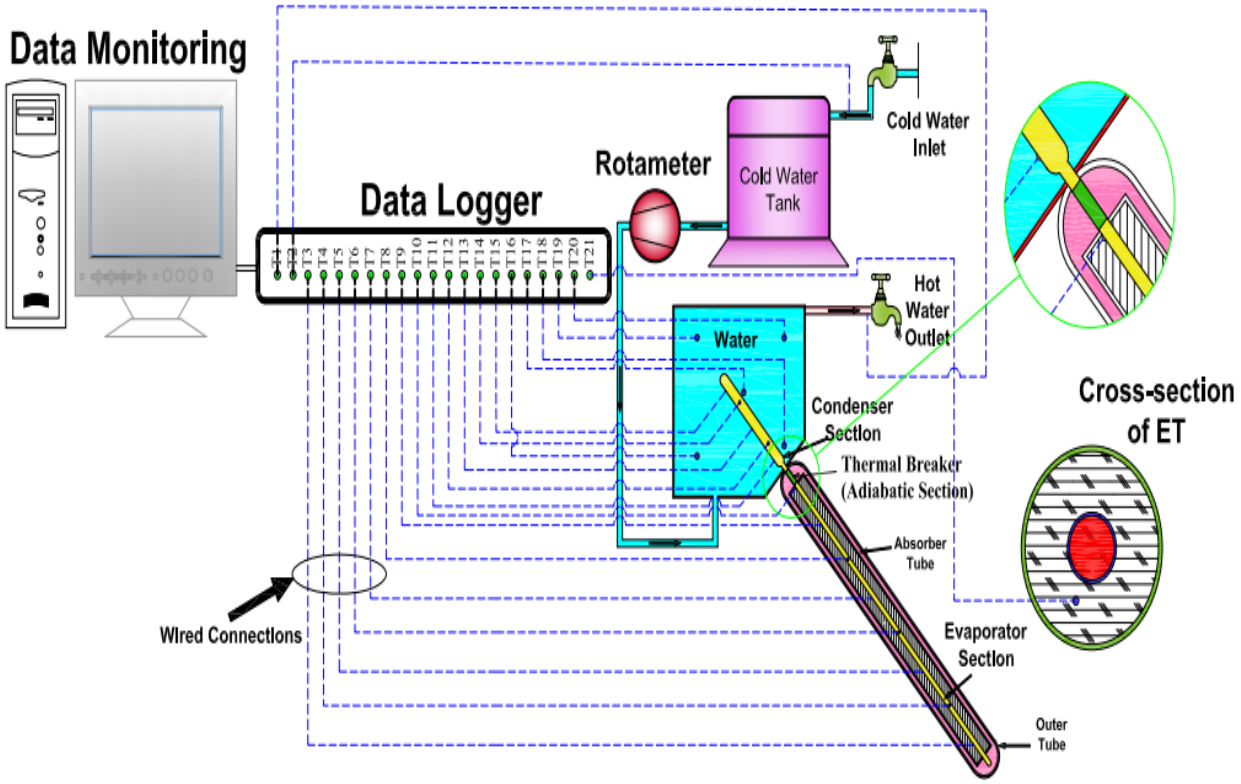

The evacuated glass tube of the ETSC which is used in this experimental work is Owens- Illinois type model 34-46-1350 -YCF supplied by ORIENTAL TRADING INC, China. The absorption coating layer contains special stainless steel and aluminum nitride (SS-ALN) that makes it possible for the ETSC to operate at very low and high temperature (water heating at a particular temperature based on various weather conditions). The specifications of the glass tube are the material of the glass is Borosilicate Glass 3.3, length of glass tube is 1.2 m, thick top notch 2.5 mm with internal and external diameter are 45 mm and 50 mm, respectively, thermal expansion coefficient is 3.3*10^-6 K^{-1}, absorptance rate $\geq$ 94 %, solar transmission rate $\geq$ 92 %, and emission ratio $\leq$ 0.06 . The internal layer contains aluminum in order to reduce the heat energy losses from the cleared glass tube area (internal space) [46].

A barium getter is a small part located at the bottom of the evacuated tube which is utilized to keep up the vacuum between the layers of the glass tube. This part is exposed

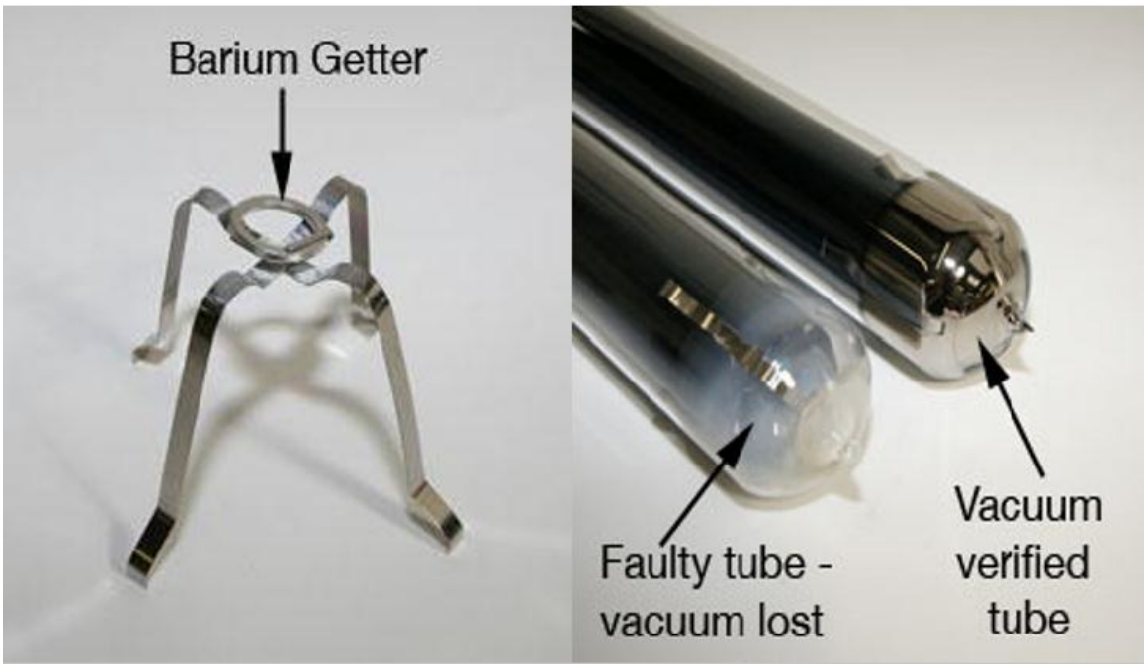

to high temperature through the production of the evacuated tube in order to coat the bottom of the tube with a barium layer. This pure layer keeps up the vacuum by absorbing some gasses such as CO2, CO, O2, N2, H2, and H2O outgassed from the glass tube throughout the operation and storage. The second benefit that this layer provides is working as an optic indicator to disclose the vacuum status to determine whether the evacuated tube is effective or not. When the color of the barium layer change from the sliver to the white color that means the vacuum is ever lost as shown in Figure (4-3) [47].

Figure (4-3): The Barium Getter and the Sealed End of the ETSC

Another part of the ETSC is the reflector which is surrounding the evacuated tube from the bottom only (as a parabolic curve). It is made from an Aluminum metal (Al) with 1 mm thickness and utilized to reflect the collected sunlight to the evacuated tube in order to increase the solar radiation intensity on the evacuated tube [27].

4.2.2. Gravity Assisted Wickless Heat Pipe (Thermosyphon)

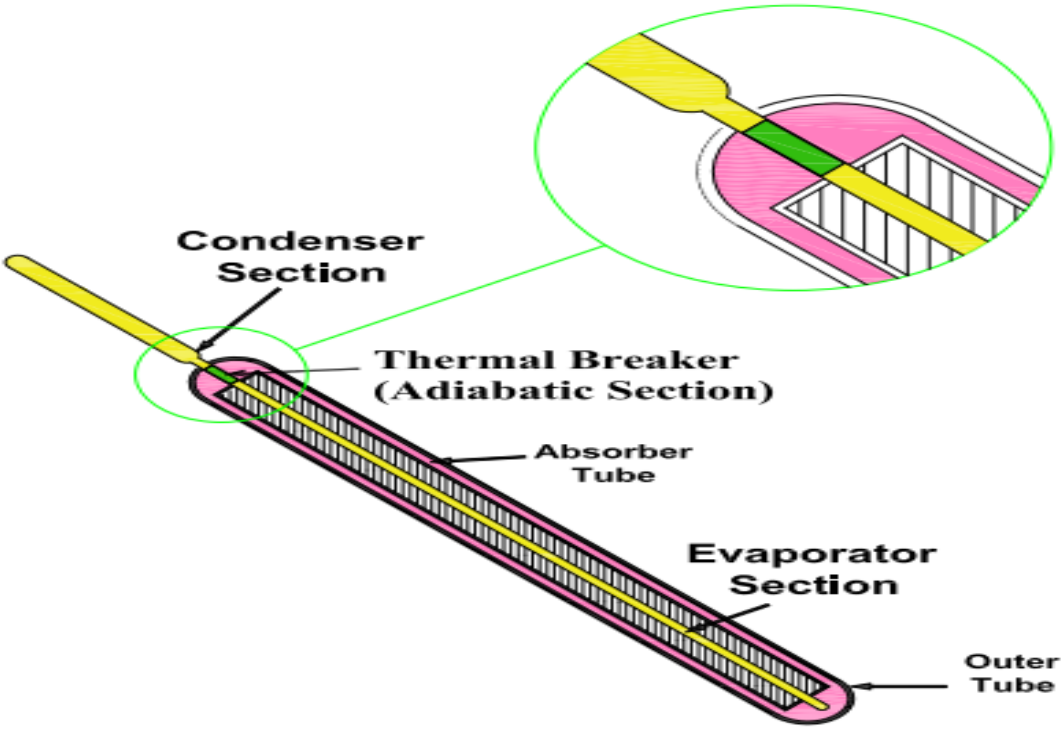

The GAHP is made from copper metal [48] and the dimensions are the length is 1.35 m and the inner and outer diameter are 14 mm and 16 mm, respectively. As described above, there are two types of thermosyphon have been used in this experimental study; first type is divided into three regions each region has a specific section that is evaporator, adiabatic (with thermal breaker), and condenser sections. Second type is divided into two regions each region has a specific section that is evaporator and condenser sections. The GAHP evaporator section length is 1.15 m located inside the evacuated glass tube and the

condenser section is 0.2 m sunken inside the water storage tank as showed in Figure (4-4)

Figure (4-4): Gravity Assisted Wickless Heat Pipe (Thermosyphon)

A small capillary pipe with a 0.2 cm diameter is utilized to link the GAHP (from the condenser side) to a pressure gauge and charging valve, and a service valve is located at the bottom of the thermosyphon at the beginning of the evaporator section. The capillary

pipe and service valve have several benefits. For instance, the service valve is used to clean the GAHP from all the undesirable atoms and discharge the working fluid (for purposes of replacing and controlling the filling ratio of the working fluid). Whereas the capillary pipe is utilized to vacuum (outgassed) the non-condensable gasses and charging the working fluid. After cleaning the GAHP, it was preserved under vacuum pressure for two days in order to check there wasn't any leakage. Then, the GAHP was charged with a small amount of the working fluid and discharge that amount under a 755 Torr for 3 hours by using a ROBINAIR vacuum pump type (250 L/min, 1 hp). Finally, the GAHP was charged by 70% filling ratio of the Acetone (the working fluid that was used in this study); a burette associated safely was utilized for charging the Acetone as illustrated in Figure (4-5A&B).

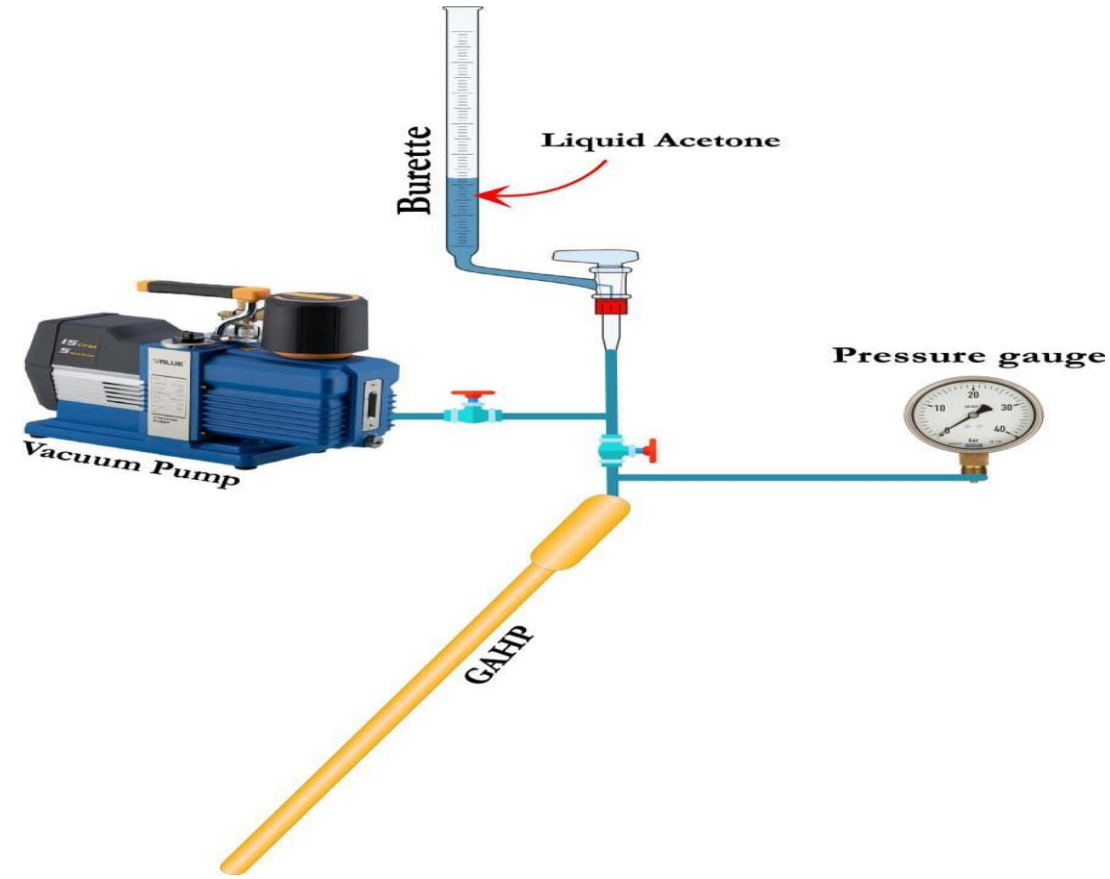

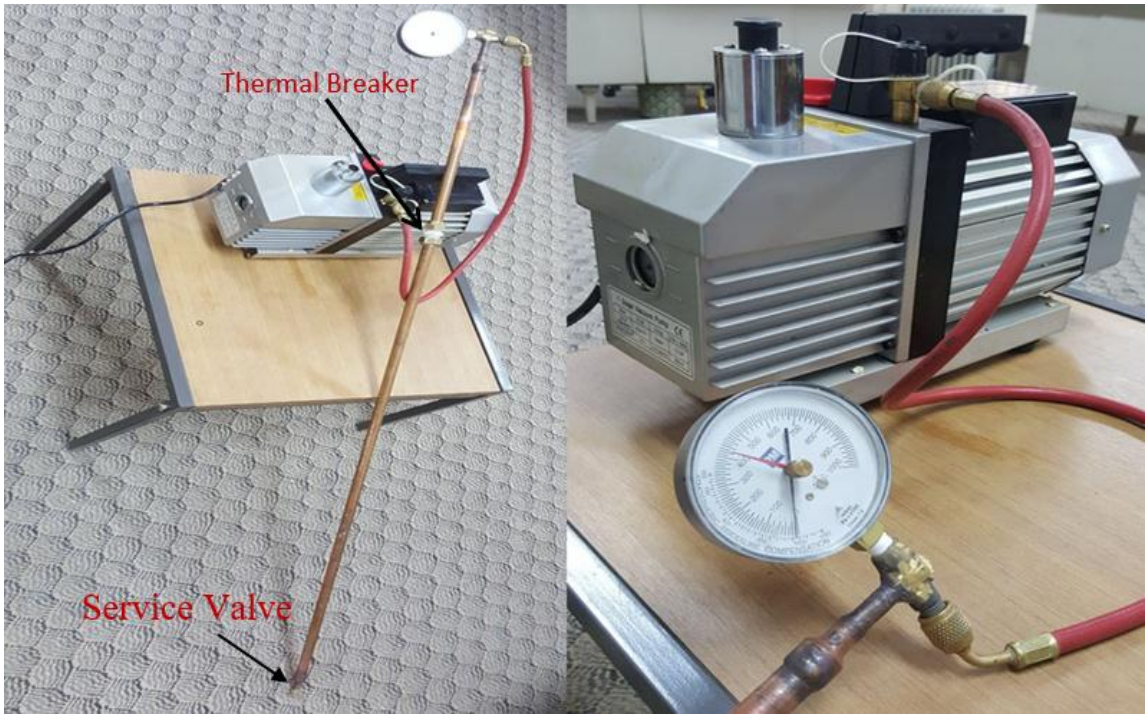

Figure (4-5A): Schematic of GAHP Vacuum and Charging Equipment

Figure (4-5B): GAHP Vacuum and Charging Experimentally

A group of 13 thermocouples K-type have been utilized along the heat pipe in order to record and estimate temperature distribution. Five of these thermocouples have been used inside the heat pipe specifically inside two sections of the heat pipe which are the evaporator and condenser to measure the temperature in the core of the heat pipe. Moreover, two of these five thermocouples were placed inside the condenser section and

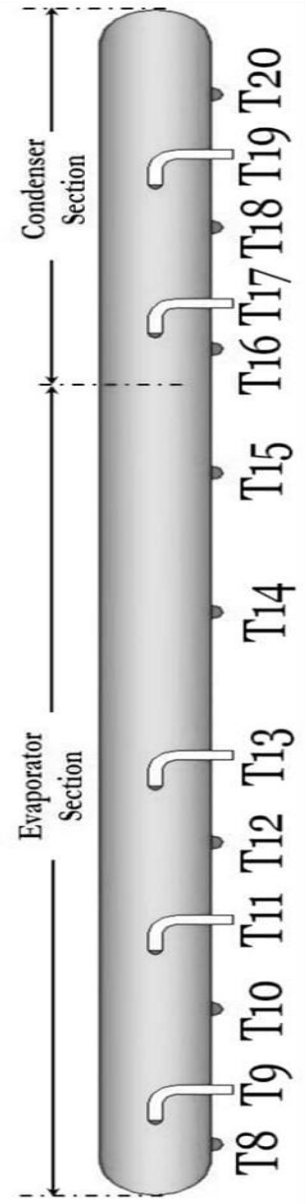

Thermo.NO.	Position (mm)
T8	10
T9	250
T10	500
T11	750
T12	1000
T13	1160
T14	1230
T15	1280
T16	30
T17	565
T18	1100
T19	1230
T20	1280

the others inside the evaporator section as clarified in Figure (4-6).

Figure (4-6): Surface and Core GAHP Thermocouples Positions

Eight of these thermocouples have been utilized on the surface of GAHP where five of them were placed on the surface of the evaporator section and three were placed on the surface of the condenser section. The eight surface thermocouples were isolated with insulating material to ensure accurate measure. While the five core thermocouples were

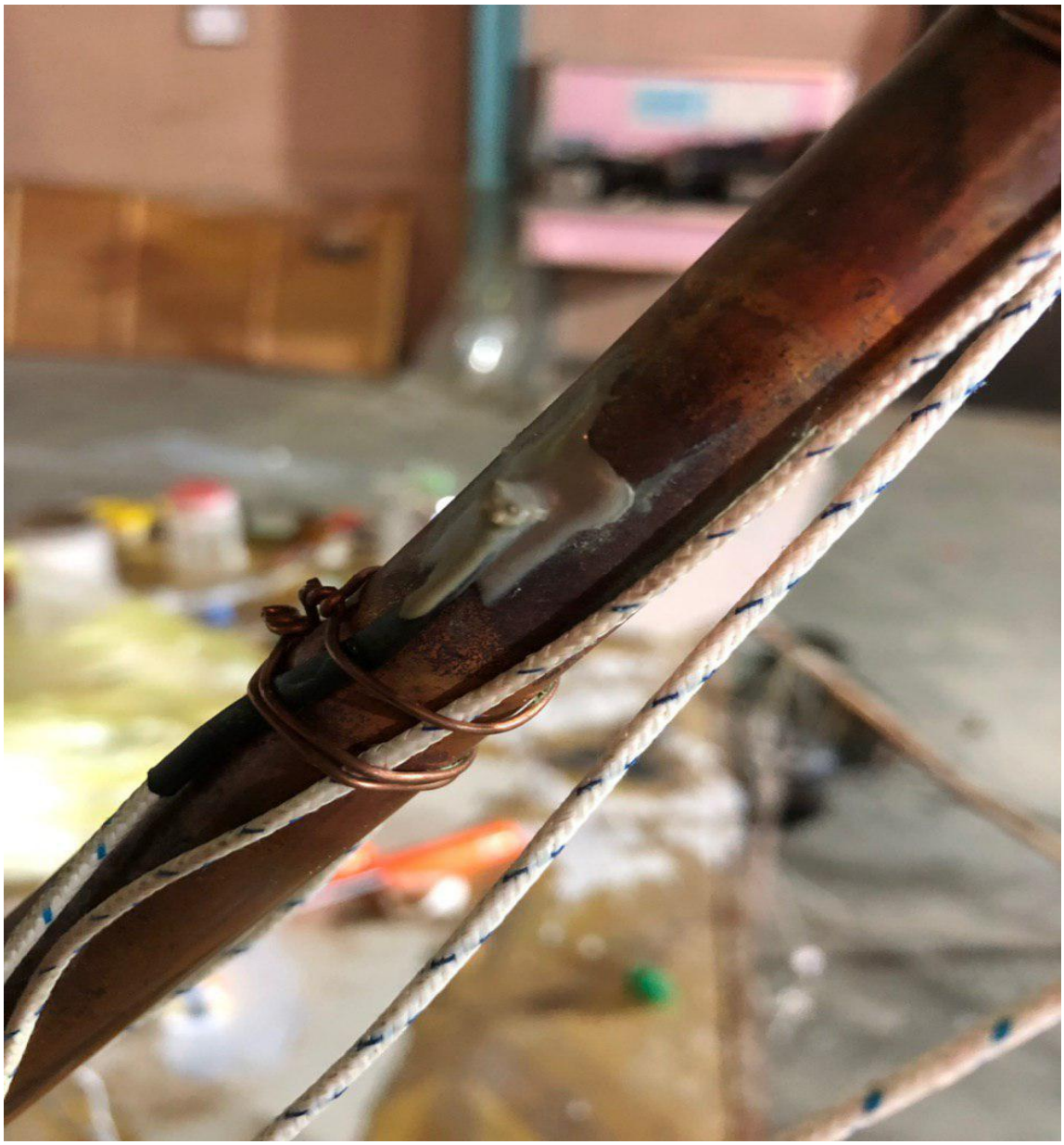

welded within the thermosyphon through small holes and covered by a special thermal

glue to ensure accurate recording for the working fluid which is inside as explained in Figure (4-7).

Figure (4-7): Core GAHP Thermocouples Install

4.2.2.1. Adiabatic Section

This prospective technique (adding the adiabatic section by using a thermal breaker between the other two sections of the GAHP) is a significant opportunity to enhance the Thermosyphon solar collector performance. The thermal breaker or thermal insulation model is a small part add to the thermosyphon after cutting a small part of it within the adiabatic section region.

The foam (Styrofoam) has been chosen to be the material of the thermal breaker due to its higher thermal resistance and lower thermal conductivity. Also, the melting point temperature for the Styrofoam is so high, inflammable, and nontoxic. The required dimensions for the thermal breaker that is needed in this experimental work are 5 cm in length and 2.5 cm in diameter. In order getting these dimensions, this model was produced by merging around six pieces of Styrofoam that are available here with 5*5*2

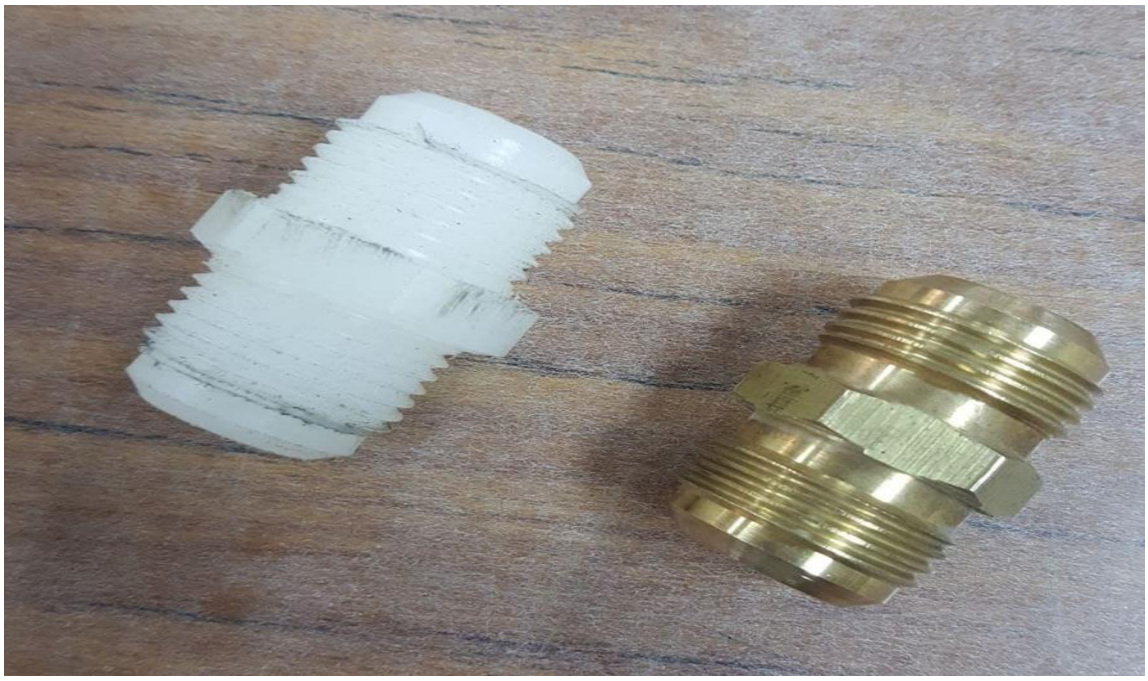

cm dimensions each together by using a special Styrofoam glue that has properties

almost similar to the original material to become a homogenous block. Thus, a CNC machine was used to forming an accurate model of the thermal breaker as shown in Figure (4-8A&B) after many attempts since the foam material is very hard to form.

Figure (4-8A): Styrofoam Thermal Breaker Model

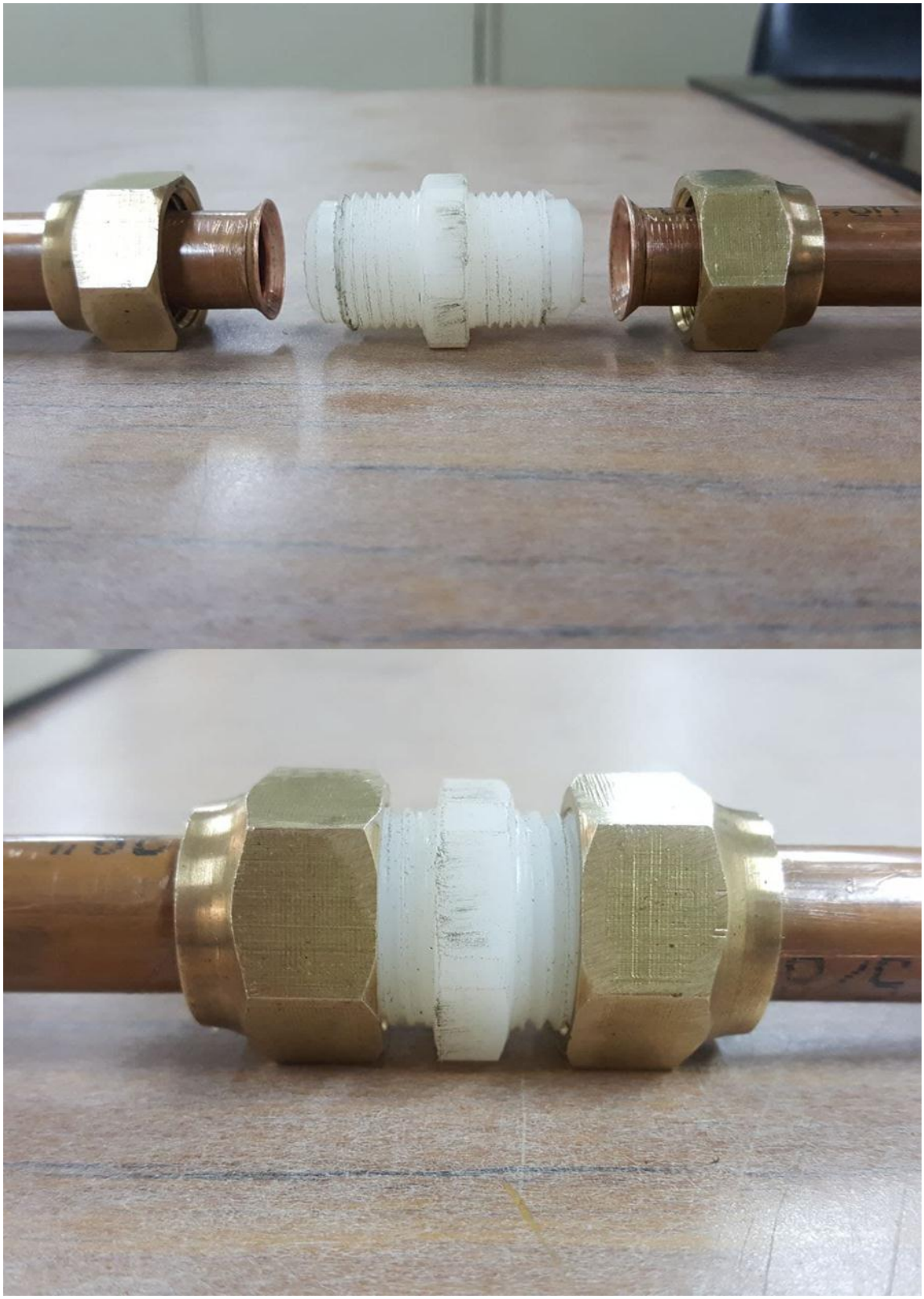

Figure (4-8B): Styrofoam Thermal Breaker Integrated Within the GAHP

Then, many laboratory tests were applied to test this model especially vacuuming pressure where the heat pipe with this model was vacuumed until getting the desired vacuum pressure which was -1 bar, and it was keeping up for one week period for leak checking purposes as illustrated in Figure (4-9).

Figure (4-9): Thermal Breaker Laboratory Test Integrated Within the GAHP

4.2.3. Storage Tank

The storage tank that is utilized in this experimental study consists of three separate tanks embedded together. One water tank is located in the middle, and two-phase change material (PCM) tanks are located on both sides of the storage tank. The water tank capacity is 5.6 liter, and the dimension of the tank are 27.5 cm in length, 7 cm in width, and 27.5 cm in depth. Both PCM tanks are identical, with capacity of 2 kg, and the dimension of the tank are 27.5 cm in length, 3 cm in width, and 27.5 cm in depth as shown in Figure (4-10).

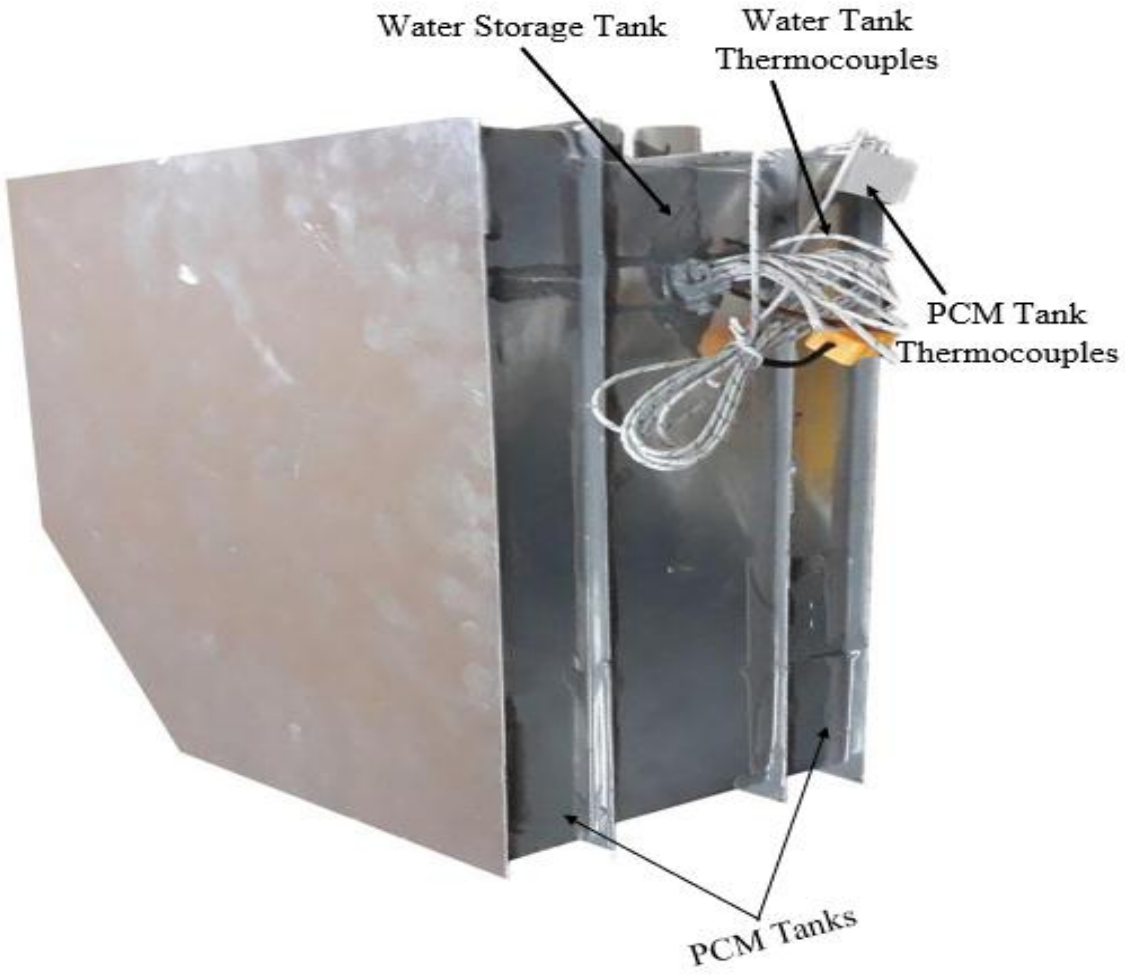

Figure (4-10): ETSC Storage Tank with Thermocouples

The three tanks are made from Aluminum material with 0.1 cm thickness each due to the characteristics of Aluminum where it has high thermal conductivity, high corrosion resistance, and low-cost price [17]. Also, the bottom corner of the face side of the storage tank had been cut down by 45° to facilitate the interfere between the GAHP (condenser section) and the water tank to be smoothly assembling [27]. A 3 cm fibrous glass layer (insulation layer) thickness was used for the purpose of minimizing heat energy loss. Where the fibrous glass layer was surrounded the storage tank from all sides. Then, it was covered by 0.25 mm aluminum sheet thickness as an extra isolated. Finally, the storage system was covered by 0.3 cm Alucobond sheets thickness uniformly for isolating the storage tank from the weather circumstances and for decorating.

Two Polypropylene Random Copolymer (PPR) pipes with 1.27 cm diameter each were inserted inside the water tank for supplying and withdrawing the water. The inlet pipe (cold water) was placed on the bottom side, and the outlet pipe (hot water) was located on the top opposite side. Also, a 0.5 cm diameter auxiliary pipe was inserted on the top side of the water tank for air vent purpose. On the other side, two PPR pipes with 1.27 cm diameter each were used to filling and draining the PCM tank with 1.8 kg paraffin wax for each PCM tank.

Twelve thermocouples were inserted and utilized to measure the temperature distribution of the storage tank. Seven thermocouples were used in the water tank, five of them are distributed and fixed on two copper wires by using special thermal epoxy glue. The two copper wires are forming a plus shape where four of these thermocouples fixed on 0.3 cm away from the four sides of the water tank walls and one thermocouple fixed in the center (core). The two remaining thermocouples, one is used to measure the temperature of the water inlet (cold water), and the other one is used to measure the temperature of the water outlet (hot water). However, five thermocouples were utilized in one of the PCM tanks only because the other one has the same conditions to measure the temperature distribution of the paraffin wax as clarified in Figure (4-2) and (4-10) above.

4.3 Measurement Tools

4.3.1 Thermocouples

The thermocouple type that has been chosen for this experimental works is Type K Thermocouple as shown in Figure (4-11). Type K Thermocouple has many characteristics that are made it the appropriate type for this study. For instance, it is most common, cheap, reliable, and accurate. Also, it has a wide range of temperatures started from the lowest -200 °C to the highest 1350 °C, and it is applicable to working under most of the chemical and environmental conditions. Additionally, it is made from Nickel-Chromium, and it doesn't require an external power source for operation. Moreover, the standard accuracy and the percentage error are around ± 0.75% and ± 0.4%, respectively. Thermocouple Reference Tables and calibrations are shown in

appendix (A).

Figure (4-11): ETSC_Type K Thermocouple

In this experimental work, around 90 type k thermocouples have been utilized to measure the temperature distribution for the four experimental devices. 25 thermocouples were used for each experimental device with PCM and 20 thermocouples for the remaining two experimental rigs without PCM. For further classification, 13 thermocouples for each GAHP of the four devices, 7 thermocouples for each water storage tank of the four devices, and 5 thermocouples for each PCM tank of the two rigs with PCM.

4.3.2 Data Logger

A multi-channel Data Logger AT4532 had used to sense and estimate the temperature throughout the thermocouples simultaneously and response quickly. Also, it has the ability to checking and testing the damaged thermocouple and high and low beep service. Additionally, it has an RS-232C connection transmission to connect to the computer easily. This Data Logger is so easy to operate and so accurate especially to the low signal that the type K thermocouple provides for this empirical work. As illustrated in Figure (4-12) where three Data Logger devices have been used in this experimental works. The specification properties of the data logger AT4532 are describes in Table (4-1). A YH-305D DC power supply was utilized to provide the electricity to the data logger.

Table (4-1): Data Logger AT4532 Specification Properties

Practicable	Thermocouple: K/E/T/J/S/N/B
Accuracy	0.2℃ ± 2 Numerals
Ranges	-200ºC ~ 1300ºC (For Type K Thermocouple)
Resolution	0.1 ºC
Channels	32 Channels (Expanded to 128 Channels)

Speeds	100 msec
Correction	Error corrects for each channel

Figure (4-12): ETSC_ Multi-Channel Data Logger

4.3.3 Solar Radiation Measurements

Solar Power Meter TENMARS TM-207 Taiwan type is the optimum device that is used to measure the solar radiance by sense the electromagnetic power which is creates

during the nuclear fusion reaction in the sun as shown in Figure (4-13). Solar Power

Display	3 1/2 digits. Max. indication 2000
Range	2000W/m²,634 BTU (ft²*h)
Resolution	0.1W/m², 0.1 BTU (ft²*h)
Accuracy	Typically within ±10 W/m² 【±3 BTU (ft²*h)】 or ±5%, whichever is greater in sunlight; additional temperature induced error ±0.38 W/m² /°C 【±0.12 BTU (ft²*h) /°C】 from 25°C

Meter calibration is performed in Appendix A. The TENMARS TM-207 characteristics and specifications are described in Table (4-2).

Table (4-2) : TENMARS TM-207 Characteristics and Specifications

Figure (4-13): ETSC_ Solar Power Meter TENMARS TM-207

4.4. Supplementation

4.4.1. Working Fluid

Pure Acetone material has utilized as a working fluid which is charged inside the GAHP. A 124 CC Acetone volume added to the GAHP which is represent 70% filling ratio [27]. A graduated glass tube (burette) used to measure the Acetone volume that was charged into the GAHP. Acetone fluid and thermal properties at 40 °C is described in Table (4-3).

Table (4-3): Acetone Fluid and Thermal Properties at 40 °C [27]

4.4.2. Phase Change Material PCM

Paraffin wax material type RT-42 have been utilized in the storage tank as a PCM. Figure (4-14) shows the pictural view of paraffin wax after and before melting. Paraffin wax material properties are described in the Table (4-4).

Liquid viscosity (kg/m*s)	Vapor pressure (Pa)	Liquid density (kg/m^3)	Vapor density (kg/m^3)	Vapor viscosity (kg/m*s)	Latent heat (J/kg)	Surface tension (N/m)
2.69×10^{-4}	6.0×10^{4}	768	1.05	0.86×10^{-5}	536×10^{3}	0.0212

Table (4-4): Paraffin Wax Material Properties [27]

T_m ^oC	C_p kJ/kg.k	k-liquid W/m.k	k-solid W/m.k	ρ-liquid kg/m^3	ρ-solid kg/m^3	Enthalpy kJ/kg
38-43	2	0.2	0.2	770	880	165

Figure (4-14): Paraffin Wax (PCM) Before (a), After Melting (b), and the Device for Estimating the Melting Point of Paraffin Wax (c)

4.5. Experimental Procedure

The four-system devices (GAHP-ETSC) have been operating at the same conditions to study and determine the performance of each experimental device individually. However, the only differences between the four devices are: one of apparatus has both an adiabatic section and PCM together, another one without both an adiabatic section and PCM which is considered the reference device. While the other two devices; one of them has an adiabatic section only and the other has PCM only.

The sequences below represent the experiment steps:

a. Fix the tilt angle (45^{o}) and filling ratio 70% with acetone as a working fluid for the four-apparatus based on previous studies.

b. Measure and record both the surface and vapor core temperatures along the GAHP as well as the storage tank system temperatures from 8:00 AM to 24:00 AM for each hour.

c. The record data of the experiment were taken place from the end of November to the tenth of April, and an average of the preferable data were selected throughout these periods, the average of the recorded data through preferable weather conditions such as clear and sunny.

4.6. Performance Calculations

During each experiment, the amount of solar energy input (I in w/m2) at evaporator region of is transferred to the condenser region and removed by the condenser . The overall thermal resistance (Rexp) for the solar collector was calculated as follows [43]:

$$R_{exp} = \frac{T_E - T_C}{2\pi r_o l_E I} \quad \text{.... (4.1)}$$

Where:

T_E: The average wall temperature at the evaporator section
T_C: The average wall temperature at the condenser section
r_o : The outer radius in mm
l_E : The length of evaporator in mm

4.6.1. Efficiency Calculations

The operation of gravity assistance heat pipe evacuated tube solar collector (GAHP-ETSC) is influenced by different factors such as the heat pipe type, the working fluid type, filling ratio, inclination angle, radiation intensity, operating conditions for hot water (inlet water temperature, mass flow rate) and ambient conditions (wind speed, clear or cloudy sky and ambient temperature). The value of the GAHP efficiency is dependent on the pervious factors above, the efficiency will be determined based on the equation [43]:

$$\eta = \frac{Q_u}{Q_{in}} \text{ .... (4.2)}$$

$$\eta = \frac{\dot{m}\, C_p (T_{wo} - T_{wi})}{A_c I} \text{ .... (4.3)}$$

- The daily efficiency can be estimates based on the equation:

$$\eta_{daily} = \frac{\dot{Q_u} dt}{\sum G_T A_{abs.} \tau_d} \text{ .... (4.4)}$$

Where $\dot{Q_u}$ = TOTAL useful energy delivered by the system

G_T= TOTAL global incident radiation (w/m^2)

τ_d= Solar Transmittance

4.6.2. Heat Energy Equivalent

The heat energy equivalent is primary depending on the heat energy useful (outlet) of the two systems with and without thermal breaker.

$$\%Q_{EQUIVALENT} = \frac{Q_{U(WT/TB)} - Q_{U(WO/TB)}}{Q_{U(WT/TB)}} \text{ .... } (4.5)$$

4.6.3. Uncertainty Analysis

Uncertainty of the measured parameters is calculated based on the methods given by Abernethy and Thompson [44]. The Uncertainty for Empirical Results is illustrated in Appendix D (Table D-1)

$$\Delta\eta = \sqrt{\left(\frac{\partial\eta}{\partial V}\Delta V\right)^2 + \left(\frac{\partial\eta}{\partial T_{wo}}\,\Delta T_{wo}\right)^2 + \left(\frac{\partial\eta}{\partial T_{wi}}\,\Delta T_{wi}\right)^2 + \left(\frac{\partial\eta}{\partial I}\,\Delta I\right)^2} \text{ .... } (4.6)$$

$$\Delta R_{exp} = \sqrt{\left(\frac{\partial R_{exp}}{\partial d_o}\Delta d_o\right)^2 + \left(\frac{\partial R_{exp}}{\partial d_i}\,\Delta d_i\right)^2 + \left(\frac{\partial R_{exp}}{\partial l_e}\,\Delta l_e\right)^2} \text{ .... } (4.7)$$

Chapter Five

Results and Discussion

5. Results and Discussion

5.1. Introduction

The primary function behind building four evacuated tube solar collector devices is to increase the daily efficiency of the solar collector system. In other words, increase the water storage tank temperature throughout the operation hours of the system especially at night. The challenge of the previous studies is the hot water in the storage tank lost its temperature gradually at night (the absence of sunlight) and the hot water demand specifically during the night. To achieve this mission, four experimental devices are utilized.

The average data has been taken for the weather measured data of February and March as illustrated in Appendix C (Table C-1 and C-2). Different two main case studies with four different system models will be presented. The first and second cases are studying the influence of applying 1 Liter/Hour load and 2 Liter/Hour load of water on the daily efficiency and performance of the four various experimental apparatus, respectively. Moreover, each case investigates the effect of applying the specific load on each experimental device individually. Additionally, the four-system apparatus are similar mostly and operating at the same time where the operating time from 8 AM to 24 AM , the four GAHP-ETSC systems operate at the same conditions and location. As results, these results are studying and investigating of applying two various loads on each specific apparatus with and without adiabatic section thermal breaker and PCM in order to illustrate and demonstrate the influence of the thermal breaker with PCM on enhancing the performance of the ETSC, especially during the demand period.

5.2. Flow Rate At (1-Liter/Hour) Load

In this section, the results (figures) represent the behavior of the temperature distribution at 1 Liter/Hour load for the whole system.

5.2.1. The Evaporator Section

The eight type-K thermocouples were utilized to measure the temperature distribution along the evaporator section which were distributed into two sects: along the surface of the evaporator (surface) and inside the evaporator (core).

Figure (5-1) shows the surface mean temperature distribution of the evaporator section for the four GAHP-ETSC models with the time. From the figure, it can be noticed that during the sunny hours (8 AM-5 PM) the surface temperature distribution with a thermal break within the adiabatic section and with and without PCM (green and blue lines) are larger than the without thermal breaker reference line because the thermal breaker allows the heat energy transfer from the evaporator to condenser sections through the working fluid (phase change convection heat transfer) only (there is no axial conduction heat transfer), and that leads to concentrate the temperature distribution on the surface of the evaporator. However, the purple and red lines (without a thermal break and with and without PCM) were transferred the heat energy to the condenser section in two ways, through the axial conduction throughout the surface of the evaporator, and through the working fluid. For these two heat transfer ways, the reference apparatus red line (without both) has the lower temperature distribution of the surface during the existence of the sunlight.

Nevertheless, the without thermal breaker and with PCM has the highest temperature during the sunny day until (18:00) because of the existence of the PCM. In the beginning, the two tanks of PCM absorb the heat energy from the water. Then, the reservoir temperature (PCM and water) will increase gradually and that is mean the conduction heat transfer through the wall will be reduced. When adding the thermal breaker, it prevents the conduction through the wall and leads the heat energy to transfer through the core only. In other words, during the sunlight, the PCM absorbs part of the transferred heat energy of the water storage tank in order to store this thermal heat energy and compensate it for the temperature reduction of the water during the night. As result, the PCM does not directly effect on the surface temperature of the evaporator, but it effects on the working fluid. Then it begins to drop and be identical to the other two apparatus during the night hours (after 18:00).

While during night hours (17:00-24:00) the surface temperature distribution with a thermal break without PCM (blue) is lower than the without a thermal break because of the axial conduction heat transfer in the without adiabatic section apparatus allows the heat energy leakage from the hot water tank storage (condenser section) to the warm or

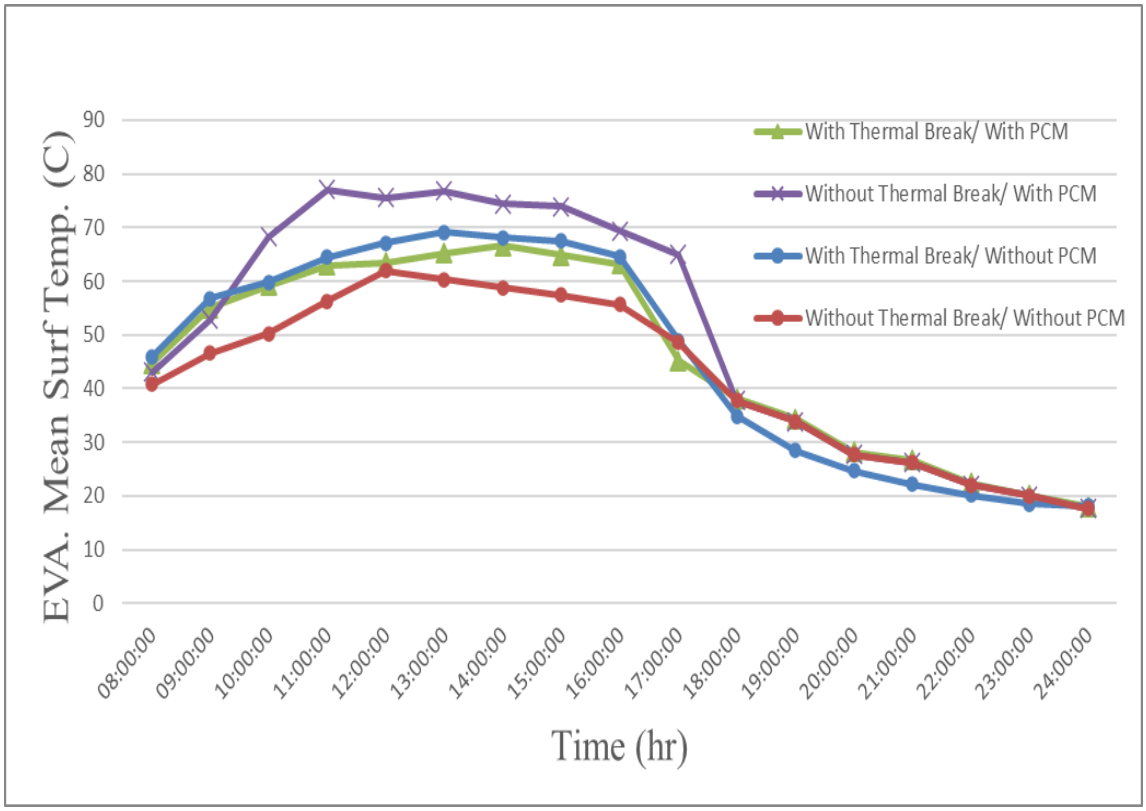

cold section (evaporator section).

Figure (5-1): One Liter/Hour Load Evaporator Mean Surface Temperature of Four Experimental Devices vs. Time

The best temperature distribution behavior device is the with both thermal breaker and PCM where during the sunlight hours until almost (17:00) it has the second lower temperature distributed (lower than purple and blue lines), and it has a uniform behavior during the night hours which is identical to the other two apparatus (without thermal breaker). This is considered the valuable advantage of adding thermal breaker and PCM together as illustrates in the figure above (less disadvantage during the sunny hours, and

more advantage during the night operating hours compared to the only with thermal breaker device and the only PCM device.

Figure (5-2) represents the core mean temperature distribution of the evaporator section for the four GAHP-ETSC devices (with and without thermal breaker and PCM) with time. It can be observed that the without thermal breaker and with PCM has the highest temperature during the sunny day until (18:00) because of the existence of the PCM. Where, during the sunlight, the PCM absorbs part of the transferred heat energy of the water storage tank in order to store this thermal heat energy and compensate it for the temperature reduction of the water during the night. In addition, the core temperature distribution during the night hours (after 18:00) was identical to the two apparatus without and with a thermal breaker.

The behavior of the core temperature for the device with thermal break and without PCM is mostly during the sunlight hours higher than the reference device except for three hours (11 AM – 1 PM) which is considered the optimum solar intensity hours. Due to the concentrate of the temperature distribution on the surface of the evaporator and it was transferred to the core through the conduction heat transfer as well as to the convection heat transfer in the working fluid itself. (There is no axial conduction heat transfer). Whilst during the night hours (16:30 -24:00) the temperature distribution line is dropped lower than the without a thermal break device's line because of the axial conduction heat transfer in the without adiabatic section apparatus allows the heat energy escape from the condenser section to the warm evaporator section.

The reference apparatus without thermal breaker and PCM behavior for three hours (11 AM – 1 PM) has recorded the highest temperature (70.55, 70.8, 68)^{o} C even higher than the blue line because of the optimum solar intensity during these hours. In other words, the advantage of the axial conduction heat transfer (without a thermal breaker) when the axial conduction slightly increases the heat transfer efficiency through the core of the evaporator to the core of the condenser section throughout the existence of the sunlight preciously (8:00-13:00). While throughout the absence of the sunlight the core temperature distribution with a thermal breaker is lower than the without a thermal break

, and this is considered the disadvantage of the axial conduction [49], and the advantage of using adiabatic section with a thermal break at the same time.

Even though in the core of the evaporator, both thermal breaker and PCM apparatus is still the more beneficial temperature distribution behavior device. Where, during the sunlight hours until almost (16:30) it has the lower temperature distributed, lower than purple and blue lines, and even the reference line for most hours of the sunlight hours. Also, it has a uniform behavior during the night hours which is identical to the other two apparatuses (without thermal breaker). Eventually, this rig is deemed the most precious device in this part of the device compared to the three other apparatus based on adding

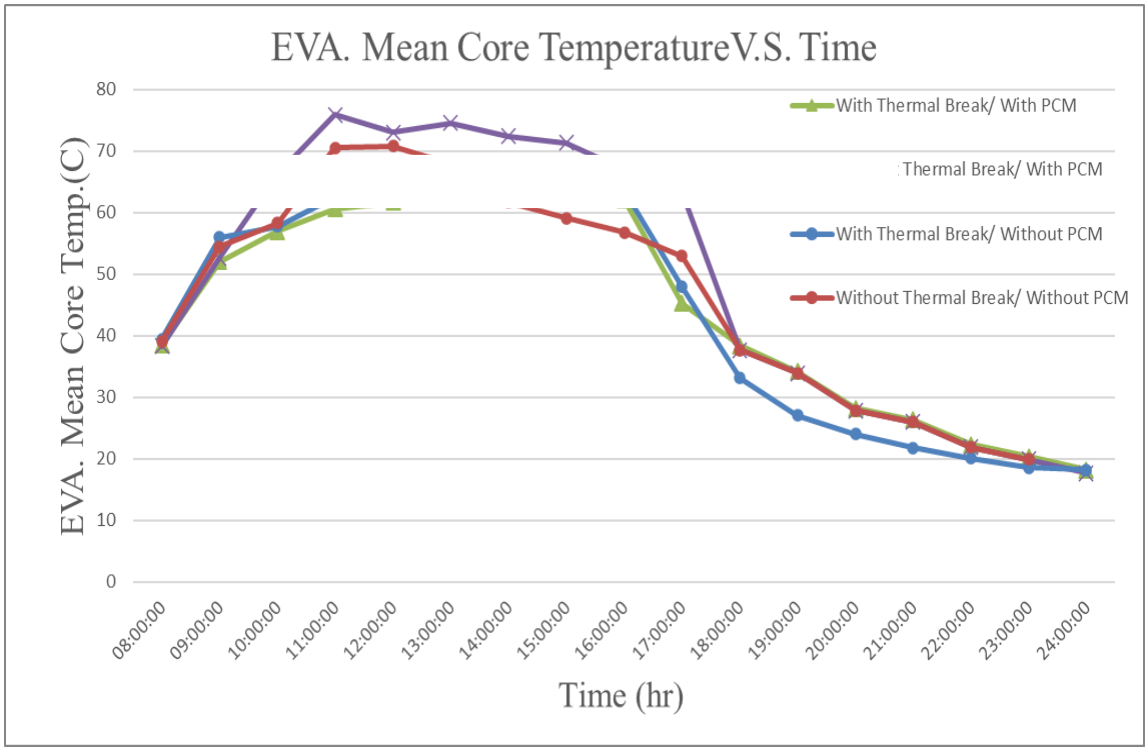

thermal breaker and PCM together as described in the figure above. In other words, it is the most advantageous and lowest disadvantage device during operating hours.

Figure (5-2): One Liter/Hour Load Evaporator Mean Core Temperature of Four Experimental Apparatus vs. Time

5.2.2. The Condenser Section

Measuring the temperature distribution steps for the condenser section of the GAHP is almost similar to the evaporator section. Where, 5 type-K thermocouples were distributed into two sects: along the surface of the condenser (surface), and inside the condenser (core).

It is clear from figure (5-3) the surface mean temperature distribution of the condenser section for the four GAHP-ETSC models with the time. It can be recognized that during the full operating hours the surface temperature distribution with a thermal break within the adiabatic section and with and without PCM are larger than the without thermal breaker reference line. This can be argued to the heat energy that is transferred from the working fluid to the surface of GAHT in the condenser section is stored (the temperature will not transfer back to the evaporator since the existence of the thermal break).

However, the without a thermal break and with and without PCM devices were received the transferred heat energy from the evaporator to the condenser section in two ways, through the axial conduction throughout the surface of the evaporator, and through the working fluid. For these two heat transfer ways, the reference apparatus (without both) has the lower temperature distribution of the surface during the full solar collector operation hours.

Whilst the without thermal breaker and with PCM is similar to the evaporator section still has almost the highest temperature during the sunny day until (17 PM) because of the existence of the PCM. But, during the night hours (17 PM- 24 AM), it begins to drop lower than the two with a thermal break apparatus. Also, the PCM compensates for the reduction temperature of the water during the absence of sunlight. Moreover, a high amount of heat energy escapes to the evaporator section through the GAHP (surface and core).

In the condenser section surface temperature distribution throughout operating hours especially the night hours, it can be realized and noticed clearly the precious benefit of using thermal breaker for the two devices with and without PCM. Where the temperature distributions of these two lines are higher than the two apparatus without a thermal breaker. In more specific, the device with both thermal breaker and PCM has the first reasonable and second-highest temperature distribution during the exitance of the sunlight until (17:30). Also, the highest temperature distribution after (17:30). That is mean the thermal breaker prevents the axial conduction from the condenser section (water storage tank) to the evaporator section, and it provides the necessary heat energy to the PCM storage tanks during sunny hours. Moreover, it resists thermally the heat energy from transferring from the storage tank (condenser section) to the evaporator section throughout the night hours, and that leads to saving most of the water temperature especially during the night.

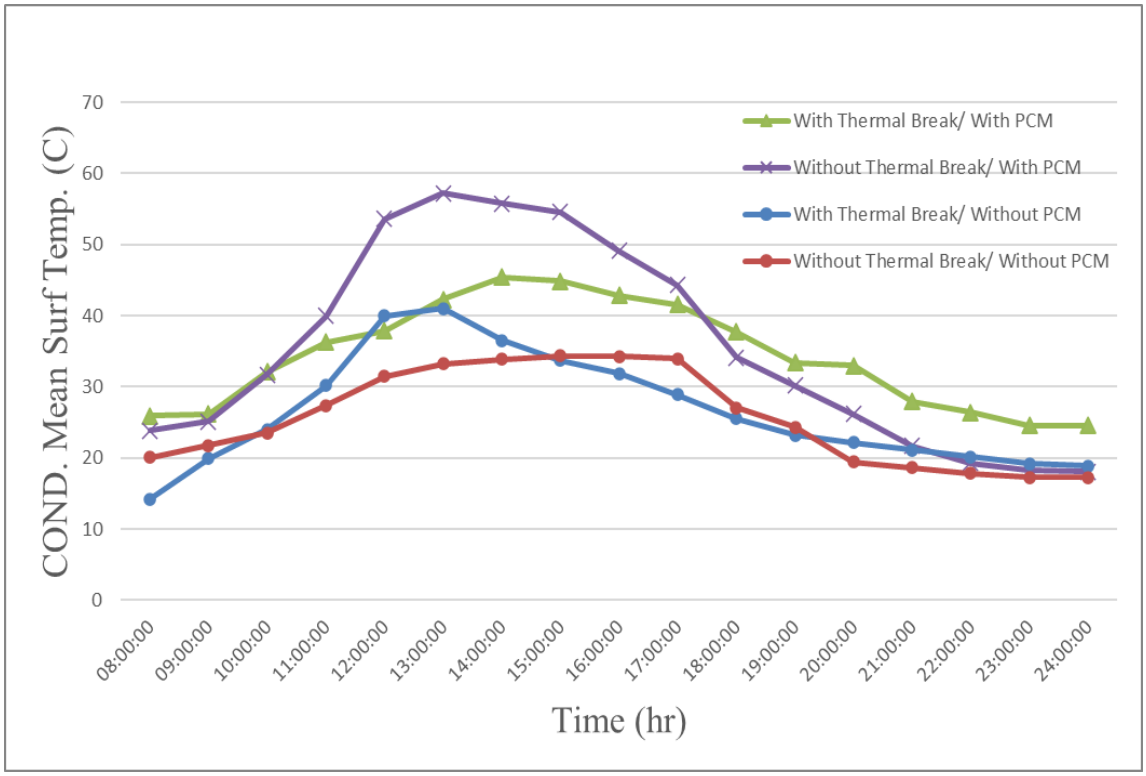

Figure (5-3): One Liter/Hour Load Condenser Mean Surface Temperature of Four Experimental Apparatus vs. Time

Figure (5-4) clarifies the core mean temperature distribution of the condenser section for the four GAHP-ETSC models (with and without thermal breaker and PCM) with the time. It can be observed that throughout the sunlight (8:00 - 17:30) operating hours the core temperature distribution without a thermal break within the adiabatic section and with and without PCM are larger than the with thermal breaker and with and without PCM . Due to the advantage of the axial conduction heat transfer for the without thermal break within GAHP when the axial conduction slightly increases the heat transfer efficiency through the core of condenser to the core of evaporator section.

Also, the without thermal breaker and with PCM device behavior is similar to the evaporator section behavior still has almost the highest temperature during the sunny day until (17:30) due to the existence of the PCM. However, through the absence of the sunlight (17:30 – 24:00), it starts to drop lower than the two with a thermal break apparatus . Also, the PCM stores the heat energy during the sunlight hours and compensates for the reduction temperature of the water during the night hours. Additionally, a respectable amount of the heat energy leaks out to the evaporator section through the GAHP (surface and core).

Additionally, the blue line temperature distribution behavior as described is the lowest line compared to the three apparatus especially the two rigs without thermal breaker because of the axial conduction for the reference device and the other device during the sunny hours until (19:20). After (19:20) operating hours, the blue line is rising up to be higher than the reference rig, and after (21:00) is higher than both without thermal breaker devices due to the advantage of the thermal breaker.

However, it can be clearly observed the benefit of adding PCM to the thermal breaker device and how this benefit improves the device to be slightly down the reference device until (13:30) due to the optimum solar intensity hours. Then, the behavior of the temperature distribution values is rising up to higher than the reference device and the with thermal breaker until (17:10), after that the green line is rising up and continuing to be the highest temperature distribution in order to save the water storage tank heat energy and keeping it possible hot during the coldest weather. In other words, the thermal break GAHP increases the thermal resistance between the two sections. That

means the experimental apparatus with both thermal breaker and PCM has valuable beneficial temperature distribution values during the full operating hours.

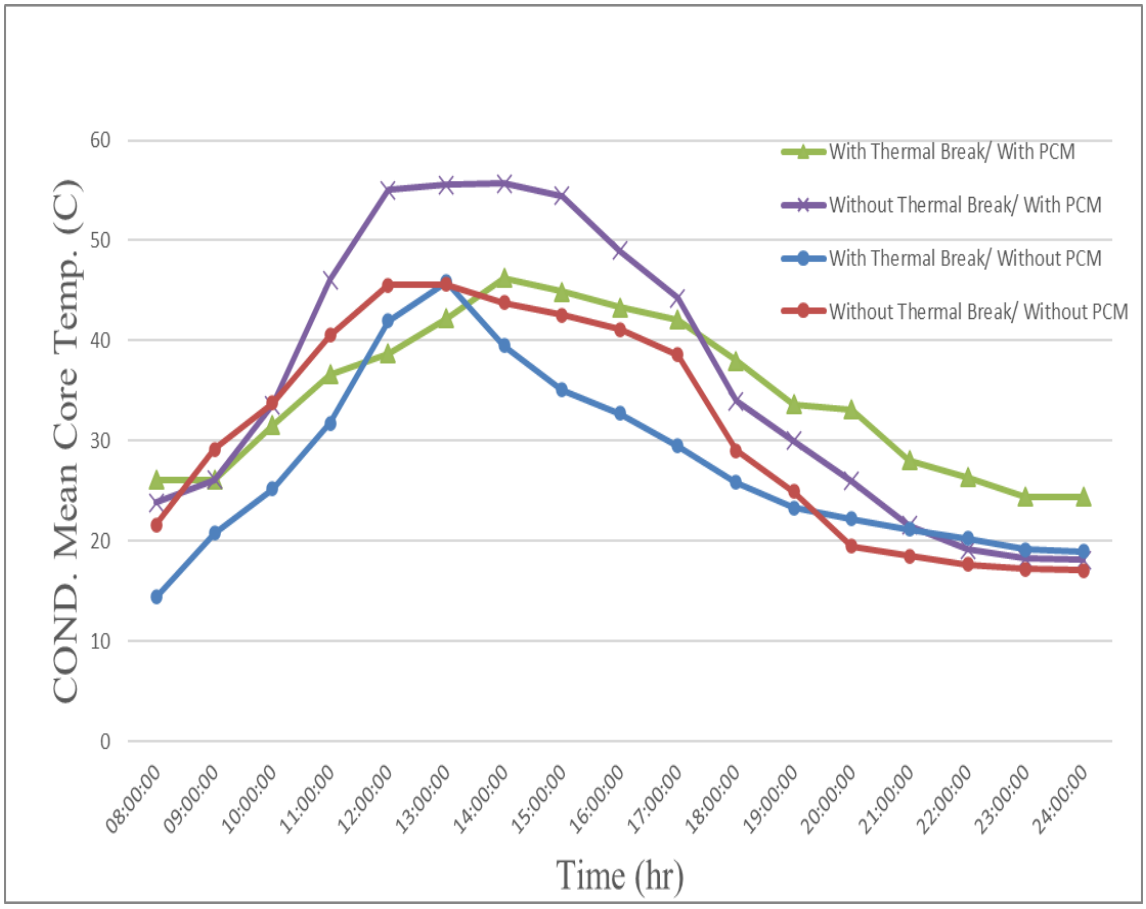

Figure (5-4): One Liter/Hour Load Condenser Mean Core Temperature of Four Experimental Apparatus vs.

5.2.3. The Water Storage Tank Section

The water storage tank is the final destination part that provides the user the demand for hot water. Multiple type-k thermocouples are utilized to measure the temperature of the water storage tank as well as measuring the input (cold) and output (hot) water temperature.

The outlet water temperature is considered the primary output of the GAHP evacuated tube solar collector that the user needs. Figure (5-5) represents the outlet water temperature of the four experimental devices. The outlet water temperature of the two apparatus without thermal breaker and with and without PCM from (8:00-15:00) are approximately identical after (15:00) the reference temperature begins to drop down to record the lowest outlet water temperature for the rest of the operating hours. However, the purple line after (15:00) is continuing to record high-temperature values, after (17:00) the water outlet temperature start to go down to be less than the apparatus with both thermal breaker and PCM , and higher than the other two devices during the absence of the sun because of the existence of the PCM (heat energy storage) that provides the heat energy to the water in the storage tank during the night. The maximum water output temperature values from (13:00-15:00) are (43, 43.5, 44)^{o} C, respectively for the reference apparatus . Also, The maximum water output temperature values from (13:00-16:00) are (43.6, 43.5, 44.4, 44)^{o}C, respectively for the with PCM device.

The output water temperature of the with thermal breaker and without PCM device from (8:00- 17:00) is nearly identical to the reference device after (17:00- 22:00) the blue line temperature is higher than the water outlet temperature of the reference device due to the exitance of the thermal break that resists the heat energy leakage from the water storage tank. Then, the blue line after (22:00-24:00) the water temperature line comes back to be identical to the temperature of the reference device. The highest water outlet temperature values that the apparatus reaches are (42.6, 42.8, 43.1)^{o} C for the period (13:00-15:00).

The output water temperature of the most beneficial device with both thermal breaker and with PCM device from (8:00- 15:00) is near to the other three experimental devices. After (17:00) the green line water temperature is continuing to be the highest water outlet temperature degrees compared to the other three devices with a high-value difference for the remaining hours of operation. The highest water outlet temperature values that the experimental device reaches are (40.2, 42.3, 43.8, 43.5)^{o} C for the period (13:00-16:00).

In other words, the water lost its heat energy for the system with both thermal break and PCM is much less than the other three systems at each hour during the operating hours

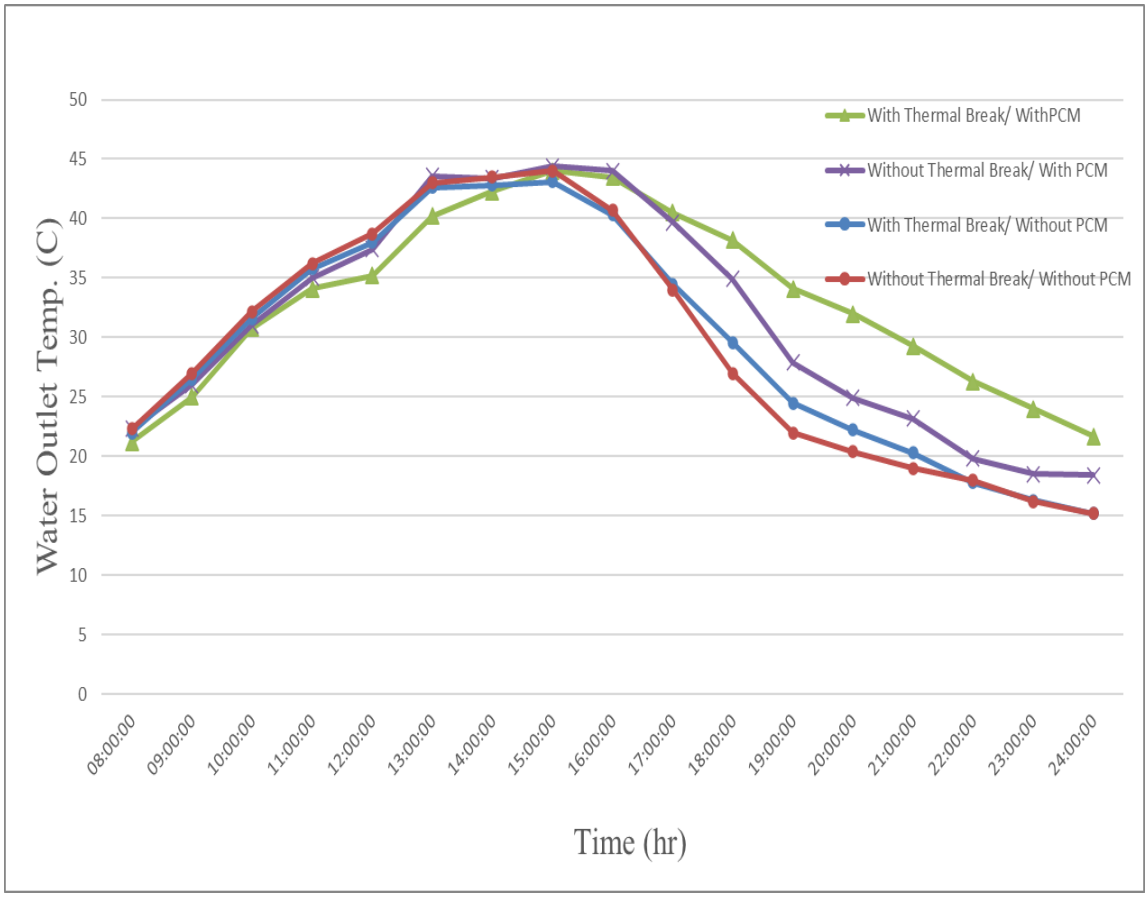

especially at night hours, and that leads to the water with both thermal breaker and PCM system maintain its heat energy mostly. That means the experimental apparatus with both thermal breaker and PCM has valuable beneficial temperature distribution values during the full operating hours.

Figure (5-5): One Liter/Hour Load Water Outlet Temperature of Four Experimental Apparatus V.S. Time

5.3. Flow Rate At (2-Liter/Hour) Load

In this section, the same procedure of applying 1 Liter/ Hour load has been repeated by applying 2 Liter/ Hour load instead. Also, All the previous results (figures) have been

remeasured based on the changing of load. Thus, the results will be shown represents the behavior of the temperature distribution in each part of the experimental model's parts individually at 2-liter/Hour load.

5.3.1. The Evaporator Section

Also, eight type-K thermocouples were utilized to measure the temperature distribution along the evaporator section which were distributed into two sects: along the surface of the evaporator (surface) and inside the evaporator (core) for 2 Lite/Hour load.

Figure (5-6) shows the surface mean temperature distribution of the evaporator section for the four GAHP-ETSC models with the time. It can be noticed the purple, green, blue, and red lines behavior are similar to the behavior of the 1 liter/hour load except the temperature distribution values of 2 liter/hour load less than 1 liter/hour load. Where, during the sunny hours (8:00-17:00) the surface temperature distribution without a thermal break within the adiabatic section and with PCM has the highest temperature distribution values because of the existence of the PCM. Thus, during the sunlight, the PCM absorbs part of the transferred heat energy of the water storage tank in order to store this thermal heat energy and compensate it for the temperature reduction of the water during the night. Then it begins to drop and be identical to the other two apparatus during the night hours (after 18:00). Also, the surface temperature distribution with a thermal break within the adiabatic section and with and without PCM are larger than the without thermal breaker reference line during most of the sunlight hours until aproximatlly17 PM because the thermal breaker allows the heat energy transfer from the evaporator to condenser sections through the working fluid , and that leads to concentrate the temperature distribution on the surface of the evaporator.

While during the night hours (17:00-24:00) the surface temperature distribution with a thermal break without PCM is sometimes nearly to be slightly lower and other times identical than the without a thermal break and because of the axial conduction heat transfer in the without adiabatic section apparatus allows the heat energy leakage from

the hot water tank storage (condenser section) to the warm or cold section (evaporator

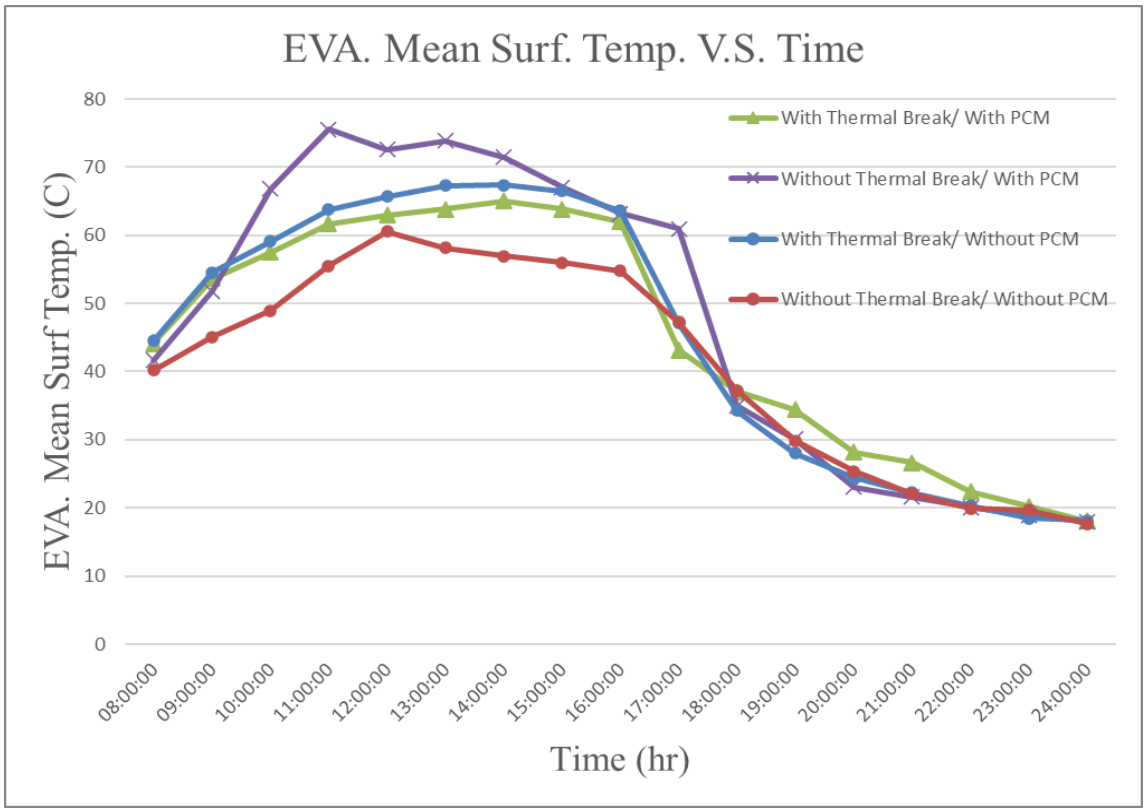

section).

Additionally, the reference apparatus (without both) has the lower temperature distribution of the surface during the existence of the sunlight due to the two-heat transfer methods to transfer the heat energy to the condenser section (through the axial conduction throughou[illegible] working fluid).

Figure (5-6): Two Liter/Hour Load Evaporator Mean Surface Temperature of Four Experimental Devices vs. Time

Even though with high load values (double mass flow rate), the preferable temperature distribution behavior device is the with both thermal breaker and PCM where during the sunlight hours until almost (16:30); It has the second lower temperature distributed (lower than purple and blue lines), and it has a uniform behavior during the night hours which is identical in some hours and slightly higher at the other hours compared to the

other two apparatus (without thermal breaker). The reason behind that is the temperature values are rapidly down due to the increase in the mass flow rate for the without thermal breaker devices. Despite increasing the load, adding thermal breaker and PCM together for the system is still and continuing has the valuable advantage as illustrates in the figure above (less disadvantage during the sunny hours, and more advantage during the night operating hours compared to the only with thermal breaker device and the only PCM device .

Figure (5-7) illustrates the core mean temperature distribution of the evaporator section for the four GAHP-ETSC devices with time. It can be observed the purple, green, blue, and red lines behavior also are similar to the behavior of the 1 liter/hour load except the temperature distribution values of 2 liter/hour load less than 1 liter/hour load. The purple line experimental apparatus has the highest core temperature distribution values during the sunshine hours until (17:00) because of the existence of the PCM (the PCM absorbs part of the transferred heat energy of the water storage tank in order to store this thermal heat energy and compensate it for the temperature reduction of the water during the night). Also, the core temperature distribution during the night hours (after 18:00) is virtually to be identical to the two apparatus with and without a thermal breaker.

The core temperature distribution values behavior of the (blue line) empirical apparatus is mainly during the sunlight hours higher than the reference device except for three hours (11:00– 13:00) which is considered the optimum solar intensity hours, and until (16:30). Due to the concentrate of the temperature distribution on the surface of the evaporator and it was transferred to the core through the conduction heat transfer as well as to the convection heat transfer in the working fluid itself (There is no axial conduction heat transfer).

Nevertheless, during the night hours (16:30-24:00) the temperature distribution line is dropped to be the lowest temperature values than the without a thermal break because of the axial conduction heat transfer in the without adiabatic section apparatus allows the heat energy escape from the condenser section to the warm evaporator section. This is considered the disadvantage of the axial conduction, and the advantage of using an adiabatic section with a thermal break at the same time.

Additionally, the reference apparatus behavior for three hours (11:00 – 13:00) has recorded the highest temperature (69.15, 70, 65.45)^{o} C higher than the blue line due to the optimum solar intensity during these hours. Videlicet, the advantage of the axial conduction heat transfer for the two devices without a thermal breaker when the axial conduction slightly increases the heat transfer efficiency through the core of the evaporator to the core of the condenser section throughout the existence of the sunlight

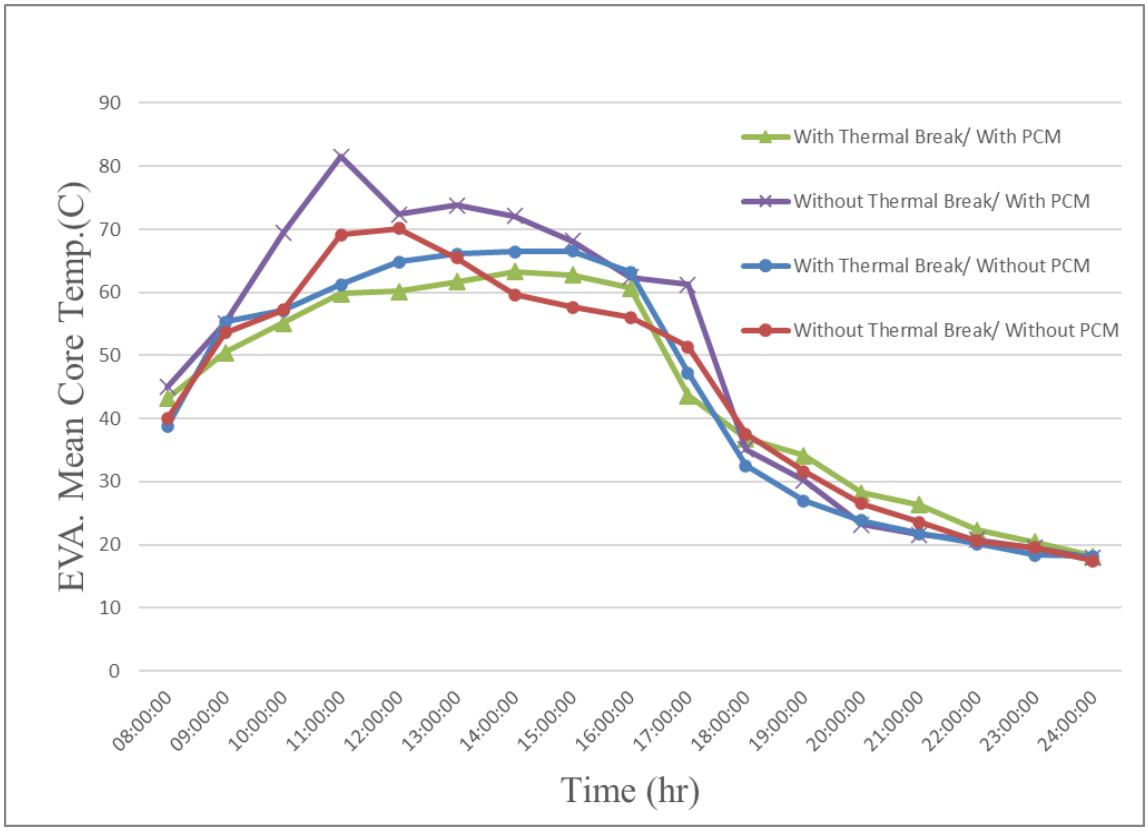

preciously (8:00-13:00).

Figure (5-7): Two Liter/Hour Load Evaporator Core Temperature of Four Experimental Apparatus vs. Time

Despite the higher load value (double mass flow rate), the core of the evaporate for both thermal breaker and PCM apparatus is still the more favored temperature distribution behavior device. Where, during the sunlight hours until almost (16:25) it has the lower temperature distributed (lower than purple and blue lines, and even the reference line for most hours of the sunlight hours). Also, it has a regular behavior too throughout the

sunset hours is identical in some hours and slightly higher at the other hours compared to the other two apparatus (without thermal breaker) due to the abruptly down in the core temperature values of the without thermal breaker devices during the increase in the mass flow rate. Eventually, this rig is deemed the most precious device in this part of the device compared to the three other apparatus based on adding thermal breaker and PCM together as described in the figure above. Namely, the most advantage and lowest disadvantage device during operating hours.

5.3.2. The Condenser Section

Using the same procedure to recording the temperature distribution steps for the condenser section of the GAHP which is almost similar to the evaporator section. Where, 5 type-K thermocouples were distributed into two sects: along the surface of the condenser (surface), and inside the condenser (core).

It's clear from figure (5-8) that the surface mean temperature distribution of the condenser section for the four GAHP-ETSC models (with and without thermal breaker and PCM) with the time. Also, it can be recognized that the green, blue, purple, and red lines conduct are similar to the conduct of the 1 liter/hour load except the temperature distribution values of 2 liter/hour load less than 1 liter/hour load. Where, during the full operating hours the surface temperature distribution with a thermal break within the adiabatic section and with and without PCM are larger than the without thermal breaker reference line. Arguably, the transferred heat energy through the working fluid to the surface of GAHT in the condenser section is stored and transferred to the water and PCM of the storage tank. In addition, the temperature will not transfer back to the evaporator since the existence of the thermal break.

Whilst the purple line without thermal breaker and with PCM is similar to the evaporator section still has almost the highest temperature during the sunny day until (17:10) because of the existence of the PCM. Later, during the night hours (17:10- 24:00), the line begins to decline to be lower than the two with a thermal break apparatus due to part

of the heat energy escape to the evaporator section through the GAHP (surface and core).

However, the reference apparatus nearly has the lower temperature distribution of the surface during the full operating hours. The reason behind that the two heat transfer

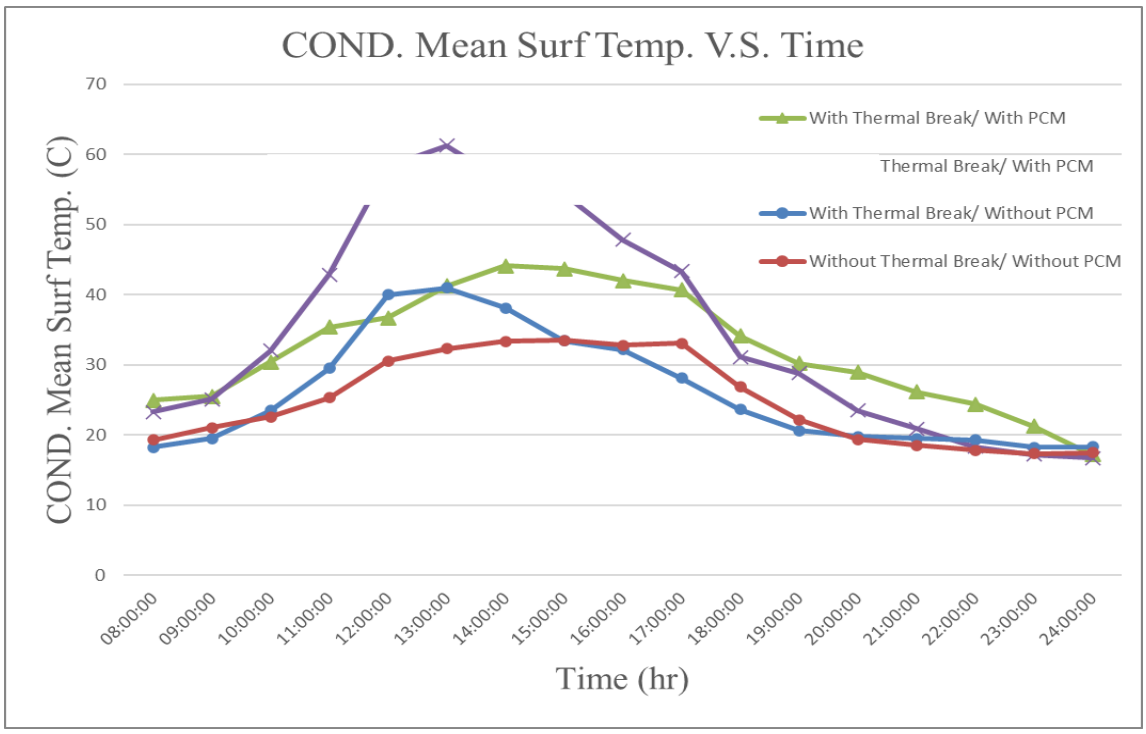

methods are utilized to transfer the heat energy to the condenser section (through the axial conduction and working fluid), and heat energy leaks out during the night hours.

Figure (5-8): Two Liter/Hour Load Condenser Mean Surface Temperature of Four Experimental Devices vs. Time

It can be easy to distinguish and noticed clearly the valuable benefit of using thermal breakers for the two devices with and without PCM throughout the operating hours especially the night hours. Where the temperature distributions of these two lines are higher than the two apparatus without thermal beaker specifically during the sunset hours. To be more precise, the device with both thermal breaker and PCM has the sensible attitude and the second-highest temperature distributions during the exitance of the sunlight until (17:10). Also, the highest temperature distribution values after (17:10)

with a noteworthy difference compared to the other three rigs. Due to the vital role of the thermal breaker that prevents the axial conduction perfectly from the water storage tank to the evaporator section during the sunset hours, while during the sunshine, it provides the necessary heat energy to the water and PCM storage tanks during the sunny hours.

Figure (5-9) clarifies the core mean temperature distribution of the condenser section for the four GAHP-ETSC models with the time. It can be observed that the green, blue, purple, and red lines attitude are similar to the attitude of the 1 liter/hour load except the temperature distribution values of 2 liter/hour load less than 1 liter/hour load. Wherever, the benefit of the axial conduction slightly increases the heat transfer efficiency through the core of the condenser to the core of evaporator from (8 AM- 13:30) and (8 AM- 17:55) for the reference apparatus and the with PCM device, respectively. For this reason, these two apparatus temperature values higher than the other two devices during that period.

Also, the purple line device has the highest temperature values for the sunshiny period until (17:50) similar to the evaporator section attitude because of the PCM. However, through the absence of the sunlight (17:50- 24:00), it starts to drop lower than the two with a thermal break apparatus. Due to a respectable amount of the heat energy leaks out to the evaporator section through the GAHP (surface and core).

Additionally, the blue line device temperature distribution behavior as described is the lowest line compared to the three apparatus especially the two rigs without thermal breaker because of the axial conduction for the reference device and the other device during the sunny hours until (20:00). After (20:00) operating hours, the blue line is rising up to be higher than the reference rig, and after (21:00) is higher than both without thermal breaker devices due to the advantage of the thermal breaker.

It can be clearly observed the benefit of adding PCM to the thermal breaker device and how this benefit improves the device to be slightly down the reference device until (13:30) due to the optimum solar intensity hours. Then, the behavior of the temperature distribution values is rising up to higher than the reference device and the with thermal breaker until (17:55), after that the green line is rising up and continuing to be the highest temperature distribution in order to save the water storage tank heat energy and

keeping it possible hot during the coldest weather. Particularly, the thermal break GAHP increases the thermal resistance between the two sections. That means the experimental

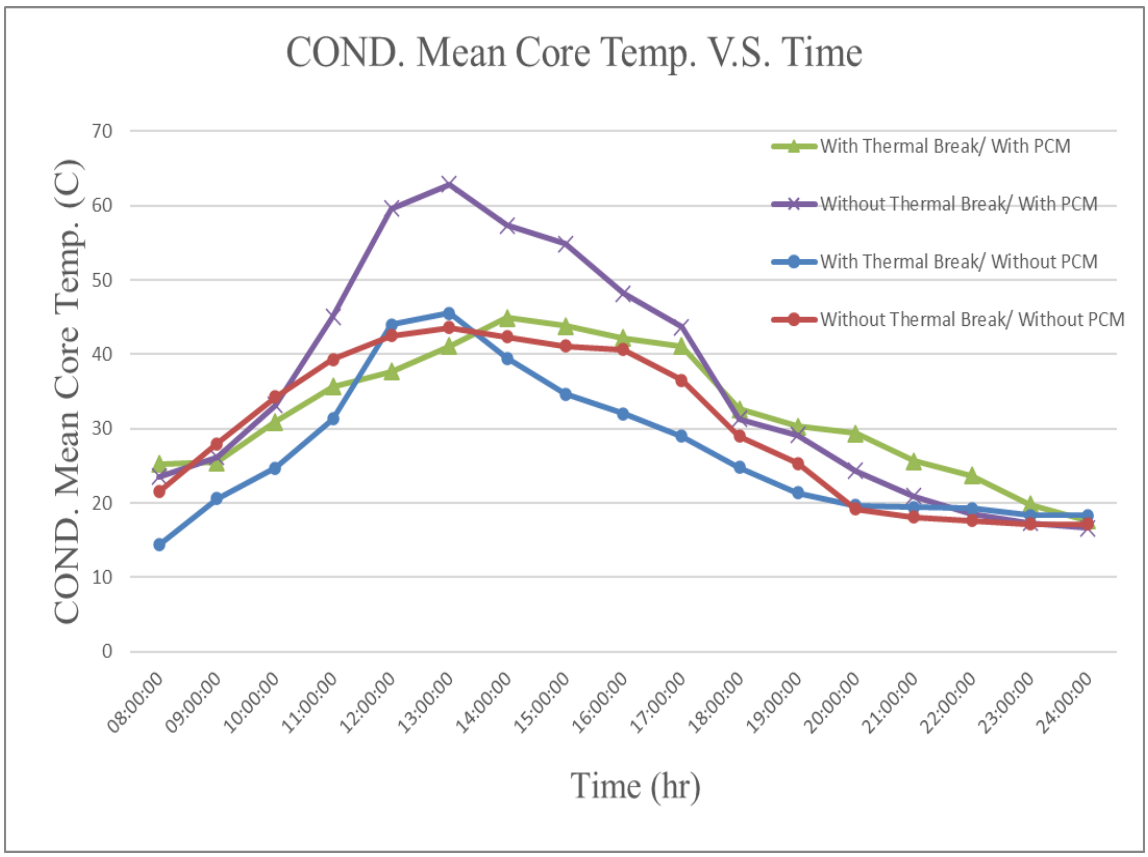

apparatus with both thermal breaker and PCM has valuable beneficial temperature distribution values during the full operating hours.

Figure (5-9): Two Liter/Hour Load Condenser Mean Core Temperature of Four Experimental Devices vs. Time

5.3.3. The Water Storage Tank Section

Seven type-k thermocouples are used to measure the temperature of the water storage tank as well as measuring the input (cold) and output (hot) water temperature. The water storage tank is considered the outcome part that supplies the user with the hot water demand. The essential output of the GAHP evacuated tube solar collector is the output

water temperature (hot water) that the user needs which is deemed the primary function of the GAHP-ETSC. Figure (5-10) represents the water output temperature of the four experimental devices. The output water temperature of the four experimental rigs behavior are similar to the conduct of the 1 liter/hour load except the temperature distribution values of 2 liter/hour load less than 1 liter/hour load.

Wheresoever, the output water temperature of the two apparatus without thermal breaker and with and without PCM from (8:00-15:00are approximately identical after (15:00) the reference temperature begins to drop down to record the lowest outlet water temperature for the rest of the operating hours. Where, the maximum water output temperature values from (13:00-15:00) are (42.1, 43, 43.5)^{o} C, respectively for the reference apparatus. Also, the water outlet temperature values of the purple line after (15:00) start to go down to be less than the apparatus with both thermal breaker and PCM and higher than the other two devices during the absence of the sun because of the existence of the PCM (heat energy storage) that provides the heat energy to the water in the storage tank during the sunset hours. The maximum water output temperature values from (13:00-16:00) are (42.4, 42.8, 43.1, 42.2)^{o} C, respectively for the with PCM device.

The outlet water temperature values of the with thermal breaker and without PCM device from (8:00- 17:00) is lower than the reference device after (17:00- 20:00) the blue line water temperature values are higher than the reference device temperature values due to the exitance of the thermal break that resists the heat energy leakage from the water storage tank. Then, the blue line after (20:00) the water temperature line drops to be identical to the temperature of the reference device. The highest water outlet temperature values for the experimental device reaches are (40.1, 41, 40.7)^{o} C for the period (13:00-15:00).

The outlet water temperature values of the most beneficial device with both thermal breaker and with PCM device from (8:00- 15:00) is near to the other three experimental devices temperature values. After (15:00) the green line water temperature is continuing to be the highest water outlet temperature degrees compared to the other three devices with a high-value difference for the remaining hours of operation.

The maximum water outlet temperature values that the experimental device reaches are (40.9, 42.8, 43, 40.8)^{o} C for the period (14:00-17:00). Particularly, the water lost its heat

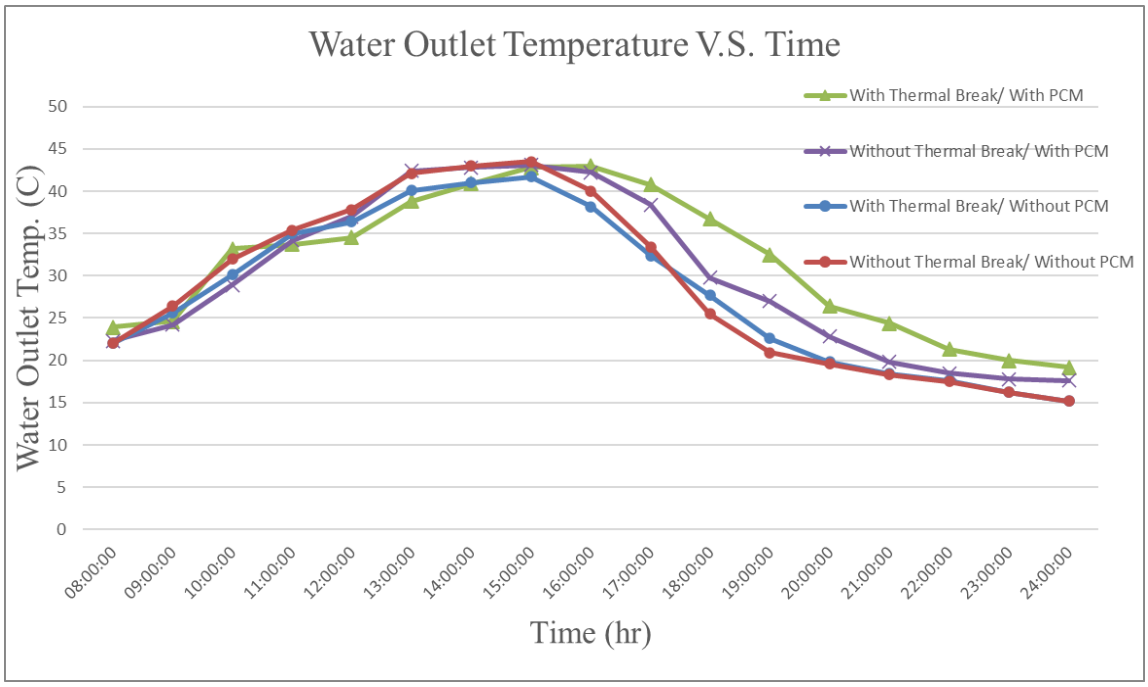

energy for the system with both thermal break and PCM is much less than the other three systems at each hour during the operating hours especially at night hours, and that leads to the water with both thermal breaker and PCM system maintain its heat energy mostly. That means the experimental apparatus with both thermal breaker and PCM has valuable beneficial temperature distribution values during the full operating hours.

Figure (5-10): Two Liter/Hour Load Water Outlet Temperature of Four Experimental Apparatus V.S. Time

5.4. The Daily Efficiency

The daily efficiency is depending on the total useful and inlet heat energy values. The factors such as a thermal breaker, PCM, and load have directly affected the daily efficiency. Figure (5-11) represents the daily efficiency for two experimental apparatus (with and without thermal breaker and both without PCM) at 1 liter/hour load. It can be observed that the daily efficiency with and without thermal breaker is 33.3% and 31.29 %, respectively due to the thermal breaker extends the operating hours of the solar collector. For example, the system without a thermal breaker was shut down at (21:00) while the with thermal breaker was shut down at (24:00 AM) (three operating hours difference) as illustrated in the figure.

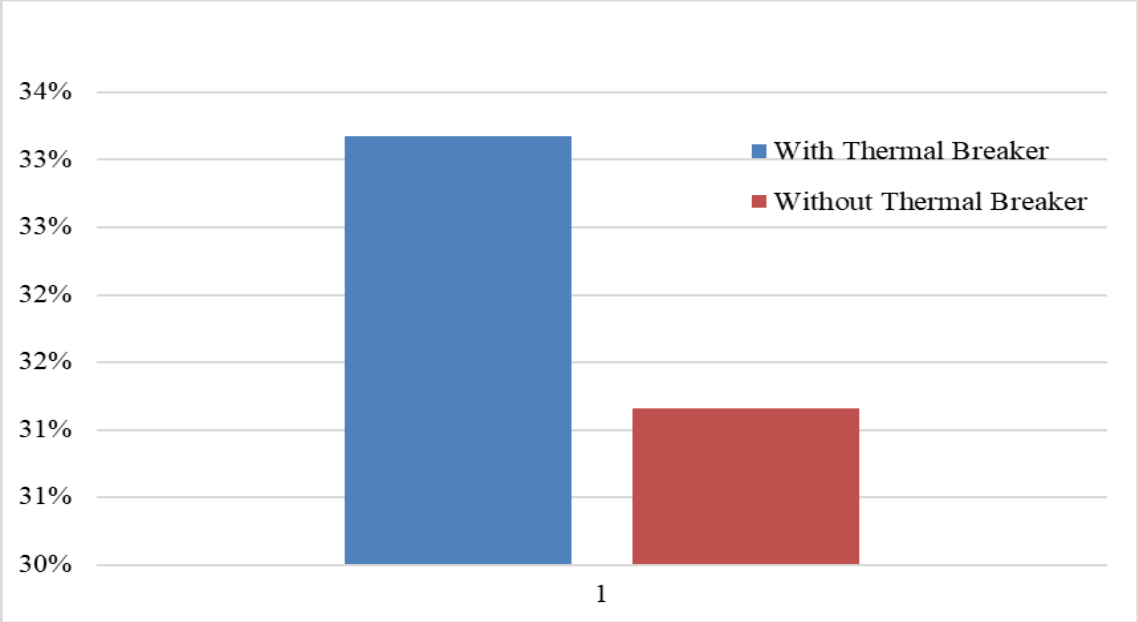

Figure (5-11): Two Systems Daily Efficiency without PCM at 1 L/H Load

Figure (5-12) clarifies the daily efficiency for two experimental apparatus (with and without thermal breaker and both with PCM) at 1 liter/hour load. It can be noticed that the daily efficiency with thermal breaker is higher than without thermal breaker too which are (41.2%) and (almost 36%). Where the system with PCM higher than the without PCM because the PCM prevents the system shutdown and compensates the heat energy lost from the water storage tank. Also, the system with both thermal breaker and

PCM has the highest daily efficiency since the thermal breaker prevents the heat energy leaks out between the sections and the PCM compensates for the reduction in the water

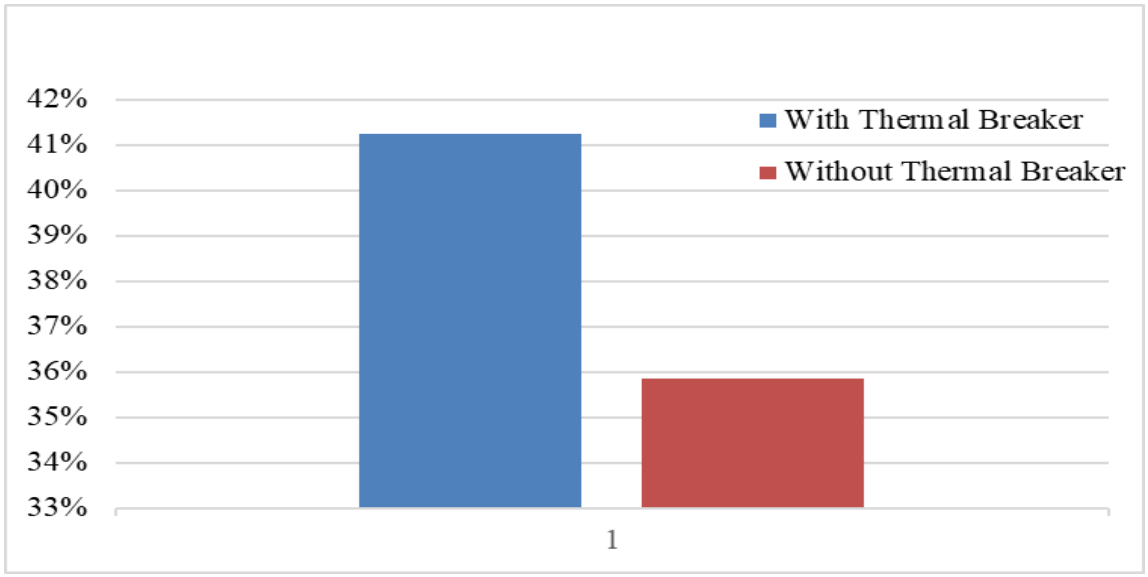

temperature as shown in the figure (5-12).

Figure (5-12): Two Systems Daily Efficiency with PCM at 1 L/H Load

Figure (5-13) represents the daily efficiency for two experimental apparatus (with and without thermal breaker and both without PCM) at a 2 liter/hour load. It can be observed

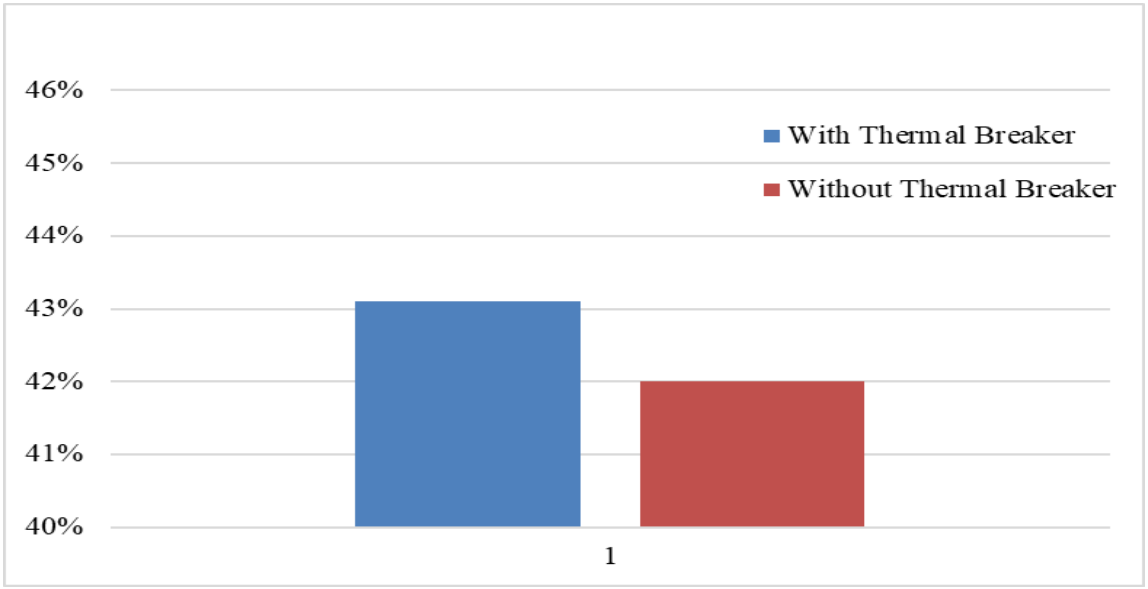

that the daily efficiency with and without thermal breaker is 43% and 42 %, respectively because the thermal breaker extends the operating hours of the solar collector.

Figure (5-13): Two Systems Daily Efficiency without PCM at 2 L/H Load

For instance, the system without a thermal breaker was shut down at (22:00) while the with thermal breaker was shut down at (24:00 AM) (two operating hours difference) as illustrated in the figure above.

Figure (5-14) clarifies the daily efficiency for two experimental apparatus (with and without thermal breaker and both with PCM) at 2 liter/hour load. It can be noticed that the daily efficiency with thermal breaker is higher than without thermal breaker too which are (47%) and (almost 44%). For the same previous reason of existing thermal breaker and PCM. There was a difference in the daily efficiency values when the load was changed. For instance, when the load is 2 Liter/Hour the daily efficiency values of the four experimental devices are higher than the daily efficiency values at 1 Liter/Hour

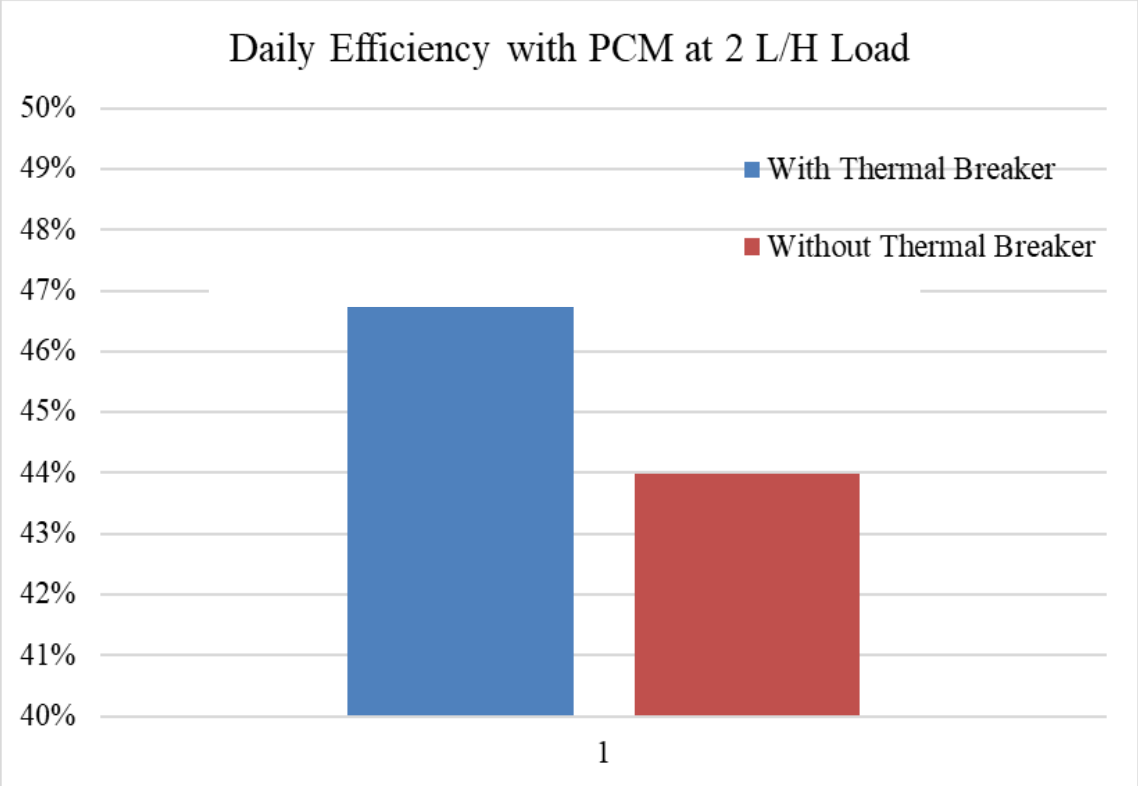

load. These are sensible results since the daily efficiency has a proportional relationship with the useful heat energy (when the load increases the mass flow rate increase too and

useful heat energy depend on the mass flow rate, so it is increased too as stated in daily efficiency equation) as described in the figure.

Figure (5-14): Two Systems Daily Efficiency with PCM at 2 L/H Load

5.5. Heat Energy Equivalent

The heat energy equivalent is called also the overall heat energy equivalent for the two solar collector systems (with and without thermal breaker) with PCM, and the other two systems without PCM at each hour for the total operating hours. The heat energy equivalent is primary depending on the heat energy useful (outlet) of the two systems with and without thermal breaker based on heat energy equivalent equation. Also, the load, PCM, and thermal breaker impact the equivalent heat energy directly. Figure (5-15) depicts the heat energy equivalent for two experimental apparatus (with and without thermal breaker and both without PCM) at 1 liter/hour load. It can be noticed that during the sunshine the useful (outlet) heat energy of the systems without thermal breaker little

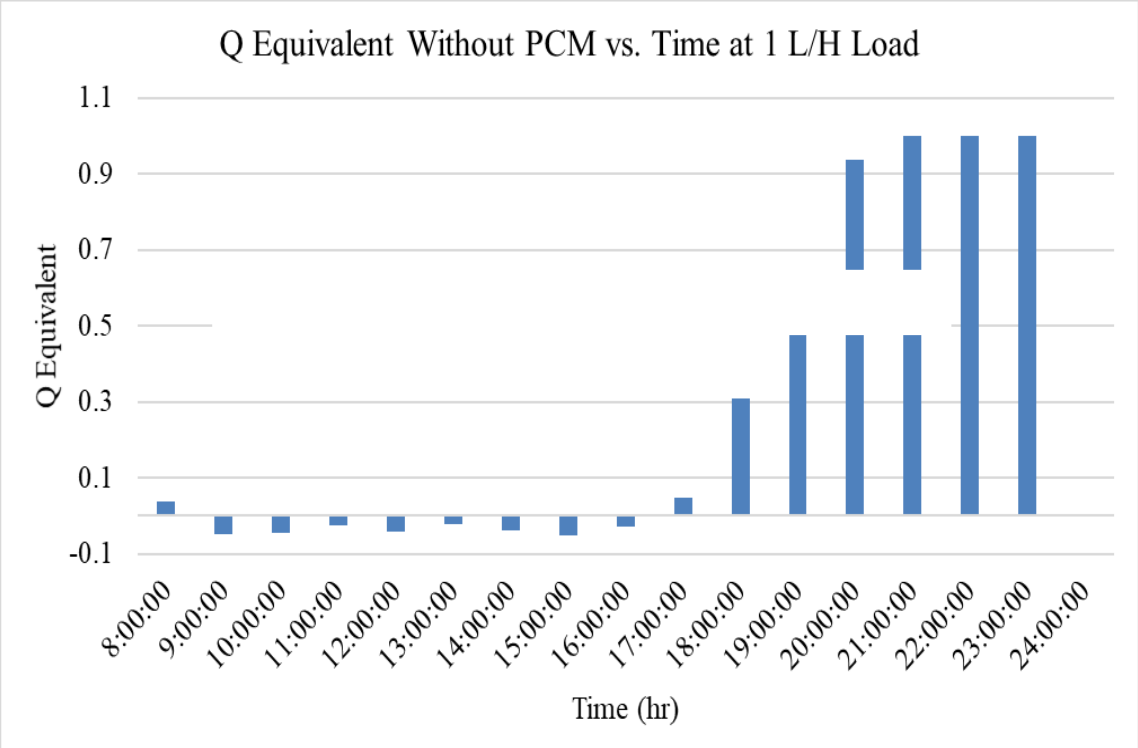

bit higher than the useful heat energy with thermal breaker until (17:00) due to the advantage of the axial conduction during the sunlight hours for the GAHP-ETSC

without thermal breaker. However, the major advantage of the thermal breaker disclosure during the sunset hours until (23:00) after that period both systems will be shut down, as described in the figure.

Figure (5-15): Two System Equivalent Heat Energy without PCM at 1 L/H Load

Figure (5-16) illustrates the heat energy equivalent for the two experimental apparatus (with and without thermal breaker and both with PCM) at 1 liter/hour load. It can be observed that during the sunshine the useful (outlet) heat energy of the systems without thermal breaker higher than the useful heat energy with thermal breaker until (16:00) because of two reasons as described in Figure (5-1) to Figure (5-5); the existence of the PCM, and the advantage of the axial conduction during the sunlight hours for the

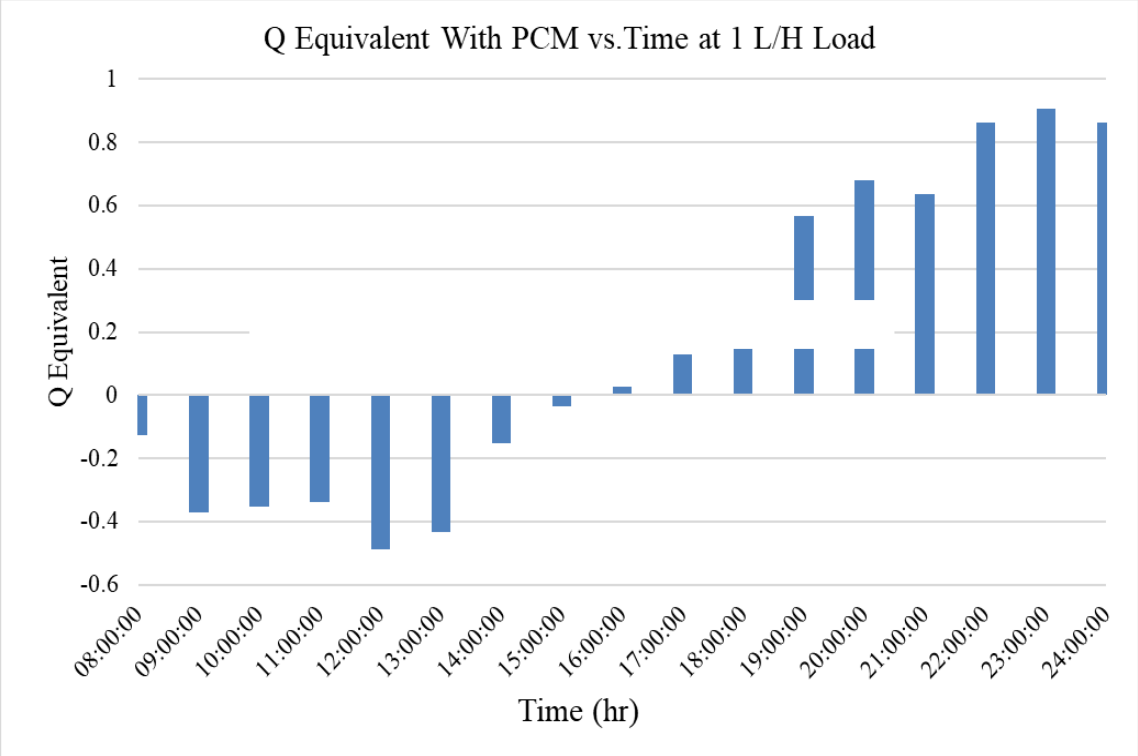

GAHP-ETSC without thermal breaker. In other words, during the sunlight, the PCM absorbs part of the transferred heat energy of the water storage tank that leads to an increase in the convection heat transfer in the working fluid (the phase change process of the acetone will be so fast transferring more heat energy). But this process is temporary

only during the high solar intensity period, thus after that time, the useful heat energy without thermal breaker decreases until the end of (15:00).

Figure (5-16): Two Systems Equivalent Heat Energy with PCM at 1 L/H Load

Later, the PCM is extending the advantage of the thermal breaker during the sunset by increasing the useful and equivalent heat energy with a thermal breaker (gained one hour compared to the system without PCM) until (24:00) since the PCM has a secondary advantage that prevents the system to shut down and compensates the heat energy lost from the water storage tank. Overall, the system with both thermal breaker and PCM has the longest positive equivalent heat energy during the full operation hours as clarified in the figure above.

Figure (5-17) clarifies the heat energy equivalent for two experimental apparatus (with and without thermal breaker and both without PCM) at 2 liter/hour load. It can be distinguished that the behavior of the equivalent heat energy without PCM at 2 L/H load is approximately nearly to the behavior of the equivalent heat energy without PCM at 1

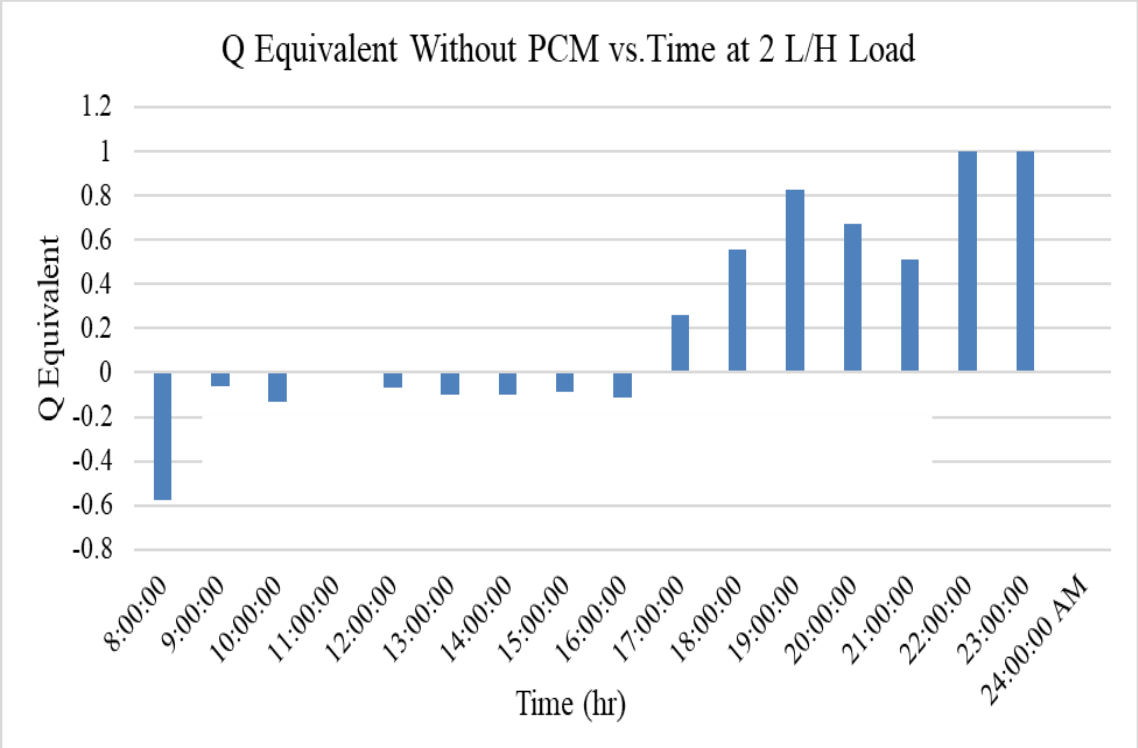

L/H load. Whereover, during the sunshine the useful (outlet), heat energy of the systems without thermal breaker at 2 L/H load less than the useful heat energy at 1 L/H load.

That means the advantage of the thermal breaker increases with increasing the load during the sunshine. Where the useful energy with thermal breaker during the sunlight insignificant than the without one until (17:00) due to the same reason (axial conduction advantage). However, the greatest advantage of the thermal breaker appears during the sunset hours until (23:00) after that period both systems will be shut down, as described in the figure.

Figure (5-17): Two Systems Equivalent Heat Energy without PCM at 2 L/H Load

Figure (5-18) represents the heat energy equivalent for the two experimental apparatus (with and without thermal breaker and both with PCM) at a 2 liter/hour load. It can be observed that the behavior of the equivalent heat energy with PCM at 2 L/H load is clearly different than the behavior of the equivalent heat energy with PCM at 1 L/H load since the advantage of adding the two features to the experimental device is obviously clear when the load increase (the advantage of axial conduction is compared to the thermal breaker advantage during the sunshine will be approximately equivalent).

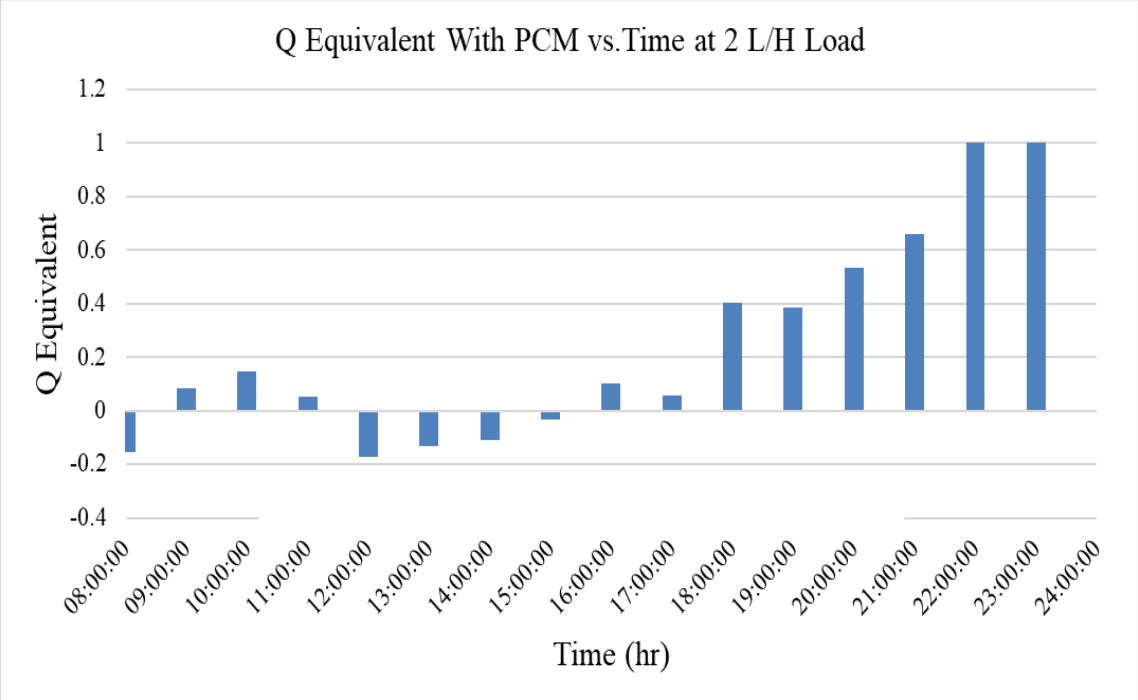

Wherever throughout the period (9 AM -11 AM) the useful heat energy with thermal

breaker higher than the without thermal breaker despite during the sunshine hours. Then, for the period (12:00-15:00) the useful heat energy without thermal breaker little bit higher due to the high solar intensity. Later, the excellent advantage of using both features (thermal breaker and PCM) is disclosure of the period (16:00-24:00). As result, When the load increases, the advantage of the thermal breaker increase too during the sunset hours, and the disadvantage decrease during the sunshine at existence of the PCM, for this reason, this solar collector system type has the optimum advantage and the longest positive equivalent heat energy over the other three systems as explained in the figure.

Figure (5-18): Two Systems Equivalent Heat Energy with PCM at 2 L/H Load

5.6. Overall Thermal Resistance

The overall thermal resistance is relying on the evaporator and condenser mean surface temperature, the evaporator length, and the solar intensity. Other factors such as PCM, thermal breaker, and load have directly affected the overall thermal resistance. Also, the calculated time for all thermal resistance results of the four experimental apparatus for the period (8:00-16:00) because after (16:00) the solar intensity values drop down to reaches zero (sunset). Figure (5-19) clarifies the overall thermal resistance for the two experimental apparatus (with and without thermal breaker and both without PCM) at 1 liter/hour load. It can be observed that the mostly the thermal resistance values of the system with a thermal breaker are higher than the without thermal breaker because the thermal breaker is considered thermal resistant prevents the axial conduction throughout the wall of the GAHP from the evaporator to condenser section and vice versa. Additionally, the phase change process of the working fluid (liquid to vapor in the evaporator section and the vapor condensate to be back liquid inside the condenser section). In the condenser section when the vapor of the working fluid condensate (condensation process), a phase change occurs from vapor to liquid during that process the latent heat is emitted to the wall of the heat pipe and then to the water. There are two types of condensation processes are film (which is the common one) and drop-wise condensation (which is more efficient). After the condensation process, the film layer

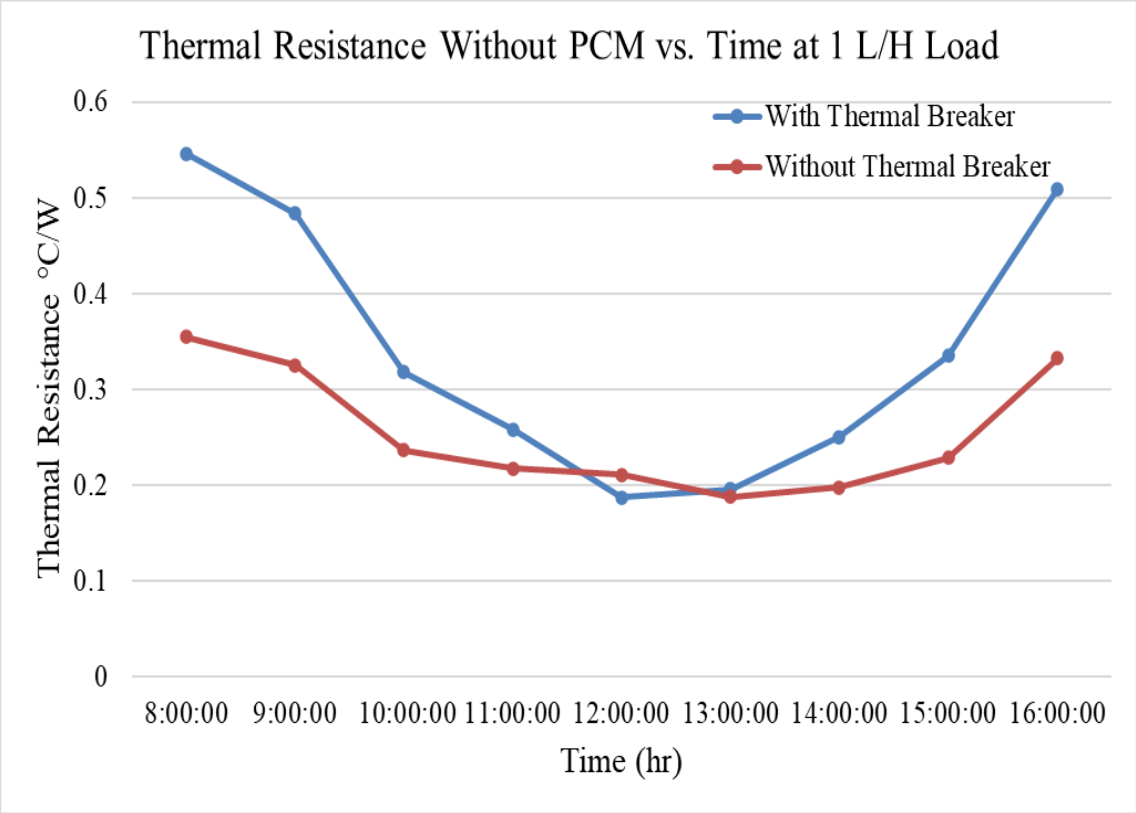

slips on the heat pipe wall by the advantage of the gravity to the evaporator section to gain latent heat and convert to vapor, and the cycle continues over and over. While, the drop-wise type, the working fluid condensate in the form of a droplet, and these droplets grown with time and drop down due to the gravity and flowing down through the GAHP wall to the evaporator section and the cycle repeated over and over. These two types (film and drop-wise) work as thermal resistance since both types (slip and flow) on the wall of the GAHP. As result, the blue line has both thermal resistance (Thermal breaker and phase change process thermal resistance), and the without thermal breaker (Red line) has only one (phase change process thermal resistance). For this reason, the experimental apparatus with a thermal breaker (Blue line) has higher thermal resistance values than the reference device (Red line) except at (12:00) due to the optimum solar intensity value at that time, thus the condenser section has almost the higher mean surface temperature.

Figure (5-19): Two Systems Thermal Resistance without PCM at 1 L/H Load

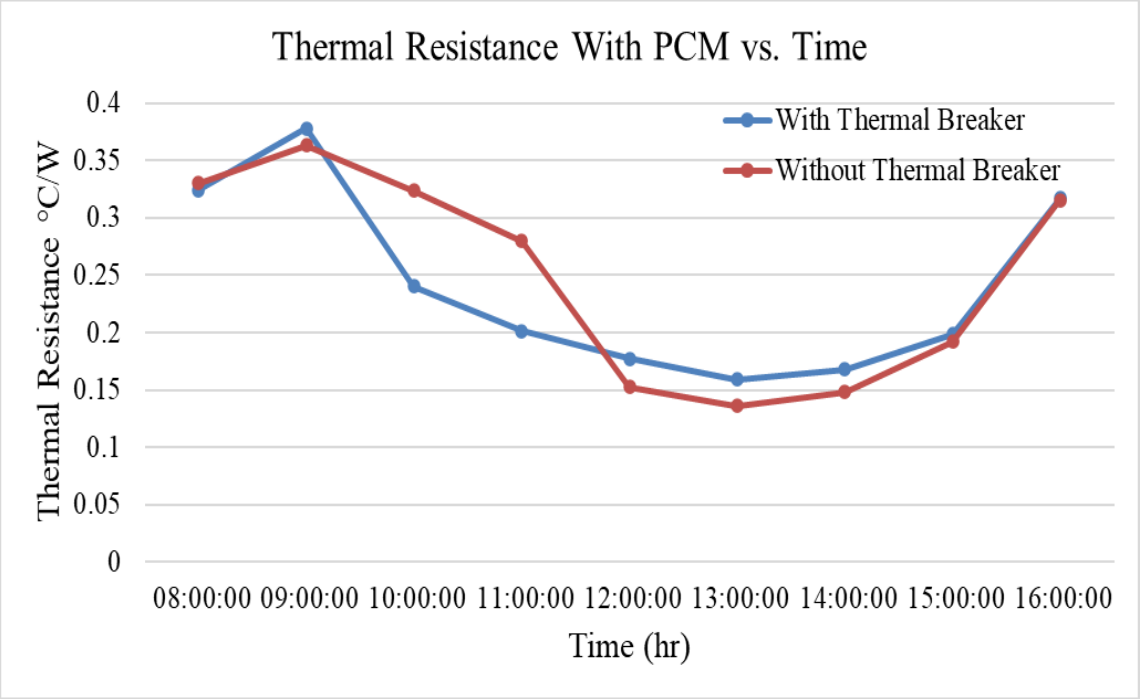

Figure (5-20) depicts the overall thermal resistance for the two experimental apparatus (with and without thermal breaker and both with PCM) at 1 liter/hour load. As described above, the difference in this figure is the PCM that affects the thermal resistance where the PCM decreases the overall thermal resistance in general for both with and without thermal breaker. Also, the blue line device with thermal breaker has slightly larger thermal resistance values than the red line device except from (9:00-11:00) as described above in figure (5-1) and (5-3) the experimental apparatus with PCM only (purple line) has the highest surface temperature distribution values in both sections because of the existence of the PCM. The PCM in the without thermal breaker apparatus during the sunshine absorbs the latent heat from the water storage tank, and that leads to an increase in the speed of the phase change process (increasing the film layer of the working fluid on the wall of the GAHP). Thus, increasing the thermal resistance during these specific operating hours.

Figure (5-20): Two Systems Thermal Resistance with PCM at 1 L/H Load

Figures (5-21) and (5-22) illustrate the overall thermal resistance for the two experimental apparatus (with and without thermal breaker and both without PCM), and

the other two devices (with and without thermal breaker and both with PCM) at 2 liter/hour load, respectively. It can be observed that the behavior of the overall thermal resistance values for the four devices at 2 liter/hour load have the same behavior of the overall thermal resistance values at 1 L/H load. Wherever the thermal resistance values

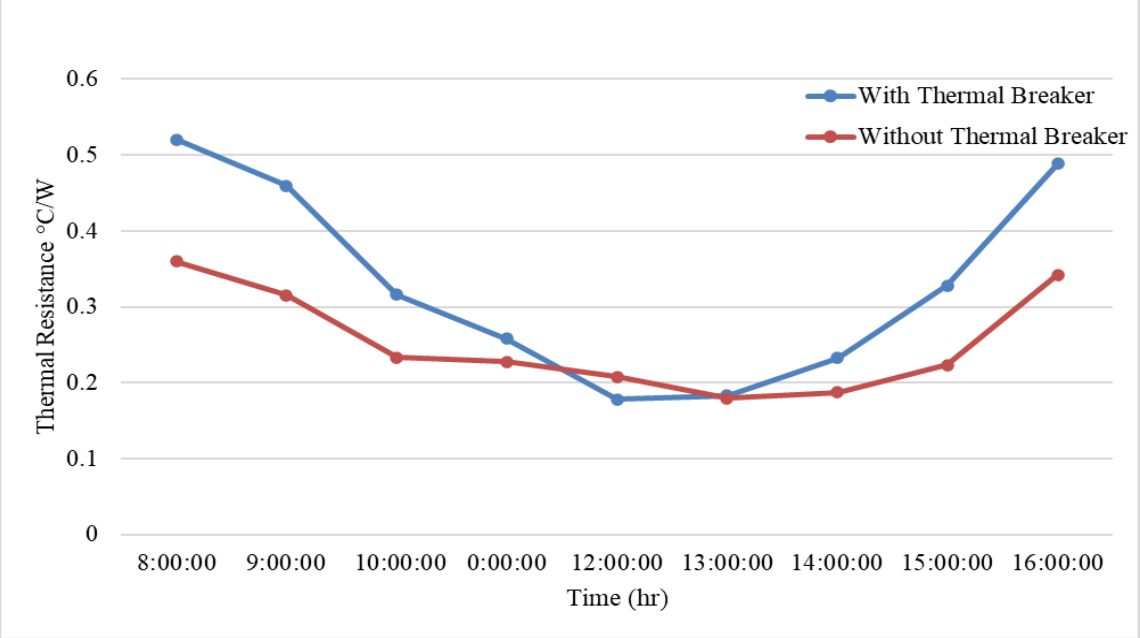

of the blue line device (with thermal breaker and without PCM) higher than the reference device (red line). Also, the blue line device with a thermal breaker with PCM has slightly larger thermal resistance values than the red line device except from (9:15-11:20) as described above in figures (5-6) and (5-8) the experimental apparatus with PCM only has the highest surface temperature distribution values in both sections because of the existence of the PCM. The only difference in the overall thermal resistance values between the 1 and 2 L/H loads is at 2 L/H load the overall thermal resistance values as general for both figures slightly lower than the values of the figures at 1 L/H. These are reasonable results because when the load increases (mass flow rate increases) the required time to transfer the demand thermal heat energy will be increasing too for all the units and parts (evaporator, condenser, water storage tank, PCM containers, and working fluid) especially gravity assistance heat pipe as described in figures (5-6) and (5-9), where the surface and core temperature distribution values through the GAHP at 2 L/H load decrease compared to the 1 L/H.

Figure (5-21): Two Systems Thermal Resistance without PCM at 2 L/H Load

Figure (5-22 ıt 2 L/H Load

5.7. Solar Intensity

The solar intensity of solar irradiance means the quantity of incoming solar radiation energy on the surface of the earth. Many factors determine the amount of this sun's energy such as the specific month of the year, time of the day, geographic location, and sun angle. As mentioned in chapter four Solar Power Meter TENMARS TM-207 measuring tool device was utilized to measure the amount of the solar irradiance during the experimental time and location. Figure (5-23) illustrates the solar intensity values during that time. It can be noticed that the solar intensity value at the first hour of the experimental apparatus operating is 502 W/m^2 at (8:00) until the sunset at (17:00) where the solar irradiance value is 0 W/m^2. Also, the optimum solar intensity value is 1249 W/m^2 at (12:00) as shown in the figure.

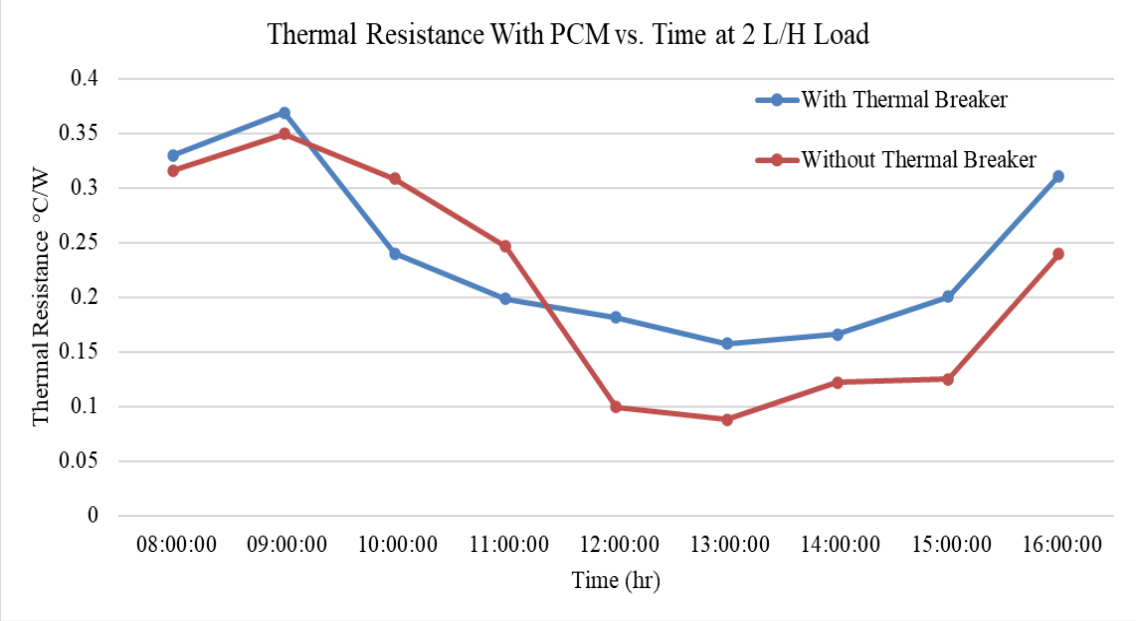

Figure ne

5.8. A Comparison between the 1&2 L/H Loads and Thermal Breaker and PCM Effects at Each Section

In this subsection, it will be discussed and compared between the temperature distribution values as well as the outlet water temperature for the four experimental

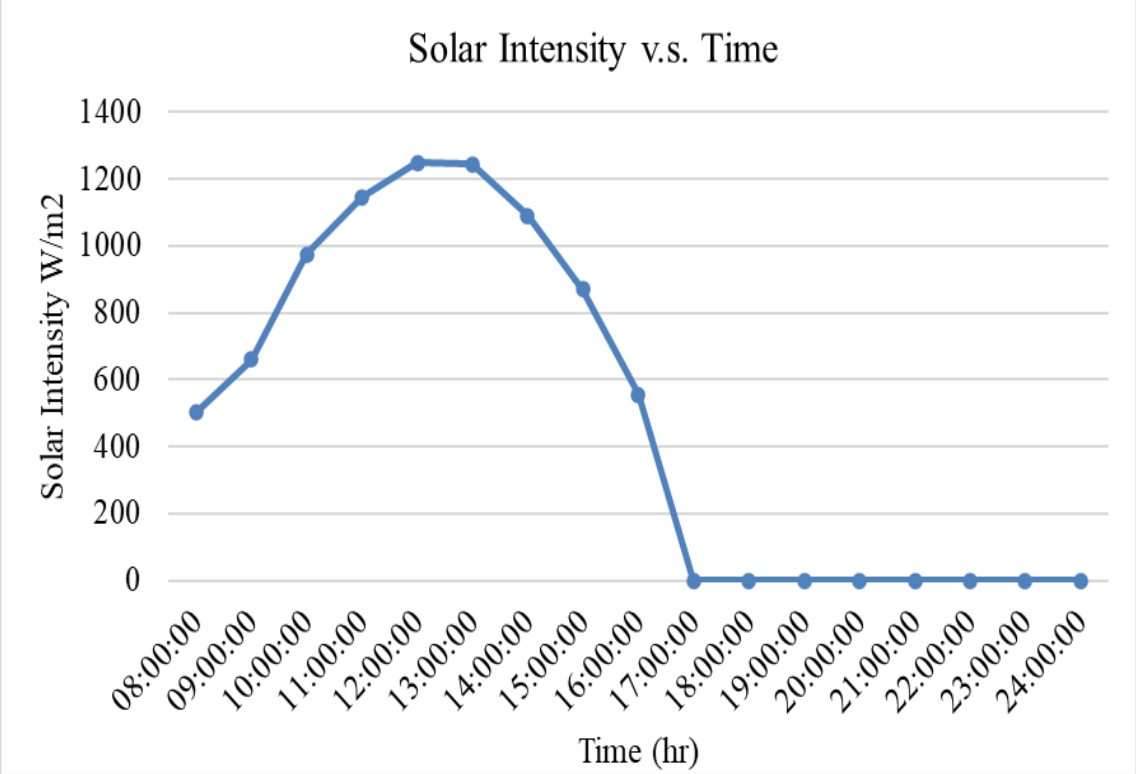

apparatus at 1 liter/Hour load and 2 liter/Hour load. For instance, comparison between the evaporator and condenser section (core and surface results) as well as, the outlet water temperature from the water storage tank for the four experimental apparatus at the two different loads as described in figure (5-1) to (5-10). Also, the daily efficiency, heat energy equivalent, and the overall thermal resistance at the two different loads as

described in figure (5-11) to (5-22). Two various periods will be chosen for the comparison during the sunshine and sunset. The comparison conducted in two periods the first was from (11:00 A.M – 1:00 P.M) and the second was from (10:00 – 12:00) P.M.

The first device without thermal breaker and with PCM (Purple line) for the evaporator section (surface and core) the temperature distribution values are (77.06, 75.6, 76.8)^{o} C and (75.95, 73.05, 74.55)^{o} C, and during the sunset are (22.06, 20.03, 17.67)^{o} C and (21.9, 19.95, 17.65)^{o} C at 1 Liter/Hour load. However, the temperature distribution values for the same period for the evaporator surface and core during the sunshine and sunset hours are (75.35, 72.56, 73.9)^{o} C and (81.5, 72.35, 73.8)^{o} C, and (20.1, 18.86, 17.96)^{o} C and (20.8, 19.5, 17.95)^{o} C at 2 Liter/Hour load.

Also, the reference device (Red line) for the evaporator section (surface and core) the temperature distribution values are (56.23, 61.96, 60.33)^{o} C and (70.55, 70.8, 68)^{o} C, and during the sunset are (22.06, 20.03, 17.67)^{o} C and (21.9, 19.95, 18.25)^{o} C at 1 Liter/Hour load. While the temperature distribution values for the same period for the evaporator surface and core during the sunshine and sunset hours are (55.53, 60.56, 58.13)^{o} C and (69.15, 70.1, 65.45)^{o} C, and (19.9, 19.7, 17.7)^{o} C and (20.65, 19.55, 17.49)^{o} C at 2 Liter/Hour load.

Furthermore, the third apparatus with thermal breaker without PCM (Blue line) the evaporator section (surface and core) the temperature distribution values are (64.43, 67.06, 69.13)^{o} C and (62.6, 64.4, 66.65)^{o} C, and during the sunsetare (20.13, 18.56, 18.2)^{o} C and (20.1, 18.6, 18.25)^{o} C at 1 Liter/Hour load. Whilst the temperature distribution values for the same period for the evaporator surface and core during the sunshine and sunset hours are (63.76, 65.7, 67.3)^{o} C and (61.25, 64.08, 66.05)^{o} C, and (20.3, 18.42, 18.13)^{o} C and (20.2, 18.4, 18.2)^{o} C at 2 Liter/Hour load.

Lastly, both thermal breaker and PCM device (Green line) for the evaporator section (surface and core) the temperature distribution values are (62.93, 63.46, 65.16)^{o} C and (60.65, 61.7, 63.45)^{o} C, and during the sunset are (22.4, 20.2, 18.03)^{o} C and (22.3, 20.4, 18.2)^{o} C at 1 Liter/Hour load. Nevertheless, the temperature distribution values for the same period for the evaporator surface and core during the sunshine and sunset hours are

(61.66, 62.96, 63.86)^{o} C and (59.85, 60.15, 61.7)^{o} C, and (22.4, 20.2, 18.03)^{o} C and (22.3, 20.4, 18.2)^{o} C at 2 Liter/Hour load.

For the condenser section (surface and core) the purple line device the temperature distribution values are (39.95, 53.6, 57.25)^{o} C and (46.05, 55.05, 55.55)^{o} C, and during the sunset are (19.25, 18.35, 18.05)^{o} C and (19.2, 18.25, 18.1)^{o} C at 1 Liter/Hour load. However, the temperature distribution values for the same period for the evaporator surface and core during the sunshine and sunset hours are (42.9, 58.25, 61.3)^{o} C and (45.05, 59.6, 62.85)^{o} C, and (18.35, 17.2, 16.7)^{o} C and (18.5, 17.35, 16.65)^{o} C at 2 Liter/Hour load.

Also, the reference device for the condenser section (surface and core) the temperature distribution values are (27.35, 31.45, 33.25)^{o} C and (40.55, 45.55, 45.6)^{o} C, and during the sunset are (17.8, 17.3, 17.25)^{o} C and (17.7, 17.2, 17.1)^{o} C at 1 Liter/Hour load. While the temperature distribution values for the same period for the evaporator surface and core during the sunshine and sunset hours are (25.35, 30.6, 32.3)^{o} C and (39.3, 42.5, 43.6)^{o} C, and (17.85, 17.35, 17.5)^{o} C and (17.6, 17.2, 17.2)^{o} C at 2 Liter/Hour load.

Furthermore, the third apparatus with thermal breaker without PCM the condenser section (surface and core) the temperature distribution values are (30.15, 40, 41)^{o} C and (31.75, 42, 45.85)^{o} C, and during the sunset are (20.2, 19.2, 18.85)^{o} C and (20.25, 19.2, 18.95)^{o} C at 1 Liter/Hour load. Whilst the temperature distribution values for the same period for the evaporator surface and core during the sunshine and sunset hours are (29.55, 40, 41)^{o} C and (19.35, 18.25, 18.35)^{o} C, and (31.35, 44, 45.55)^{o} C and (19.25, 18.35, 18.3)^{o} C at 2 Liter/Hour load.

Finally, both thermal breaker and PCM device for the condenser section (surface and core) the temperature distribution values are (36.25, 37.9, 42.3)^{o} C and (36.65, 38.75, 42.25)^{o} C, and during the sunset are (26.4, 24.55, 24.55)^{o} C and (26.4, 24.4, 24.45)^{o} C at 1 Liter/Hour load. Nevertheless, the temperature distribution values for the same period for the evaporator surface and core during the sunshine and sunset hours are (35.4, 36.75, 41.25)^{o} C and (35.65, 37.65, 41.1)^{o} C, and (24.45, 21.3, 17.2)^{o} C and (23.7, 19.8, 17.6)^{o} C at 2 Liter/Hour load.

The maximum outlet water temperature values for the (Purple line) device at the period (1:00-4:00) P.M are (43.6, 43.5, 44.4, 44)^{o}C at 1 Liter/Hour load. However, the values at 2 Liter/Hour load for the same period are (42.4, 42.8, 43.1, 42.2)^{o} C.

The maximum outlet water temperature values for the reference apparatus which are at the period (1:00-3:00) P.M which are (43, 43.5, 44)^{o}C at 1 Liter/Hour load. However, the values at 2 Liter/Hour load for the same period are (42.1, 43, 43.5)^{o} C.

The maximum outlet water temperature values for the (Blue line) apparatus are at the period (1:00-3:00) P.M which are (42.6, 42.8, 43.1)^{o}C at 1 Liter/Hour load. However, the values at 2 Liter/Hour load for the same period are (40.1, 41, 40.7)^{o} C.

The maximum outlet water temperature values for the both features (Green line) apparatus which are at the period (1:00-4:00) P.M are (40.2, 42.3, 43.8, 43.5)^{o}C at 1 Liter/Hour load. However, the values at 2 Liter/Hour load for the same period are (38.8, 40.9, 42.8, 43)^{o} C.

Generally, according to the results above, the effect and the precious benefit of adding a thermal breaker within the adiabatic section in the GAHP, PCM within the storage tank system, or adding both thermal breaker and PCM together in the solar collector apparatus will be discussed clearly for the whole sections of the experimental device. For instance, the thermal breaker allows the heat energy transfer from the evaporator to condenser sections through the working fluid (phase change convection heat transfer) only (there is no axial conduction heat transfer), and that leads to concentrate the temperature distribution on the surface of the evaporator. However, the PCM absorbs part of the transferred heat energy of the water storage tank in order to store this thermal heat energy and compensate it for the temperature reduction of the water during the night. As result, the PCM is not directly affecting the surface temperature of the evaporator, but it affects the working fluid.

In the condenser section, the GAHP with thermal breaker devices higher than the without devices. It could be debated to the heat energy that is transferred from the working fluid to the surface of GAHT in the condenser section is stored (the temperature will not transfer back to the evaporator since the existence of the thermal break). Also,

the PCM compensates for the reduction temperature of the water during the absence of sunlight. Moreover, a high amount of heat energy escapes to the evaporator section through the GAHP (surface and core).

For the solar collector system with both features (Thermal breaker and PCM), where the thermal breaker prevents the axial conduction from the condenser section (water storage tank) to the evaporator section, and it provides the necessary heat energy to the PCM storage tanks during the sunny hours. Moreover, it resists thermally the heat energy from transferring from the storage tank (condenser section) to the evaporator section throughout the night hours, and that leads to saving most of the water temperature especially during the night. Particularly, the water lost its heat energy for the system with both thermal break and PCM is much less than the other three systems at each hour during the operating hours especially at night hours. That leads to the water with both thermal breaker and PCM system maintain its heat energy mostly (keeping it possible hot during the coldest weather). That means the experimental apparatus with both thermal breaker and PCM has valuable beneficial temperature distribution values during the full operating hours. Eventually, this device is deemed the most precious device compared to the three other apparatus based on adding thermal breaker and PCM together. In other words, it is the most advantageous and lowest disadvantage device during operating hours.

The temperature distribution values difference between the four experimental apparatus at each specific part (evaporator, condenser, and water storage tank) have been discussed briefly above in each section. It can be observed that the behavior of the surface, core, and outlet water temperature distribution for the four experimental apparatus at 2 liter/hour load is mostly similar to the behavior of the surface, core, and outlet water temperature distribution for the 1 liter/hour load. Only except for the 2 liter/hour load the temperature distribution values for the four empirical devices sections are lower than the temperature distribution values of 1 liter/hour load. These are reasonable results because when the mass flow rate increases the required time to transfer the demand thermal heat energy will be increasing too for all the units and parts (evaporator, condenser, water storage tank, PCM containers, and working fluid), especially to the water storage tank.

Also, when the load increases (flow rate increase) the thermal breaker disadvantage through the sunshine will be decreasing until there is not any considerable disadvantage through the sunshine. On the other hand, the advantage of the thermal breaker during sunset will be noticeable and increased especially when adding a PCM compared to the without thermal breaker apparatus.

For the daily efficiency, the thermal breaker enhances the daily efficiency by extending the total operating hours of the solar collector around (3 Hours). Also, the system with PCM higher than the without PCM because the PCM prevents the system shutdown (working with thermal breaker) and compensates for the heat energy lost from the water storage tank. Also, the system with both thermal breaker and PCM has the highest daily efficiency since the thermal breaker prevents the heat energy leaks out between the sections and the PCM compensates for the reduction in the water temperature. Additionally, there was a difference in the daily efficiency values when the load was changed. For example, when the load is 2 Liter/Hour the daily efficiency values of the four experimental devices are higher than the daily efficiency values at 1 Liter/Hour load since the daily efficiency has a proportional relationship with the useful heat energy (when the load increases the mass flow rate increase too and useful heat energy depend on the mass flow rate, so it is increased too.

For the heat energy equivalent, the PCM is extending the advantage of the thermal breaker during the sunset by increasing the useful and equivalent heat energy with the thermal breaker (gained one hour compared to the system without PCM) until (24:00). The behavior of the equivalent heat energy with PCM at 2 L/H load is clearly different from the behavior of the equivalent heat energy with PCM at 1 L/H load since the advantage of adding the two features to the experimental device is obviously clear when the load increase (the advantage of axial conduction is compared to the thermal breaker advantage during the sunshine will be approximately equivalent). Overall, this solar collector system type has the optimum advantage and the longest positive equivalent heat energy over the other three systems as explained in the figure below.

Lastly, the thermal breaker is considered thermal resistant prevents the axial conduction throughout the wall of the GAHP from the evaporator to the condenser section and vice

versa. Additionally, the phase change process of the working fluid (liquid to vapor in the evaporator section and the vapor condensate to be back liquid inside the condenser section) is deemed a secondary thermal resistance. The only difference in the overall thermal resistance values between the 1 and 2 L/H loads is at 2 L/H load the overall thermal resistance values as general for the four systems slightly lower than the values at 1 L/H. When the load increases (mass flow rate increases) the required time to transfer the demand thermal heat energy will be increasing too for the system as described above in figures (5-6) and (5-9), where the surface and core temperature distribution values through the GAHP at 2 L/H load decrease compared to the 1 L/H.

Finally, when the load increases (flow rate increase) the thermal breaker disadvantage through the sunshine will be decreasing until there is not any considerable disadvantage through the sunshine. On the other hand, the advantage of the thermal breaker during sunset will be noticeable and increased especially when adding a PCM compared to the without thermal breaker apparatus. Lastly, the apparatus with both thermal breaker and PCM is considered the most advantageous and lowest disadvantage device during operating hours.

5.9. The Numerical Results

The Gravity Assistance Heat Pipe mathematical model has been analyzed by solving the partial differential equations to obtain the temperature distribution profiles of the present system by utilizing a numerical analysis (MATLAB Software) for recommended future works. The MATLAB code creates to solve cylindrical coordinates (Transient Heat Problem) by utilizing a Finite Difference Method (FDM). Also, the type of the boundary conditions (BC) is Dirichlet Conditions that are used in the creating code and the fix

initial condition (Temperature). The Graphical results below represent the two regions of the GAHP evaporator sections (Liquid and vapor) at different time throughout the operating time of the GAHP-ETSC system at 2 Liter/ Hour load (with and without thermal breaker and both with PCM) as shown in Figure (5-24) to figure (5-31). Figure (5-24) and figure (5-25) represent the GAHP evaporator section of an experimental apparatus without thermal breaker and with PCM, and with both thermal breaker and PCM, respectively at a 2 L/H load during (10 AM). It can be noticed that the maximum temperature of the system without a thermal breaker is around 69^{o} C since the axial conduction heat transfer during the sunshine as explained. However, the maximum temperature of the system with a thermal breaker is around 57^{o} C as shown in the figures, respectively.

Also, Figures (5-26) and (5-27) clarify the GAHP evaporator section of an experimental apparatus without thermal breaker and with PCM, and with both thermal breaker and PCM, respectively at a 2 L/H load during (17:00). It can be observed that the maximum temperature of the system without thermal breaker is around 64^{o} C and the system with

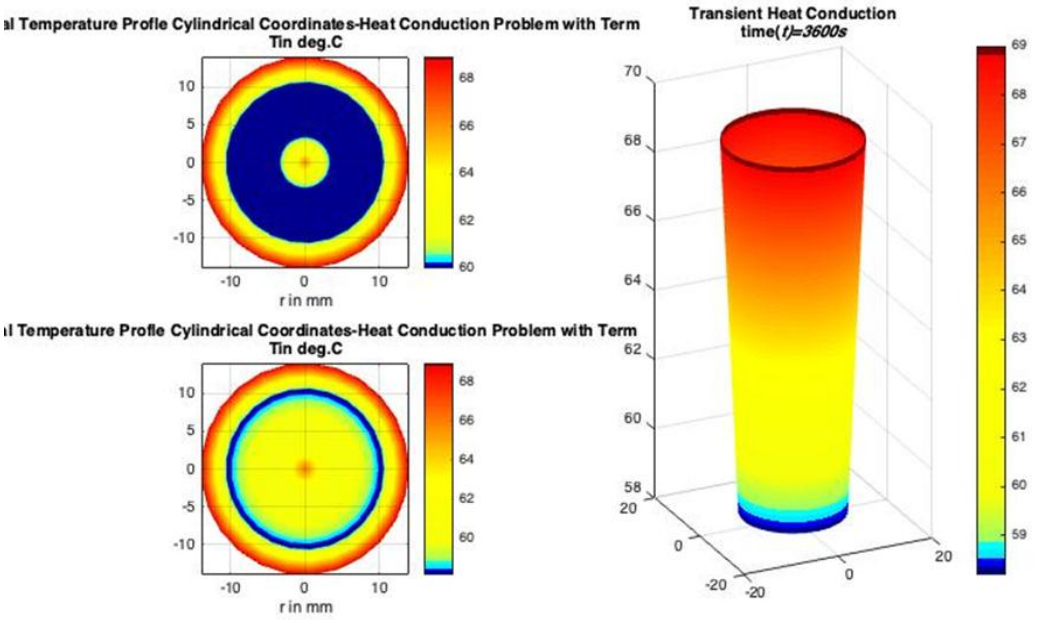

thermal breaker is around 44^{o} C. Similarly, figures (5-28) and (5-29) represent the GAHP evaporator section of an experimental apparatus without thermal breaker and with PCM, and with both thermal breaker and PCM, respectively at a 2 L/H load during (22:00). It can be observed that the maximum temperature of the system without a thermal breaker is around 27^{o} C and the system with a thermal breaker is around 19^{o} C. The reason behind that is, as described before at (17:00) the solar intensity value starts to be zero, and it continues to be zero until (24:00), thus the two systems without thermal breaker have a respectable amount of the heat energy leaks out to the evaporator section through the GAHP (surface and core) from the condenser section (water storage tank). However, the other two systems with thermal breaker have lower temperature values than the without thermal breaker systems due to the advantage of the thermal breaker during the sunset, as illustrated in the figures, respectively.

Figure (5-24): Temperature Profiles without Thermal Br. and with PCM at 10 AM

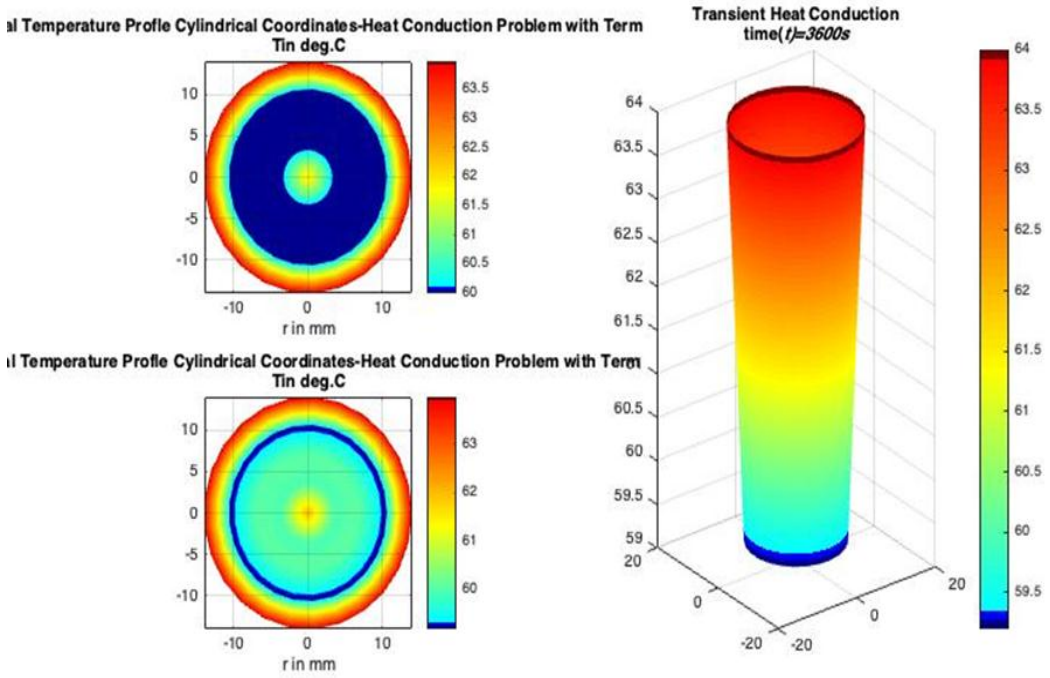

Figure (5-25): Temperature Profiles with Both Thermal Breaker & PCM at 10 AM

Figure (5-26): Temperature Profiles without Thermal Br. and with PCM at 5 PM

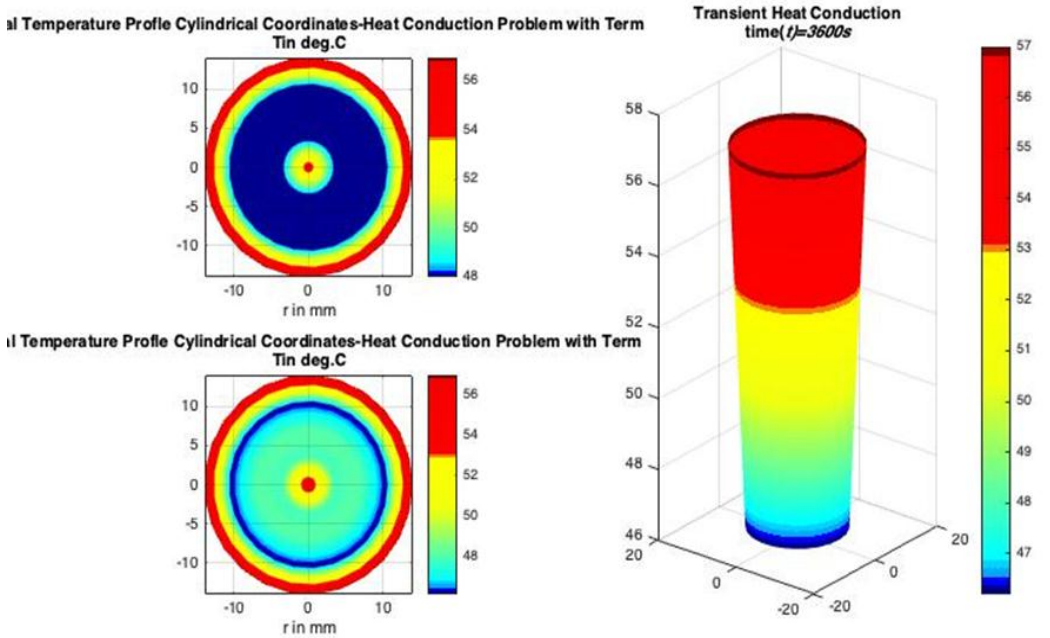

Figure (5-27): Temperature Profiles with Both Thermal Breaker & PCM at 5 PM

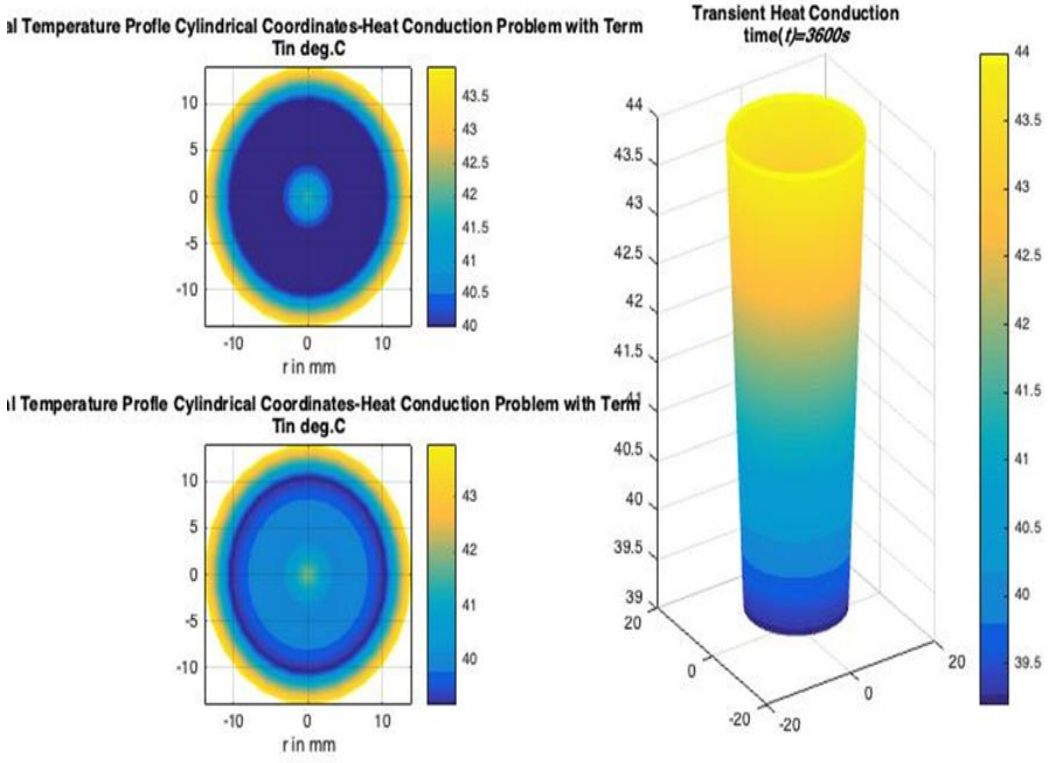

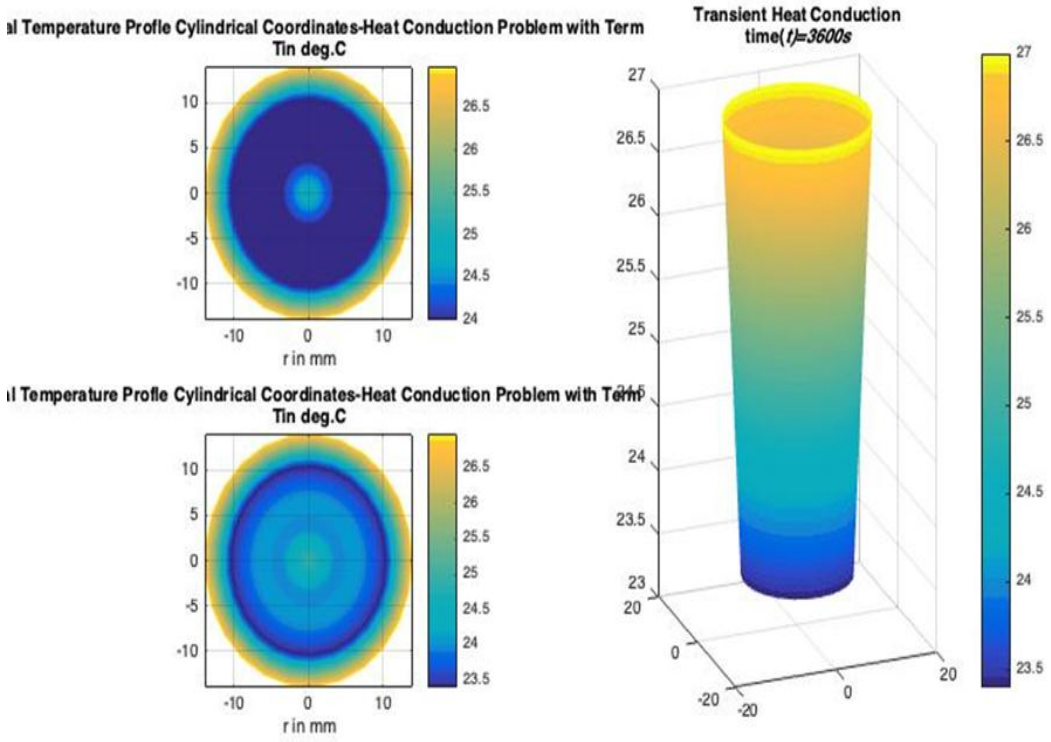

Figure (5-28): Temperature Profiles without Thermal Br. and with PCM at 10 PM

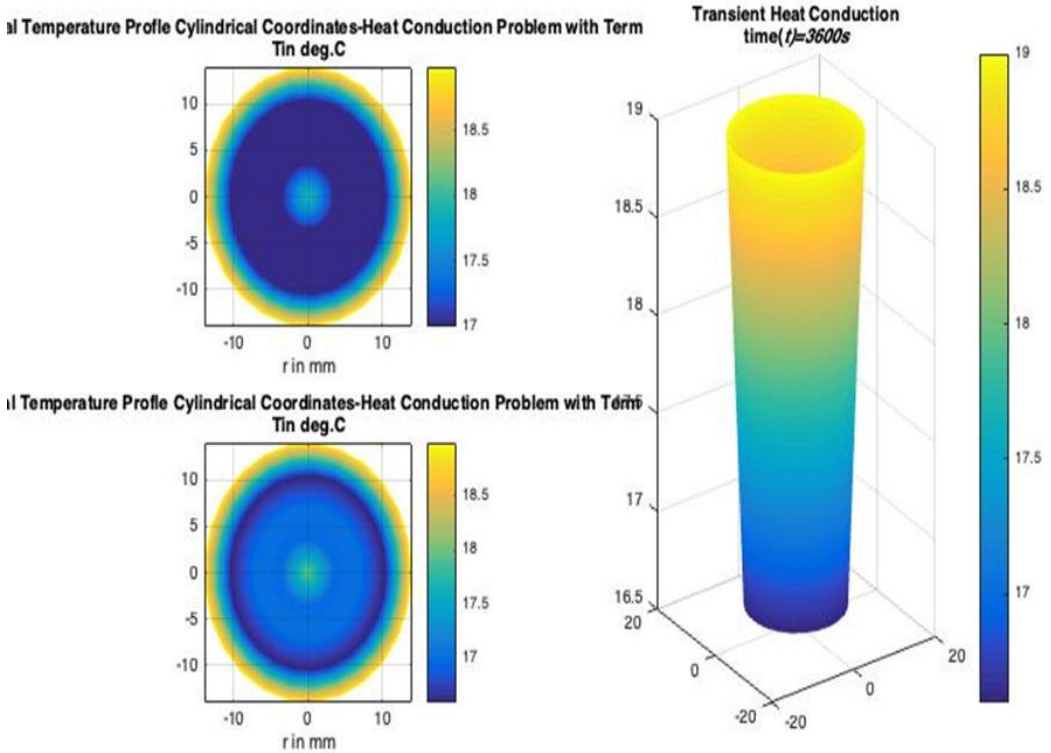

Figure (5-29): Temperature Profiles with Both Thermal Breaker & PCM at 10 PM

5.10. Validation of Numerical and Experimental Results

In this section, two validations between the numerical and experimental results have been presented for the surface temperature distribution along the evaporator section (two regions vapor and liquid). Figures (5-30) and (5-31) represent the validation between the numerical and experimental results for the device with both thermal breaker and PCM, and the other device without thermal breaker and with PCM, respectively; both cases at a 2 Liter/Hour load.

It can be observed that the minimum and maximum percentage of error values between the numerical and experimental results are (2.54 %) at (10:00) and (9.52%) at (22:00), respectively for the solar collector with both thermal breaker and PCM as shown in figure (5-30). However, the minimum and maximum percentage of error values between the numerical and experimental results are (3.2 %) at (10:00) and (16.53%) at (22:00), respectively for the solar collector without thermal breaker and with PCM as presented in figure (5-31).

In figure (5-30), the numerical results have an excellent validity along the GAHP evaporator section (vapor and liquid regions) with experimental results, and after (20:00) the experimental results started to rise above the blue line due to the high advantage of using both thermal breaker and PCM together especially during the sunset hours. Also, the PCM melting point temperature is 43°C that used in the numerical simulation. However, a range of the PCM melting point temperature values are (38°C) to (43°C) which are utilized in the experimental calculation.

However, in figure (5-31) the numerical results have a very good validity along the GAHP evaporator section (vapor and liquid regions) with experimental results. Also, the behavior of both results is almost similar where the experimental results temperature distribution values are lower than the numerical results due to the absence of the thermal breaker advantages specifically throughout the evening hours. Also, the PCM melting point temperature is 43°C that used in the numerical simulation (only one PCM melting

temperature value). However, a range of the PCM melting point temperature values are

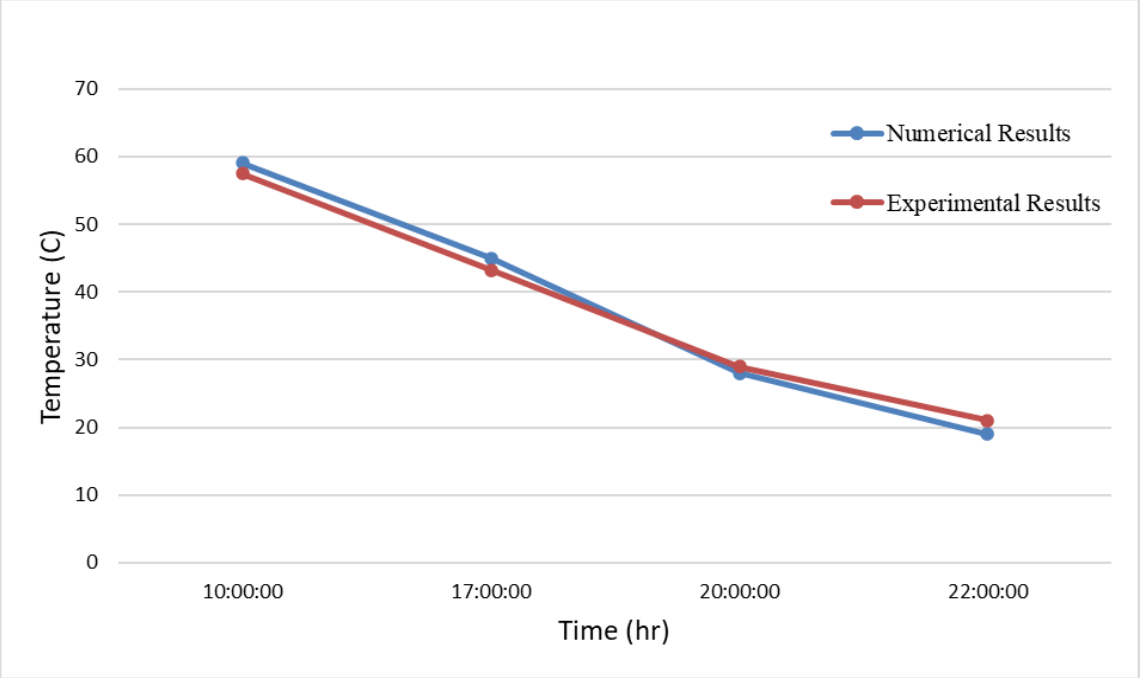

(38°C) to (43°C) which are utilized in the experimental calculation.

Figure (5-30): Validation Between Numerical and Experimental Results with Both

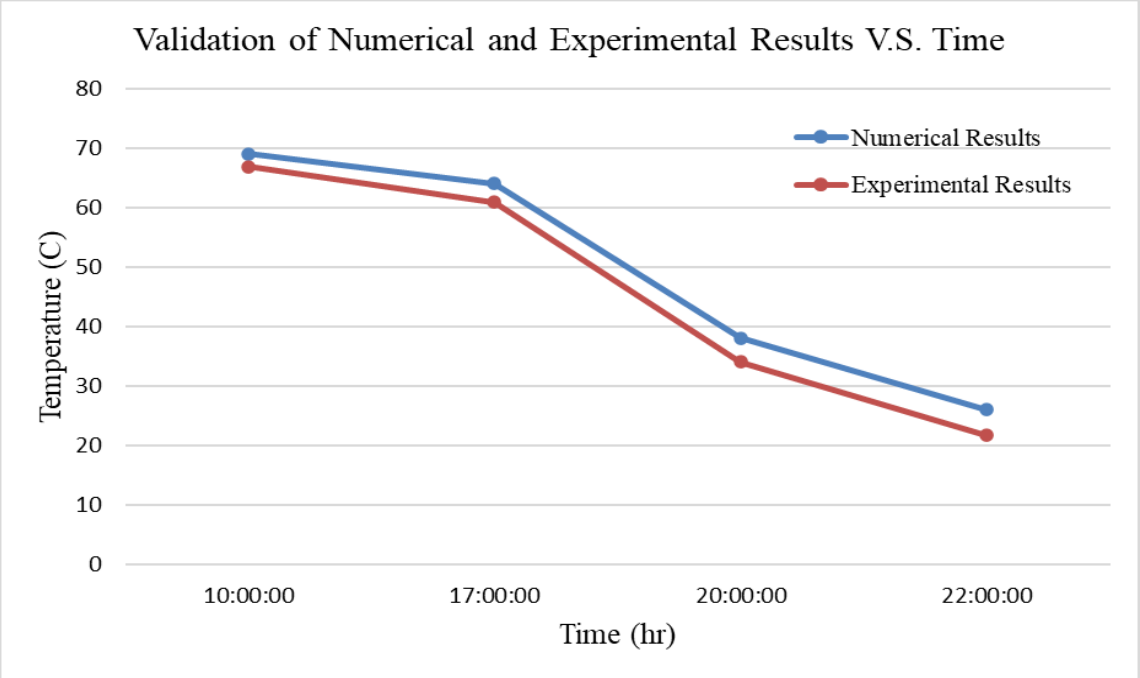

Thermal Breaker & PCM at 2 Liter/Hour Load

Figure (5-31): Validation Between Numerical and Experimental Results without Thermal Breaker and with PCM at 2 Liter/Hour Load

CHAPTER SIX

Conclusion & Recommendations

6.1. Conclusion

The fundamental targets and objectives of this thesis have been accomplished. Four experimental apparatuses models are two GAHP-ETSC with and without PCM and both with thermal breaker, and the other two with and without PCM and both without thermal breaker have been manufactured, developed, and operated to achieve the assessments of the desired system.

In this thesis, two cases studies with the four various system models were performed which were divided based on the water load amount. The first and second cases are studying the influence of applying 1 L/H load and 2 L/H load of water on the daily efficiency and performance of the four various experimental devices, respectively. Also, each case investigates the effect of applying the specific load on each experimental device individually in order to illustrate and demonstrate the influence of the thermal breaker with PCM on enhancing and improving the performance of the ETSC, especially during the demand period.

The thermal breaker allows the heat energy transfer from the evaporator to condenser sections through the working fluid only. However, the PCM absorbs part of the transferred heat energy of the water storage tank in order to store this thermal heat energy and compensate it for the temperature reduction of the water during the night.

The behavior of the surface, core, and outlet water temperature distribution for the four experimental apparatus at (1&2) liter/hour load are mostly similar. Only except for the temperature distribution values for the four empirical devices sections at 2 liter/hour load are lower than at 1 liter/hour load. These are reasonable results because when the mass flow rate increases the required time to transfer the demand thermal heat energy will be increasing too for all parts, especially to the water storage tank.

The thermal breaker enhances the daily efficiency by extending the total operating hours of the solar collector around (3 Hours). The system with both thermal breaker and PCM has the highest daily efficiency since the thermal breaker prevents the heat energy leaks out between the (condenser-evaporator) sections, and the PCM compensates for the reduction in the water temperature. Also, the PCM is extending the advantage of the

thermal breaker during the sunset by increasing the useful and equivalent heat energy with the thermal breaker (gained one hour compared to the system without PCM) until (24:00). Particularly, the water lost its heat energy for the system with both thermal break and PCM is much less than the other three systems at each hour during the operating hours especially at night hours. That leads to the water with both thermal breaker and PCM system maintain its heat energy mostly (keeping it possible hot during the coldest weather).

When the load increases (mass flow rate increases) the required time to transfer the demand thermal heat energy will be increasing too for the system. Also, the thermal breaker disadvantage through the sunshine will be decreasing until there is not any considerable disadvantage through the sunshine. On the other hand, the advantage of the thermal breaker during sunset will be noticeable and increased especially when adding a PCM compared to the without thermal breaker apparatus. Where, the improvement percentage between the apparatus with both thermal breaker and PCM and the apparatus without both is 55% and 55.5% at 1 L/H and 2 L/H load, respectively based on the water outlet temperature.

Lastly, the apparatus with both thermal breaker and PCM is considered the most advantageous and lowest disadvantage device during operating hours and has the optimum advantage and the longest positive equivalent heat energy over the other three systems.

Validation between the present work and previous studies has been achieved. Two previous researchers' studies were utilized to compare with the present work in order to disclose the advantage and the better performance of the present work than others. The validation showed that the present work had the highest efficiency and thermal resistance among the other two researchers.

6.2. Future Works & Recommendations

For future works, the Gravity Assistance Heat Pipe mathematical model has been analyzed by solving the partial differential equations to obtain the temperature distribution profiles of the present system by utilizing a numerical analysis (MATLAB Software). The MATLAB code creates to solve cylindrical coordinates (Transient Heat Problem) by utilizing a Finite Difference Method (FDM).

Two validations between the numerical and experimental results have been presented for the surface temperature distribution along the evaporator section (two regions vapor and liquid). The first device with both thermal breaker and PCM, and the other device without thermal breaker and with PCM, respectively; both cases at a 2 Liter/Hour load. The minimum and maximum percentage of error values between the numerical and experimental results are (2.54 %) at (10:00) and (9.52%) at (22:00), respectively for the solar collector with both thermal breaker and PCM. However, (3.2 %) at (10:00) and (16.53%) at (22:00), respectively for the solar collector without thermal breaker and with PCM.

The following suggestions can be recommended for future works:

- Develop the presented MATLAB code to solve and simulate the whole GAHP-ETSC system.
- Add additive materials to the space between the evacuated tube glass and the GAHP such as (Nanofluids, Nanoparticles, and PCM, …etc.,).
- Try to use another type of PCM with higher thermal conductivity.
- Integrate a sun tracking system to embedded with the solar collector system to increase the solar intensity that falling on the ETSC.
- Install fins on the surface of the GAHP to enhance thermal efficiency.

References

References

[1] S. Mekhilef, R. Saidur, and A. Safari, "A review on solar energy use in industries," *Renew. Sustain. Energy Rev.*, vol. 15, no. 4, pp. 1777–1790, 2011, doi: 10.1016/j.rser.2010.12.018.

[2] A. N. Al-Shamani, M. D. Faisal, and H. H. Abada, "Proposed Solar Powered Water Heating System for Babylon – Iraq Using Transient System Simulation (Trnsys) Tool," *J. Mech. Contin. Math. Sci.*, vol. 15, no. 5, pp. 101–111, 2020, doi: 10.26782/jmcms.2020.05.00009.

[3] S. Kumar, "Renewable Energy: Emerging Trends, Potential in India and Its Improvement," pp. 57–69.

[4] International Energy Agency, "Snapshot of Global Photovoltaic Markets - 2018," *Rep. IEA PVPS T1-332018*, pp. 1–16, 2018.

[5] B. I. Gaëtan, Masson and B. I. Mary, Brunisholz, "Snapshot of global photovoltaic markets," *Rep. IEA PVPS*, pp. 1–19, 2016.

[6] IEA-Pvp, "Snapshot of Global PV Markets 2020," *Www.Iea-Pvps.Org*, pp. 1–16, 2020, [Online]. Available: http://www.iea-pvps.org/fileadmin/dam/public/report/technical/PVPS_report_-_A_Snapshot_of_Global_PV_-_1992-2014.pdf.

[7] Africa-EU Renewable Energy Cooperation Programme (RECP), "Global Market Outlook - For Solar Power/2017-2021," *Sol. Power Eur.*, p. 58, 2017.

[8] K. Chopra, A. K. Pathak, V. V. Tyagi, A. K. Pandey, S. Anand, and A. Sari, "Thermal performance of phase change material integrated

heat pipe evacuated tube solar collector system: An experimental assessment," *Energy Convers. Manag.*, vol. 203, no. November 2019, 2020, doi: 10.1016/j.enconman.2019.112205.

[9] I. Budihardjo, G. L. Morrison, and M. Behnia, "Natural circulation flow through water-in-glass evacuated tube solar collectors," *Sol. Energy*, vol. 81, no. 12, pp. 1460–1472, 2007, doi: 10.1016/j.solener.2007.03.002.

[10] F. Abdalla, P. Tuohy, D. Evans, and P. Blackwell, "A Review of Integrated Phase Change Materials for Evacuated Tube Solar Collector System," pp. 379–390, 2018.

[11] P. Feliński and R. Sekret, "Effect of PCM application inside an evacuated tube collector on the thermal performance of a domestic hot water system," *Energy Build.*, vol. 152, pp. 558–567, 2017, doi: 10.1016/j.enbuild.2017.07.065.

[12] A. Kumar, Z. Said, and E. Bellos, "An up-to-date review on evacuated tube solar collectors," *J. Therm. Anal. Calorim.*, no. June, 2020, doi: 10.1007/s10973-020-09953-9.

[13] A. A. Eidan, M. J. Alshukri, M. Al-fahham, A. AlSahlani, and D. M. Abdulridha, "Optimizing the performance of the air conditioning system using an innovative heat pipe heat exchanger," *Case Stud. Therm. Eng.*, vol. 26, no. May, p. 101075, Aug. 2021, doi: 10.1016/j.csite.2021.101075.

[14] R. Daghigh and A. Shafieian, "An experimental study of a heat pipe evacuated tube solar dryer with heat recovery system," *Renew.*

Energy, vol. 96, pp. 872–880, 2016, doi: 10.1016/j.renene.2016.05.025.

[15] H. Olfian, S. S. M. Ajarostaghi, and M. Ebrahimnataj, "Development on evacuated tube solar collectors: A review of the last decade results of using nanofluids," *Sol. Energy*, vol. 211, no. July, pp. 265–282, 2020, doi: 10.1016/j.solener.2020.09.056.

[16] R. Andrzejczyk, "Experimental investigation of the thermal performance of a wickless heat pipe operating with different fluids: Water, ethanol, and SES36. Analysis of influences of instability processes at working operation parameters," *Energies*, vol. 12, no. 1, 2019, doi: 10.3390/en12010080.

[17] R. AL-HARIS, "EXPERIMENTAL AND THEORETICAL INVESTIGATION OF HEAT PIPE COLLECTOR USING PHASE CHANGE MATERIALS PCM," 2018.

[18] A. Sharma, V. V. Tyagi, C. R. Chen, and D. Buddhi, "Review on thermal energy storage with phase change materials and applications," *Renew. Sustain. Energy Rev.*, vol. 13, no. 2, pp. 318–345, 2009, doi: 10.1016/j.rser.2007.10.005.

[19] A. Abhat, "Low temperature latent heat thermal energy storage: Heat storage materials," *Sol. Energy*, vol. 30, no. 4, pp. 313–332, 1983, doi: 10.1016/0038-092X(83)90186-X.

[20] M. J. Alshukri, A. A. Eidan, and S. I. Najim, "Thermal performance of heat pipe evacuated tube solar collector integrated with different types of phase change materials at various location," *Renew. Energy*,

vol. 171, pp. 635–646, Jun. 2021, doi: 10.1016/j.renene.2021.02.143.

[21] R. Daghigh and A. Shafieian, “Energy-exergy analysis of a multipurpose evacuated tube heat pipe solar water heating-drying system,” *Exp. Therm. Fluid Sci.*, vol. 78, pp. 266–277, 2016, doi: 10.1016/j.expthermflusci.2016.06.010.

[22] P. Behnam and M. B. Shafii, “Examination of a solar desalination system equipped with an air bubble column humidifier, evacuated tube collectors and thermosyphon heat pipes,” *Desalination*, vol. 397, pp. 30–37, 2016, doi: 10.1016/j.desal.2016.06.016.

[23] T. ting Zhu, Y. hua Zhao, Y. hua Diao, F. F. Li, and Z. hua Quan, “Experimental investigation and performance evaluation of a vacuum tube solar air collector based on micro heat pipe arrays,” *J. Clean. Prod.*, vol. 142, pp. 3517–3526, 2017, doi: 10.1016/j.jclepro.2016.10.116.

[24] M. A. Essa and N. H. Mostafa, “Theoretical and experimental study for temperature distribution and flow profile in all water evacuated tube solar collector considering solar radiation boundary condition,” *Sol. Energy*, vol. 142, pp. 267–277, 2017, doi: 10.1016/j.solener.2016.12.035.

[25] S. Sobhansarbandi, P. M. Martinez, A. Papadimitratos, A. Zakhidov, and F. Hassanipour, “Evacuated tube solar collector with multifunctional absorber layers,” *Sol. Energy*, vol. 146, pp. 342–350, 2017, doi: 10.1016/j.solener.2017.02.038.

[26] W. Kong *et al.*, “Test method for evaluating and predicting thermal

performance of thermosyphon solar domestic hot water system," *Appl. Therm. Eng.*, vol. 146, pp. 12–20, 2019, doi: 10.1016/j.applthermaleng.2018.09.086.

[27] A. A. Eidan, A. AlSahlani, A. Q. Ahmed, M. Al-fahham, and J. M. Jalil, "Improving the performance of heat pipe-evacuated tube solar collector experimentally by using Al2O3 and CuO/acetone nanofluids," *Sol. Energy*, vol. 173, no. July, pp. 780–788, Oct. 2018, doi: 10.1016/j.solener.2018.08.013.

[28] S. Ali, "Controlled Vibration System to Enhance the Performance of Heat pipe Evacuated Tube solar collector Integrated with PCM," 2020.

[29] P. Feliński and R. Sekret, "Experimental study of evacuated tube collector/storage system containing paraffin as a PCM," *Energy*, vol. 114, pp. 1063–1072, 2016, doi: 10.1016/j.energy.2016.08.057.

[30] W. Guo and D. W. Nutter, "An experimental study of axial conduction through a thermosyphon pipe wall," *Appl. Therm. Eng.*, vol. 29, no. 17–18, pp. 3536–3541, 2009, doi: 10.1016/j.applthermaleng.2009.06.008.

[31] M. J. Alshukri, A. A. Eidan, and S. I. Najim, "The influence of integrated Micro-ZnO and Nano-CuO particles/paraffin wax as a thermal booster on the performance of heat pipe evacuated solar tube collector," *J. Energy Storage*, vol. 37, p. 102506, 2021, doi: https://doi.org/10.1016/j.est.2021.102506.

[32] R. Tang and Y. Yang, "Nocturnal reverse flow in water-in-glass

evacuated tube solar water heaters," *Energy Convers. Manag.*, vol. 80, pp. 173–177, 2014, doi: 10.1016/j.enconman.2014.01.025.

[33] F. P. I. and D. P. Theodor L., Adrienne S., *Fundamentals of Heat and Mass Transfer*, SEVENTH ED. 111 River Street, Hoboken, NJ: John Wiley & Sons, Inc., 2011.

[34] G. E. Myers, *Analytical methods in conduction heat transfer*. United States: McGraw-Hill Book Company, 1971.

[35] B. K. Dutta, *Scilab Textbook Companion for Principles Of Heat Transfer Book Description*. 2014.

[36] J.P. Holman (Department of Mechanical Engineering and Southern Methodist University, *Experimental Methods for Engineers*, E I G H T., vol. s1-VIII, no. 193. 1221 Avenue of the Americas, New York, NY 10020: McGraw-Hill, a business unit of The McGraw-Hill Companies, Inc., 2011.

[37] Q. Li, C. Wang, Y. Wang, Z. Wang, H. Li, and C. Lian, "Study on the effect of the adiabatic section parameters on the performance of pulsating heat pipes," *Appl. Therm. Eng.*, vol. 180, no. July, p. 115813, Nov. 2020, doi: 10.1016/j.applthermaleng.2020.115813.

[38] R K Rajput, *Heat and Mass Transfer rajput.pdf*, Revised Ed., vol. 2 &3. 2002.

[39] L. M. Jiji, *Heat Convection*. Berlin, Heidelberg: Springer Berlin Heidelberg, 2006.

[40] Y. Cao, A. Faghri, and Won Soon Chang, "A numerical analysis of

Stefan problems for generalized multi-dimensional phase-change structures using the enthalpy transforming model," *Int. J. Heat Mass Transf.*, vol. 32, no. 7, pp. 1289–1298, Jul. 1989, doi: 10.1016/0017-9310(89)90029-X.

[41] S. H. Cho and J. E. Sunderland, "Heat-Conduction Problems With Melting or Freezing," *J. Heat Transfer*, vol. 91, no. 3, pp. 421–426, Aug. 1969, doi: 10.1115/1.3580205.

[42] E. Bender, "Numerical heat transfer and fluid flow. VonS. V. Patankar. Hemisphere Publishing Corporation, Washington - New York - London. McGraw Hill Book Company, New York 1980. 1. Aufl., 197 S., 76 Abb., geb., DM 71,90," *Chemie Ing. Tech.*, vol. 53, no. 3, pp. 225–225, 1981, doi: 10.1002/cite.330530323.

[43] A. A. Eidan, S. E. Najim, and J. M. Jalil, "Experimental and numerical investigation of thermosyphone performance in HVAC system applications," *Heat Mass Transf.*, vol. 52, no. 12, pp. 2879–2893, Dec. 2016, doi: 10.1007/s00231-016-1800-y.

[44] J. W. Abernethy, R.B., Thompson, *Handbook uncertainty in gas turbine measurements In: Measurement Uncertainty Handbook. Sponsored by Instrument Society of America ISA*. 1980.

[45] M. Ricci, E. Bocci, E. Michelangeli, A. Micangeli, M. Villarini, and V. Naso, "Experimental tests of solar collectors prototypes systems," *Energy Procedia*, vol. 82, pp. 744–751, 2015, doi: 10.1016/j.egypro.2015.11.804.

[46] A. A. Eidan, A. Alsahlani, and K. J. Alwan, "Experimental

investigation on the performance of evacuated tube solar collector with wickless heat pipe under Iraq climatic conditions," *Adv. Nat. Appl. Sci.*, vol. 11, no. September, pp. 11–18, 2017.

[47] L. 1st Sunflower Renewable Energy Co., "Sunflower Renewable Energy," 2021. http://www.sunflower-solar.com.

[48] M. Kannan and E. Natarajan, "Thermal Performance of a Two-Phase Closed Thermosyphon for Waste Heat Recovery System," *J. Appl. Sci.*, vol. 10, no. 5, pp. 413–418, Feb. 2010, doi: 10.3923/jas.2010.413.418.

[49] Q. Liao, T.-C. Jen, Q. Chen, L. Li, and W. Cui, "Heat transfer performance in 3D internally finned heat pipe," *Int. J. Heat Mass Transf.*, vol. 50, no. 7–8, pp. 1231–1237, Apr. 2007, doi: 10.1016/j.ijheatmasstransfer.2006.09.010.

[50] A. Al Sahlani and A. A. Eidan, "Controllable vibrating system to enhance the performance of heat pipe evacuated tube solar collector," *J. Mech. Eng. Res. Dev.*, vol. 41, no. 3, pp. 67–73, 2018, doi: 10.26480/jmerd.03.2018.67-73.

Appendices

Appendix (A)

The Calibration of Instruments Used in The Experiments

A.1. Calibration of solar collector meter:

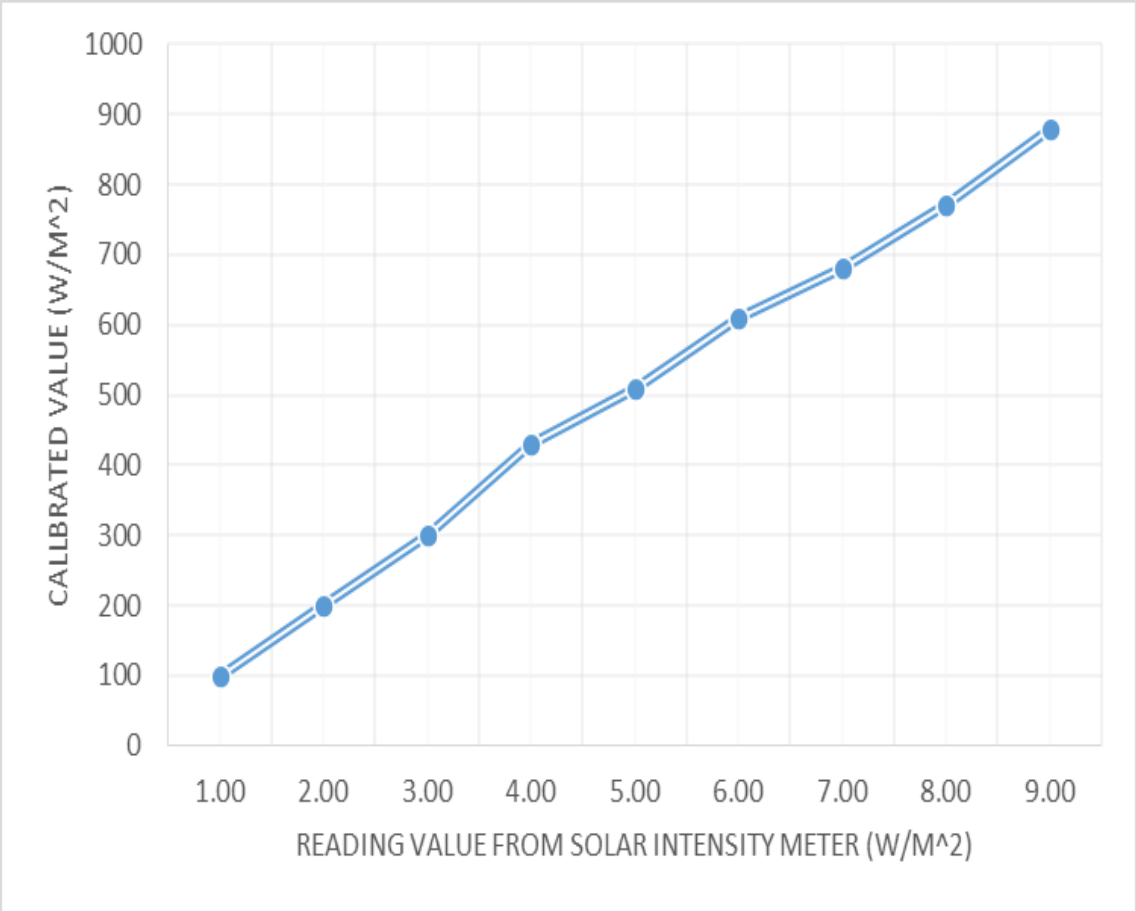

Fig. A.1: Calibration of solar radiation meter

A.2. Calibration of Thermocouple:

Fig. A.2: Calibration of Thermocouple

Appendix (B)

Experiments Data

Time	3 OUT EVA.	4 OUT EVA.	5 OUT EVA.	2 IN EVA.	3 IN EVA.	2 OUT COND.	3 OUT COND.	1 IN COND.	2 IN COND.	Length mm	1 W	4 W	5 W	INTLET WATER	OUTLET WATER
8:00:00	48	46.7	43.2	48	31	14.6	13.9	14.6	14.3	250	13.1	13.1	13.2	14.4	22
9:00:00	59.4	57.6	53.4	59	53	21.1	18.7	21.2	20.4	350	18.3	18.7	19	16.2	26.5
10:00:00	60.3	59.3	60	59.4	56.2	25.5	22.5	25.7	24.7	450	21.8	23.1	23.6	18	31.6
11:00:00	65	64.3	64	64.3	60.9	32.6	27.7	32.7	30.8	550	28.1	31	31.8	19.8	35.8
12:00:00	67.5	67	66.7	65.4	63.4	53.2	44	53.5	52.3	650	35	38	38.9	21.7	38
13:00:00	69.3	69	69.1	67.8	65.5	47.4	38.7	47.3	44.4	750	37	42.8	43	24.1	42.6
14:00:00	69.3	67.5	67.6	68	66.9	39.4	33.7	39.4	37.3	850	38.1	41.4	40.9	25.1	42.8
15:00:00	68	67.2	67.3	67.5	66.6	35.9	31.6	36	34.2	950	39.2	41	40.8	25.5	43.1
16:00:00	65.1	64.4	64.3	64	63.1	33.2	30.5	33.1	32.4	1050	35.1	36.8	37	25.3	40.3
17:00:00	49.1	49	48.8	48.4	47.6	29.8	28	29.8	29.2	1150	24.2	24.4	24.5	24.2	34.5
18:00:00	36.9	34.6	33.1	36.7	29.6	26	25.1	26	25.7	1250	23.4	23.4	23.5	21.2	29.6
19:00:00	30.4	29.4	25.8	30.1	24.1	23.3	23.1	23.3	23.3	1350	22.6	22.6	22.7	19.7	24.5
20:00:00	26	25.3	22.8	25.7	22.3	22.2	22.1	22.2	22.2	1450	21.8	21.8	21.9	19	22.2
21:00:00	22.9	22.4	21.1	22.5	21	21.2	21.1	21.2	21.2	1550	20.9	20.9	21	18.2	20.3
22:00:00	20.5	20.2	19.7	20.2	20	20.2	20.2	20.2	20.3	1650	20.1	20	20.1	17.6	17.8
23:00:00	18.7	18.5	18.5	18.3	18.9	19.2	19.2	19.2	19.2	1750	19.1	18.9	19	16.2	16.3
24:00:00	18.3	18.1	18.2	17.9	18.6	18.9	18.8	19	18.9	1850	18.8	18.6	18.8	15.2	15.2

Table (B-1): Without PCM with Thermal Break at 1 L/H Load

Time	3 OUT EVA.	4 OUT EVA.	5 OUT EVA.	2 IN EVA.	3 IN EVA.	2 OUT COND.	3 OUT COND.	1 IN COND.	2 IN COND.	1 W	4 W	5 W	1 PCM'	2 PCM'	OUTLET WATER	INLET WATER
08:00:00	47.5	45.6	41.1	47.2	29.8	26	25.8	26.3	26	24.7	26	26.1	26.1	26.6	21.2	17.3
09:00:00	58.7	55.2	51.2	58.4	45.8	26.4	26	26.7	25.5	22.3	25.3	25.4	25.7	25.9	25	19.3
10:00:00	59.4	59	59.2	58.3	55.7	32.2	32	32.6	30.6	24.6	29.8	29.8	27.1	26.7	30.8	22.2
11:00:00	63	63.3	62.5	62	59.3	37.2	35.3	37	36.3	26.3	34.4	34.1	30.5	29.8	34.1	23.8
12:00:00	64	63.4	63	63.6	59.8	38.6	37.2	39	38.5	29.8	37	36.8	33.7	33.1	35.2	25.1
13:00:00	65.4	65.1	65	64.1	62.8	43.2	41.4	43.3	41.2	36.1	40.1	39.7	37.1	36	40.2	26.1
14:00:00	66.7	66.6	66.6	65.7	64.4	46.7	44.2	47.5	45	38.9	42.9	42.8	40	39	42.3	25
15:00:00	65.1	64.9	64.5	64.3	63.3	45.7	44	45.2	44.6	40.1	44	43.9	42.2	41.3	44	24.3
16:00:00	63.5	63.3	62.9	62.6	61.8	43.2	42.5	43.4	43.3	39.5	42.6	42.5	40.9	40.6	43.5	23.9
17:00:00	45.1	45.3	45.2	45.4	45.2	41.7	41.4	41.9	42.3	39.1	41.7	41.5	39.7	39.6	40.5	22.7
18:00:00	38.2	38.4	37.9	38.6	38.2	37.8	37.7	37.9	38.1	36.4	37.7	37.7	37.4	37.7	38.2	22.9
19:00:00	34.4	34.5	34.4	34.3	34.1	33.4	33.4	33.5	33.8	32.4	33.5	33.5	34.1	34.8	34.1	20.1
20:00:00	28.1	28.4	28	28.4	28.1	33	33	33	33.3	31.9	33	33	32.6	33	32	18.6
21:00:00	26.8	26.5	26.7	26.5	26.2	28	27.9	28	28.1	27.2	27.9	28	29	30.2	29.3	17.8
22:00:00	22.3	22.5	22.4	22.3	22.3	26.5	26.3	26.5	26.3	25.5	26.3	26.3	26.6	27.3	26.3	17.1
23:00:00	20.3	20	20.3	20.4	20.4	24.4	24.7	24.4	24.4	23	24.6	24.6	25.4	25.9	24	16.7
24:00:00	18	18.1	18	18.1	18.3	24.5	24.6	24.6	24.3	23.3	24.4	24.5	25.2	25.7	21.7	16.7

Table (B-2): Without PCM without Thermal Break at 1 L/H Load

Table (B-3): With PCM with Thermal Break at 1 L/H Load

Time	3 OUT EVA.	4 OUT EVA.	5 OUT EVA.	2 IN EVA.	3 IN EVA.	2 OUT COND.	3 OUT COND.	1 IN COND.	2 IN COND.	1 W	4 W	5 W	INLET WATER	OUTLET WATER
8:00:00	47	40.7	34.6	68.8	32.2	21.1	19	22.2	21.1	18.9	21.2	21.3	14.4	22.3
9:00:00	58.1	39.9	41.9	70.4	38.6	24	19.6	33.3	25.1	19.1	23.8	23.9	16.2	27
10:00:00	60.3	43.9	46.5	74	42.7	27.2	19.9	38.1	29.5	19.5	27.1	27.3	18	32.2
11:00:00	65	50.6	53.1	92.9	48.2	31.9	22.8	43.3	37.8	22.3	32	32.1	19.8	36.2
12:00:00	67.4	55	63.5	89.7	51.9	37.1	25.8	47.9	43.2	25.2	37.4	37.5	21.7	38.7
13:00:00	70.4	53.8	56.8	84	52	39.4	27.1	48.1	43.1	26.6	40	40.1	24.1	43
14:00:00	70.2	51.7	54.5	73.2	50.3	39.4	28.3	47	40.6	27.8	39.8	39.9	25.1	43.5
15:00:00	68.6	50.3	53.2	69.4	48.9	39.2	29.5	45.8	39.3	28.9	39.2	39.4	25.5	44
16:00:00	66	49.2	51.9	65.7	47.9	38.6	30	43.7	38.5	29.4	38.6	38.7	25.3	40.7
17:00:00	49.4	47.1	49.4	60	46	36.9	31	40.6	36.6	30.4	36.7	36.8	24.2	34
18:00:00	38	38	37.5	37.3	38	29.8	24.3	28.4	29.7	24	30.3	30.4	21.2	27
19:00:00	34	34.1	33.6	34	33.8	25.8	22.9	24.8	25.1	22.4	25.5	25.7	19.7	22
20:00:00	27.5	28	27.6	27.7	28	19.9	19	19.4	19.6	19	19.8	19.8	19	19.2
21:00:00	26.2	26	26.4	26	25.9	19	18.2	18.5	18.6	18.1	18.8	18.9	18.2	18.2
22:00:00	22	22.2	22	21.8	22	18.1	17.5	17.7	17.7	17.4	17.9	18	17.6	17.6
23:00:00	20	20.1	20	20	19.9	17.6	17	17.2	17.2	17	17.3	17.5	16.2	16.2
24:00:00	17.6	17.8	17.6	17.5	17.8	17.5	17	17.1	17.1	16.9	17.2	17.3	17.1333	15.2

Table (B-4): With PCM without Thermal Break at 1 L/H Load

Time	3 OUT EVA.	4 OUT EVA.	5 OUT EVA.	2 IN EVA.	3 IN EVA.	2 OUT COND.	3 OUT COND.	1 IN COND.	2 IN COND.	1 W	4 W	5 W	INLET WATER	OUTLET WATER
08:00:00	47.3	44.5	37.3	47.7	29	23.9	23.8	23.6	24.1	24.2	24	23.1	17.8	22.3
09:00:00	57.9	51.7	49	58.1	47.2	25.2	25.1	26.3	25.9	23	22.5	20.1	18	26
10:00:00	73.2	66.7	64.9	73.1	59.5	33.2	30.3	34	33.2	25.3	25	21.1	19.1	31
11:00:00	83.8	73.3	74.1	83.3	68.6	44.5	35.4	47.8	44.3	34.9	34.3	25.9	20.9	35
12:00:00	74.7	75.2	76.9	74.3	71.8	59.9	47.3	62	48.1	45.7	45.3	32.5	22	37.4
13:00:00	76.6	76.7	77.2	75.9	73.2	62.6	51.9	59.7	51.4	51	51.6	39.6	22.9	43.6
14:00:00	74.2	74.1	75.1	74.4	70.4	57.7	53.9	57.3	54	53.5	53.3	42.8	23	43.4
15:00:00	72	72.7	76.9	71.9	70.8	56	53.1	55.6	53.3	53	52.9	43.8	23.5	44.4
16:00:00	67.9	68.4	71.9	67.7	66.5	49.3	48.9	49.1	48.9	49.5	48.6	32.9	24.5	44
17:00:00	64.2	64.4	66.4	63.9	62.8	44.4	44.2	44.3	44.2	44.6	44.1	31.7	23.8	39.7
18:00:00	38	38	37.5	37.3	38	32.8	35.4	32.8	35.1	39.2	34.6	24.5	23.2	34.9
19:00:00	34	34.1	33.6	34	33.8	29.8	30.5	29.6	30.5	32.1	30.4	24.4	21.7	27.9
20:00:00	27.5	28	27.6	27.7	28	25.8	26.5	25.6	26.4	28.1	26.4	21.9	20.5	24.9
21:00:00	26.2	26	26.4	26	25.9	21.4	22	21.2	22	23.9	22	19.1	18.9	23.2
22:00:00	22	22.2	22	21.8	22	19.3	19.2	19.1	19.3	20	19.4	18.7	18.5	19.8
23:00:00	20	20.1	20	20	19.9	18.4	18.3	18.2	18.3	18.7	18.5	17.9	17.8	18.5
24:00:00	17.6	17.8	17.6	17.5	17.8	18.1	18	18	18.2	18.5	18.4	17.7	17.7	18.4

Table (B-5): Without PCM with Thermal Break at 2 L/H Load

Time	3 OUT EVA.	4 OUT EVA.	5 OUT EVA.	2 IN EVA.	3 IN EVA.	2 OUT COND.	3 OUT COND.	1 IN COND.	2 IN COND.	1 W	4 W	5 W	INLET WATER	OUTLET WATER
8:00:00	46	40.6	34	66.3	32	20.1	18.5	22	21	18.2	20.8	21	14.4	22
9:00:00	56	38.6	40.7	70.2	37.1	22.9	19.2	31.6	24.4	19	23.4	23.5	16.2	26.4
10:00:00	58.2	42.7	45.8	72.4	42	25.7	19.5	38.4	30.2	19.3	28.8	26	18	32
11:00:00	63.7	50.5	52.4	90.7	47.6	28.7	22	42.7	35.9	22	31	30.9	19.8	35.4
12:00:00	66	54.3	61.4	89.4	50.8	35.8	25.4	44.4	40.6	25.6	35.6	36.2	21.7	37.8
13:00:00	68.3	51.7	54.4	79.6	51.3	38	26.6	45.4	41.8	16.2	38.4	38.7	24.1	42.1
14:00:00	68.1	50	52.8	70.9	48.4	38.8	28	45.3	39.4	27	38	38.4	25.1	43
15:00:00	66.8	49.2	52	67.6	47.8	38	29.1	44.7	37.5	28.4	37.8	38	25.5	43.5
16:00:00	64.2	48.8	51.4	64.4	47.6	36	29.6	43.6	37.7	29.1	37.5	37.7	25.3	40
17:00:00	48	45.9	47.9	57.7	45	35.4	30.8	37.9	35.2	30.2	35.5	35.7	24.2	33.4
18:00:00	37.6	37	37.2	38.3	36.9	29.7	24	28.9	29.1	22.3	29.5	29.6	21.2	25.5
19:00:00	31.3	30.5	27.7	31.1	32.2	22	22.4	25.3	25.4	18.4	25.7	25.8	19.7	20.9
20:00:00	26.6	25.8	23.7	26.4	26.7	19.8	19	19	19.3	18	19.3	19.3	19	19.6
21:00:00	22.9	22.3	21.1	22.8	24.4	19	18.1	18.1	18.1	17.9	18.2	18.4	18.2	18.3
22:00:00	20.4	20	19.3	20.3	21	18.2	17.5	17.8	17.4	17.4	17.4	17.4	17.6	17.6
23:00:00	19.8	19.9	19.4	19.3	19.8	17.5	17.2	17.2	17.2	17.2	17.2	17.2	16.2	16.2
24:00:00	17.6	18.2	17.3	17.4	17.5	17.6	17.4	17.2	17.2	17.1	17.2	17.1	15.2	15.2

Time	3 OUT EVA.	4 OUT EVA.	5 OUT EVA.	2 IN EVA.	3 IN EVA.	2 OUT COND.	3 OUT COND.	1 IN COND.	2 IN COND.	Length mm	1 W	4 W	5 W	INTLET WATER	OUTLET WATER
8:00:00	45	45.9	42.6	47	30.4	14.8	13.8	14.5	14.2	250	13	13.1	13	14.4	19.1
9:00:00	54.2	56	53.5	55.2	52.4	20.8	18.2	21	20.2	350	18	18.4	18.3	16.2	25.6
10:00:00	58.9	59	59.4	58.7	55.5	25	22	25.2	24.2	450	20.7	22.3	22.8	18	30.1
11:00:00	64.2	63.7	63.4	63.3	59.2	32.1	27	32.1	30.6	550	27.4	30.3	30.6	19.8	35
12:00:00	66	65.4	65.7	65.3	64.3	50.4	44	52.8	52	650	34	37.2	38	21.7	36.4
13:00:00	67.4	66.2	68.4	67.1	65	47	38	47	44.1	750	36.2	41.4	42.3	24.1	40.1
14:00:00	68.3	67	66.9	67.3	65.6	43	33.2	38.7	37.1	850	37.3	40.2	40.5	25.1	41
15:00:00	66.6	66	66.8	65	66	35.7	31.2	35.3	34	950	38.5	40	40.4	25.5	41.7
16:00:00	63.7	63.1	64	64.2	62.3	34.4	30	32	32.1	1050	34.3	36.2	36.4	25.3	38.2
17:00:00	47.2	47	47.2	47.5	47	29.2	27	29	29	1150	23.4	23.6	24	24.2	36.4
18:00:00	35.8	34.5	32.6	35.7	29.4	23	24.3	24.7	24.8	1250	22.3	22.8	22.9	21.2	30.7
19:00:00	29.1	29.3	25.6	29.8	24.2	20.1	21.2	21.4	21.3	1350	22	22.4	22.5	19.7	26.6
20:00:00	25.7	25.6	21.8	25.7	22	19.8	19.8	19.7	19.6	1450	20.4	20.6	21	19	20.8
21:00:00	23	22.7	21	22.6	21	19.5	19.6	19.5	19.4	1550	20.3	20.3	20.4	18.2	18.4
22:00:00	20.5	20.9	19.6	20.4	20	19.3	19.4	19.2	19.3	1650	19.8	20	20	17.4	17.6
23:00:00	18.8	18.2	18.4	18.3	18.5	18.2	18.3	18.3	18.4	1750	18.7	18.7	18.7	16	16.2
24:00:00	18.2	18.1	18.1	18	18.4	18.4	18.3	18.4	18.2	1850	18.7	18.6	18.6	15.2	15.2

Time	3 OUT EVA.	4 OUT EVA.	5 OUT EVA.	2 IN EVA.	3 IN EVA.	2 OUT COND.	3 OUT COND.	1 IN COND.	2 IN COND.	1 W	4 W	5 W	1 PCM'	2 PCM'	OUTLET WATER	INLET WATER
08:00:00	46.7	44.9	40.8	46.3	40.2	25.2	24.8	25.4	25.1	20.4	24.5	24.7	24.2	24.3	20.9	17.1
09:00:00	56.3	54.2	50.6	57.4	43.6	25.8	25.3	25.3	25.6	22	24.6	25	24.8	24.9	24.6	18
10:00:00	57.3	56.8	58.4	56.8	53.5	30.7	30.2	31.6	30.2	24.2	29.2	29.4	26.5	27.4	30.2	19
11:00:00	61.8	61.7	61.5	61.3	58.4	36.2	34.6	36.2	35.1	26	32.4	32.9	30.3	30.7	33.7	20
12:00:00	63.2	63	62.7	62.4	57.9	37.1	36.4	37.9	37.4	29.6	36.3	36	33.6	32.4	34.5	22
13:00:00	64.3	63.8	63.5	62	61.4	42	40.5	41.9	40.3	35.6	39.8	39.4	36.5	35.9	38.8	22
14:00:00	65.3	65	64.8	63.9	62.7	45.2	43.1	45.8	44.1	38.6	42.1	42	39.3	38.7	40.9	23.5
15:00:00	64.2	63.9	63.4	63.5	62.1	44.5	42.9	44.1	43.5	40	43.4	43.1	41.8	41.2	42.8	24.3
16:00:00	62.4	62	61.7	60.9	60.6	42.1	42	42.4	42	38.8	42	42	40.5	40	43	23.8
17:00:00	43.2	43.4	43	44.1	43.2	40.9	40.6	41.2	41	38.5	41.5	41.4	40	39	37.8	22.7
18:00:00	36.8	36.5	37.9	37.2	36.5	34.6	33.7	33.4	31.8	34.2	34.2	35.1	36.5	36.2	33.7	22.9
19:00:00	34.4	34.5	34.4	34.3	34.1	30.9	29.6	30.6	30	30.9	31.2	31.8	33.7	33.1	28.5	20.1
20:00:00	28.1	28.4	28	28.4	28.1	29.3	28.6	29.6	29.1	30	30.3	30.6	31.2	30.6	23.4	18.6
21:00:00	26.8	26.5	26.7	26.5	26.2	26.2	26.2	26	25.3	25.3	25.2	25.6	27.3	27	20.4	17.8
22:00:00	22.3	22.5	22.4	22.3	22.3	24.5	24.4	24	23.4	22.1	22	22	23.4	23.4	17.3	17.1
23:00:00	20.3	20	20.3	20.4	20.4	22.1	20.5	20.3	19.3	19.2	18.9	19.2	22.2	22.3	17	16.7
24:00:00	18	18.1	18	18.1	18.3	17.2	17.2	17.6	17.6	17.5	17.3	17.4	19.8	19.4	16.7	16.7

Table (B-6): Without PCM without Thermal Break at 2 L/H Load

Table (B-7): With PCM with Thermal Break at 2 L/H Load

Table (B-8): With PCM without Thermal Break at 2 L/H Load

Appendix (C)

Average Data

Table (C-1): Average Date for February 2021

Time	Wind Speed (m/s)	Solar Radiation (W/m2)	Ta ^{o}C
8:00 AM	0.2	115.625	18.975
9:00 AM	0.2	241	19.6375
10:00 AM	0.2	338.625	20.5
11:00 AM	1.6	511.625	21.0125
12:00 PM	1	561.875	20.5625
1:00 PM	1.2	627.875	20.675
2:00 PM	0.8	737.375	21.1875
3:00 PM	0.6	714.875	21.625
4:00 PM	0.6	332	21.5875
5:00 PM	0.6	170.25	20.4375
6:00 PM	1.2	0	21.025
11:00 PM	0.4	0	23.275
12:00 AM	1.4	0	22.1625

Time	3 OUT EVA.	4 OUT EVA.	5 OUT EVA.	2 IN EVA.	3 IN EVA.	2 OUT COND.	3 OUT COND.	1 IN COND.	2 IN COND.	1 W	4 W	5 W	INLET WATER	OUTLET WATER
08:00:00	46.2	42.1	36.6	46	44	23.2	23.4	23.5	23.6	22.8	22.7	23	17.8	22.3
09:00:00	57	50.4	48	56.7	53.6	25	25.3	26	26.3	24.4	23.7	24.1	18	24.2
10:00:00	72.1	65.2	63.2	72	66.9	31.8	32.3	33	33.4	30.9	31.2	30.8	19.1	28.9
11:00:00	83	72	71.6	82.3	80.7	42.6	43.2	45.3	44.8	36.4	36.2	35.3	20.9	34.2
12:00:00	73.9	72.5	71.3	73.5	71.2	58.1	58.4	60.3	58.9	49.8	49.1	48.7	22	37
13:00:00	75.8	73.8	72.1	73.8	73.8	61.1	61.5	63.2	62.5	53.4	52.2	51.2	22.9	42.4
14:00:00	73	70.9	70.4	72.8	71.4	55.9	56.2	57.8	56.9	53.1	52.3	49.4	23	42.8
15:00:00	68.3	66.8	66	68	68.3	54.3	54.6	55.4	54.4	51.9	50.8	51	23.5	43.1
16:00:00	64.2	63.3	62.2	62.7	62.2	47.7	48	48.7	47.6	44.7	43.3	43.1	24.5	42.2
17:00:00	61.8	60.8	60.2	61	61.5	43.1	43.7	44	43.4	41.5	41.2	40.8	23.8	38.4
18:00:00	34.2	35.4	35.3	35	35.2	31.2	31.1	31.3	31.3	32.1	30.8	30	23.2	29.8
19:00:00	29.3	30.4	30.5	30.4	30.1	28.7	28.9	28.9	29.4	29.4	28.6	27.8	21.7	27
20:00:00	22.3	23.3	23.6	23.3	23.1	23.4	23.6	24.4	24.2	24	23.5	23.4	20.5	22.8
21:00:00	21.2	21.6	22	21.7	21.5	20.8	21	21	20.8	20.7	20.1	19.4	18.9	19.8
22:00:00	19.8	20.1	20.4	20.9	20.7	18.3	18.4	18.6	18.4	18.7	18.6	18.7	18.5	18.5
23:00:00	18.4	19	19.2	19.5	19.5	17.2	17.2	17.4	17.3	17.3	18.5	17.9	17.8	17.8
24:00:00	17.6	18.1	18.2	18	17.9	16.7	16.7	16.8	16.5	16.7	18.4	17.7	17.7	17.7

Table (C-2): Average Date for March 2021

Time	Wind Speed (m/s)	Solar Radiation (W/m2)	Ta (C)
8:00 AM	3.4125	193	12.9625
9:00 AM	4	376.75	15.0875
10:00 AM	4	462.125	17.175
11:00 AM	3	587	18.625
12:00 PM	6.0125	749	19.7
1:00 PM	5.6125	611.375	20.7
2:00 PM	4.8125	546.25	21.475
3:00 PM	4.4125	386.75	21.6375
4:00 PM	5.2125	283	21.625
5:00 PM	3.6	153.875	21
6:00 PM	2.4	16.25	19.8625
7:00 PM	3	0	18.3875
8:00 PM	2.4	0	17.5375
9:00 PM	2.2	0	16.7375
10:00 PM	2.6125	0	16.075
11:00 PM	1.6	0	15.4375
12:00 AM	3.0125	0	13.8

Appendix (D)

Table D-1: Uncertainty for Empirical Results

Details	Average Worth	Gross Worth	Gross (%)
Temp. (C^o)	45	±0.41	±0.91
Pyro. (W/m^2)	400	±0.5	±1.6
Volumetric Flow Ra. (l/h)	1	±0.4	±1.4
Thermal Resistance (m^2.K /W/)	0.198	±0.8	±2.3
Heat Pipe Eff. (η), %	42	±1.3	±3.2

Appendix (E)

List of publications

1. The Paper has been Published (https://doi.org/10.1063/5.0069702)

2nd International Conference on Engineering and Science (ICES2021)
26 -27 MAY 2021
AL-SAMAWAH, IRAQ

Final Acceptance Letter

Manuscript Number: ICES2021-102 **Decision ID : FAL-ICES-009**

Dear Noora Saleh

Co-Authors : Mohamed Al-fahham /Adel A. Eidan

Congratulations!

It's a great pleasure to inform you that, after the peer review process, your manuscript entitled

(Influence of The Adiabatic Section Thermal Break on The Thermal Performance of A Gravity-Assisted Heat Pipe Integrating With Evacuated Tube Solar Collector)

Has been **ACCEPTED** for participating in the **2nd International Conference on Engineering and science,** and considered for publication in **(AIP Conference proceeding).**

Thank you for your valuable participation in the ICES2021 conference.

Dr.Ahmed Razzaq H. Al-Manea
ICES2021 Scientific Committee | AIP Conference Proceeding Editor
26 - 27 MAY 2021 | SAMAWA| IRAQ

Al-Furat Journal of Innovations in Mechanical and Sustainable Energy Engineering
(FJIMSE) Publish by Al-Furat Al-Awsat Technical University (ATU) / Iraq

ISSN :- 2710-3374

Manuscript Acceptance Letter

Dear Authors: Noora S. Mahdi, Adel A. Eidan & Mohamed Al-Fahham

Al-Furat Journal of Innovations in Mechanical and Sustainable Energy Engineering FJIMSE, Editorial Board, is pleased to inform you that your manuscript entitled "**Thermal Performance of a Gravity-Assisted Heat Pipe Evacuated Tube Solar Collector Integrating with The Adiabatic Section Thermal Break and Phase Change Material**" has been accepted and approved for publication within the 1st Volume, 4th Issue of "FJIMSE-Journal".

The decision was made based on the fact that your manuscript had successfully passed the review process and revisions made by you. The manuscript was also checked for plagiarism by Turnitin software that showed acceptable similarity index (SI ≤ 20%), and all the similarities in the manuscript belong to the "General Knowledge Domain". All of the accepted manuscripts in this journal will go under advanced English editing by our native editors. The authors will also receive the galley proof of the final revision after all the quality control checks and before publishing the article.

Thank you for publishing your work with FJIMSE Journal.

Sincerely Yours

Dr. Essam Al-Zaini
FJIMSE-Journal Editorial Manager
Furat-fjimse@atu.edu.iq
+9647706234439
23August 2021

الخلاصة

الجيل القادم من مجمعات الطاقة الشمسية، وتحديدًا مفاهيم مبادئ نظام مجمعات الطاقة الشمسية الأنبوبية (ETSC) يقوم الباحثون بتضمين تقنيات جديدة وإحداث العديد من التطورات في الطاقة الحرارية الكامنة. ومع ذلك، هناك بعض التحديات المرتبطة بأحدث التقنيات أن العلماء يخططون لاستخدامها في الجيل المقبل من تجميع الطاقة الشمسية. على سبيل المثال، انخفاض الطاقة الحرارية أثناء غياب اشعة الشمس. إحدى التقنيات الفريدة في استخدام قسم ثابت الحرارة داخل نظام أنابيب تسخين مساعدة الجاذبية (GAHP-ETSC) ، مثل قاطع حراري داخل قسم ثابت الحرارة من GAHP يختلف بشكل كبير عن نظام HP-ETSC التقليدي. إضافة على ذلك، يتم دمج تقنية أخرى وهي مادة تغيير الطور (PCM) ضمن التقنية الفريدة السابقة لتعزيز الكفاءة الحرارية أثناء غروب الشمس.

أربعة نماذج تجريبية GAHP-ETSC هي طرازا GAHP-ETSC مع وبدون PCM (مادة متغيرة الطور) وكلاهما مع قاطع حراري، والآخران مع وبدون PCM (مادة متغيرة الطور) وكلاهما بدون قاطع حراري تم تصنيعهما وتطويرهما وتشغيلهما لتحقيق الفوائد المطلوبة. تمت دراسة أربعة نماذج مختلفة من خلال تقسيم في حالتين على أساس كمية حمولة المياه (الحمل) في الخزان. تدرس الحالتان الأولى والثانية تأثير تطبيق حمولة ١ لتر / ساعة وحمل ٢ لتر / ساعة من الماء على الكفاءة اليومية والأداء للأجهزة التجريبية الأربعة المختلفة، على التوالي. حيث تقوم كل حالة بالتحقيق وتبيان تأثير تطبيق كل حمل على كل جهاز تجريبي كلاً على حدة لتوضيح وإثبات تأثير القاطع الحراري مع PCM على تعزيز وتحسين أداء نظامGAHP-ETSC ، خاصة خلال فترة الطلب (بعد غروب الشمس).

تم العمل الدراسة التجريبية في مدينة النجف الاشرف العراقية في ظروف خارجية للفترة من شهر ايلول ٢٠٢٠ الى شهر نيسان ٢٠٢١. حيث تم استخدام المواصفات الاتية: زاوية الميل (٤٥ درجة) ونسبة الملء ٧٠٪ بالأسيتون كسائل عامل و٣.٦ كيلوغرام من شمع البرافين باعتباره PCM (مادة متغيرة الطور) لكل جهاز من الأجهزة الأربعة المختلفة. أظهرت النتائج أن القاطع الحراري يعزز الكفاءة اليومية من خلال إطالة إجمالي ساعات التشغيل المجمع الشمسي حوالي (٣ ساعات) أثناء الليل. كذلك، يتمتع النظام المزود بكل من القاطع الحراري و PCM بأعلى كفاءة يومية مقارنة

بالأجهزة الأخرى، حيث زادت الكفاءة من ٣١٪ إلى ٤١٪ عند حمل ١ لتر / ساعة، ومن ٤٢٪ إلى ٤٧٪ عند حمل ٢ لتر / ساعة. علاوة على ذلك، فإن نسبة التحسين في درجة حرارة الماء الخارج من المجمع الشمسي (المنتج المهم من(GAHP-ETSC) بين الجهاز مع كلاً من الميزتين القاطع الحراري و PCM والجهاز بدون كليهما هي ٥٥٪ و ٥٥.٥٪ عند حمل ١ لتر / ساعة و ٢ لتر / ساعة، على التوالي.

كذلك تم تحليل نموذج رياضي لـ GAHP عن طريق حل المعادلات التفاضلية PDE من أجل الحصول على صورة ومظهر توزيع درجة الحرارة للنظام الحالي باستخدام التحليل العددي واستخدام برنامج (MATLAB Software) للبحوث المستقبلية. تم بناء وعمل النموذج الرياضي (كود MATLAB) لحل الإحداثيات الأسطوانية (لمشاكل الحرارة العابرة) باستخدام طريقة الفروق المحدودة (FDM). كذلك أيضًا، تم عمل عمليات التحقق من الصحة بين النتائج العددية والتجريبية لجهازين بحمل ٢ لتر / ساعة بناءً على توزيع درجة حرارة السطح على طول قسم المبخر في GAHP (منطقتان بخار وسائل). الجهاز الأول مع كلاً من القاطع الحراري و PCM، والجهاز الآخر بدون قاطع حراري ومع PCM. الحد الأدنى والحد الأقصى لنسبة الخطأ بين النتائج العددية والتجريبية هي (٢.٥٤٪) عند (١٠:٠٠) و (٩.٥٢٪) عند (٢٢:٠٠) على التوالي للمجمع الشمسي بكلاً من القاطع الحراري وPCM. أما (٣.٢٪) عند الساعة (١٠:٠٠) و (١٦.٥٣٪) عند الساعة (٢٢:٠٠) على التوالي لمجمع الطاقة الشمسية بدون قاطع حراري ومع PCM.

من خلال تحديد وفهم التحديات والإمكانيات الرئيسية التي توفرها التكنولوجيا، تساهم هذه الرسالة بشكل أكبر في تحديد خارطة طريق لنظام ETSC للتكنولوجيا الجديدة لتسهيل البحوث المستقبلية.

جمهورية العراق

وزارة التعليم العالي والبحث العلمي

جامعة الفرات الاوسط التقنية

الكلية التقنية الهندسية – نجف

دراسة تجريبية لأنتقال الحرارة محوريا بالتوصيل خلال انبوب مجمع شمسي مفرغ معزز بمادة متغيرة الطور

رسالة مقدمة الى

قسم تقنيات ميكانيك القوى

كجزء من متطلبات نيل درجة الماجستير تقني في هندسة الميكانيكية (حراريات)

تقدم بها الطالب

نوره صالح مهدي

(بكالوريوس هندسة ميكانيك ٢٠١٣)

اشراف

الدكتور محمد عبد الرضا الفحام

هـ 1443